Regulation of hepatic miRNAs by hypoosmolarity

Inaugural-Dissertation

zur Erlangung des Doktorgrades
der Mathematisch-Naturwissenschaftlichen Fakultät

der Heinrich-Heine-Universität Düsseldorf

vorgelegt von

Nils Bardeck

aus Essen

Düsseldorf, März 2022

Aus der Klinik für Gastroenterologie, Hepatologie und Infektiologie

der Heinrich-Heine-Universität Düsseldorf

Gedruckt mit der Genehmigung der Mathematisch-Naturwissenschaftlichen Fakultät der Heinrich-Heine-Universität Düsseldorf

Berichterstatter:

1. Prof. Dr. Stephan vom Dahl

2. Prof. Dr. Holger Gohlke

Tag der mündlichen Prüfung: 09.12.2022

Table of Contents

List of abbreviations

Δp	hydrostatic pressure
$\Delta \pi$	osmotic pressure
3'UTR	three prime untranslated region
5'UTR	five prime untranslated region
ACADL	acyl-CoA dehydrogenase
ACTB	beta actin
AGO	argonaute protein
ANOVA	one-way analysis of variance
ATG5	autophagy related protein 5
ATP	adenosine triphosphate
BCL2	Bcl2 apoptosis regulator
BSEP	bile salt export pump
C. elegans	*Caenorhabditis elegans*
CAMSAP1	calmodulin regulated spectrin associated protein 1
CAV1	caveolin 1
CCNB2	cyclin b2
CCND1	cyclin d1
CD95	cluster of differentiation 95
CDC25A	cell division cycle 25a
CDK8	cyclin dependent kinase 8
CDKN1A	cyclin dependent kinase inhibitor 1a
CIRCKEAP1	kelch like ech associated protein 1
DGCR8	DiGeorge syndrome critical region 8
DMXL1	dmx like 1
DSTYK	dual serine/threonine and tyrosine protein kinase
DUOXA2	dual oxidase maturation factor 2
EGFR	epidermal growth factor receptor
EML4	emap like 4
EMT	epithelial-to-mesenchymal transition
FAK	adhesion kinase $p125^{FAK}$
FBP1	fructose bisphosphatase 1
FBXW7	f-box and wd repeat domain containing 7
FCS	fetal calf serium
FDR	false discovery rate
FOS	fos proto oncogene
FXR1	fragile x mental retardation related protein 1
GJA1	gap junction protein alpha 1
GO	Gene Ontology enrichment
GUCY2C	guanylate cyclase 2c
GW182	trinucleotide repeat-containing gene 6A protein
HCC	hepatocellular carcinoma
HIF1A	hypoxia inducible factor 1 subunit alpha
HSF1	heat shock transcription factor 1
HSP70	heat shock protein 70
HSPA1A	heat shock protein family a member

HSPB1	heat shock protein family b member 1
IL-6	interleukin 6
JNK	c-jun n terminal kinase
LAMC2	laminin subunit gamma 2
L_p	hydraulic conductivity
LPC	liver progenitor cells
LUC7L3	LUC7 like 3 pre mRNA splicing factor
MAP	mitogen activated protein
MAP1LC3B	microtubule-associated protein 1 light chain 3 beta
MAP4K4	mitogen activated protein kinase 4
MIEF1	mitochondrial elongation factor 1
MCS	multiple cloning site
miR-141-3p	mature microRNA-141-3p
MIRISC	microRNA-induced silencing complex
miRNA	microRNA
MREs	microRNA response elements
mRNA	messenger ribonucleic acid
mRNP	messenger ribonucleoproteins
MRP2	multidrug resistance associated protein 2
MSANTD2	MYB/SANT DNA binding domain containing 2
MVB	multivesicular bodies
NAGS	n-acetylglutamate synthase
NFAT5	nuclear factor of activated t cells 5
NF-YA	nuclear transcription factor y subunit alpha
NF_KB	nuclear factor kappa b
NOX	NADPH oxidase
NTCP	sodium/taurocholate co transporting polypeptide
ODC1	ornithine decarboxylase
PEPCK	phosphoenolpyruvate carboxykinase
PHX	partial hepatectomy
PRMT1	protein arginine methyltransferase 1
qPCR	quantitative real-time PCR
RAB30	member ras oncogene family
rER	rough endoplasmic reticulum
RGD	tripeptide Arg-Gly-Asp attachment site
RGS20	regulator of G-protein signaling 20
RISC	RNA-induced silencing complex
ROS	reactive oxygen species
RPM	revolutions per minute
RPS6	ribosomal protein S6
RTASE	reverse transcriptase
RVD	regulatory volume decrease
RVI	regulatory volume increase
SCNN1A	sodium channel epithelial 1 subunit alpha
SEM	standard error of the mean
SG	stress granules
siRNA	small interfering RNA
SLC1A7	solute carrier family 1 member 7
SLC22A5	solute carrier family 22 member 5

SLC39A10	solute carrier family 39 member 10
SLC9A3	solute carrier family 9 member A3
SMAD	sma- and mad-related protein
SOCS	suppressors of cytokine signaling
STAT	signal transducer and activator of transcription
SYNE1	nesprin 1
TAT	tyrosine aminotransferase
TFEB	transcription factor EB
TGN	trans-golgi network
TIMP1	timp metallopeptidase inhibitor 1
TNF-α	tumor necrosis factor alpha
TUBB	tubulin
VIM	vimentin
WNT	wingless-type MMTV integration site family
XP1	exportin-1
XPO5	nuclear transporter protein exportin-5
XRN4	5' - 3' exoribonuclease 1
ZEB1	zinc finger e box binding homeobox 1
ZEB2	zinc finger e box binding homeobox 2
ZFP18	zinc finger protein 18
ZMPSTE24	zinc metallopeptidase STE24

Zusammenfassung

Leberzellen sind durch ihre kritische anatomische Lage mit dem Portalgefäßsystem und dem restlichen Blutkreislauf in stetiger Verbindung. Folglich sind sie großen Konzentrationsveränderungen von gelösten Stoffen wie Aminosäuren, Gallensäuren und Glukose ausgesetzt. Die gelösten Stoffe erzeugen einen osmotischen Gradienten und induzieren eine transmembrane Wasserbewegung. Damit das ursprüngliche Zellvolumen wiederhergestellt werden kann, erfolgt eine adaptive Reaktion, welche eine passive Wasserbewegung induziert. Veränderungen des Zellvolumens sind wichtige Regulatoren von Zellfunktionen und der damit einhergehenden Genexpression. Sie können als eine Art Transmitter als Reaktion auf verschiedene Stimuli, wie die durch die Hormone Insulin und Glukagon, wirken. Zellvolumenänderungen durch eine Verschiebung der Osmolarität treten auch bei einer Vielzahl von Krankheiten auf, wie der Leberzirrhose und der hepatischen Enzephalopathie. Der mechanische Stimulus, welcher auf die Leberzellen durch Hypoosmolarität ausgeübt wird, tritt ebenfalls bei regenerativen Prozessen in der Leber auf.

In der Vergangenheit konnte gezeigt werden, dass eine Zellschwellung, welche durch Hypoosmolarität induziert wird, zu einer erhöhte Zellproliferation führt. Mit dem Ziel, eine Beteiligung von microRNA Prozessen zu identifizieren, welche durch Zellschwellung induziert werden, wurden Leberperfusionen durchgeführt. Anschließend wurden diese über Transkriptomanalysen und quantitativer PCR untersucht. In der vorliegenden Doktorarbeit konnten spezifische Veränderungen auf Transkriptomebene als eine direkte Reaktion auf Hypoosmolarität gezeigt werden. Weiterhin konnte die microRNA miR-141-3p als eine osmotisch sensitive microRNA identifiziert werden. Durch die Bindung an die 3'UTR der mRNA von spezifischen Genen, wie der *Cyclin-abhängigen Kinase 8* (*Cdk8*), übt miR-141-3p einen antagonistischen Effekt auf Prozesse wie die Zellproliferation aus. Eine Untersuchung von isolierten primären Hepatozyten zeigte ebenfalls eine Heraufregulation der miR-141-3p nach einer Zellschwellung. Durch Inhibitor-Perfusionen konnte nachgewiesen werden, dass miR-141-3p über den MAP-Kinase-Weg durch die Kinasen Erk-1/2 und $p38^{MAPK}$ reguliert wird. Weiterhin konnte eine Beteiligung der miR-141-3p und deren Zielgen *Cdk8* an regenerativen Prozessen der Leber nach einer partiellen Hepatektomie nachgewiesen werden.

Die vorgelegte Arbeit weist der microRNA miR-141-3p eine mögliche Schlüsselrolle bei der Zellproliferation zu. Die hier aufgezeigten Befunde legen die Vermutung nahe, dass miR-141-3p durch die Modulierung von spezifischen Zielgenen eine Terminierung von proliferativen Effekten hervorruft, um die Zelle vor einer möglichen Entstehung eines hepatozellulären Karzinoms (HCC) zu bewahren.

Summary

Liver cells are connected to the portal vasculature and the rest of the bloodstream by their critical anatomical location. Consequently, they are exposed to large concentration changes of solutes such as amino acids, bile acids, and glucose. These solutes create an osmotic gradient which induces transmembrane water movement. In order for the original cell volume to be restored, an adaptive response occurs that induces passive water movement. Alterations of cell volume are important regulators of cell function and associated gene expression. They can act as a type of second messenger in response to various stimuli, such as those produced by hormones like insulin and glucagon. Cell volume changes due to a shift in osmolarity also occur in a variety of diseases, such as liver cirrhosis and hepatic encephalopathy.

In the past, it has been shown that cell swelling induced by hypoosmolarity leads to increased cell proliferation. With the aim to identify an involvement of microRNAs in processes induced by hypoosmolarity, liver perfusions were performed and subsequently investigated via transcriptome analyses and quantitative PCR. In the present PhD thesis, specific changes at the transcriptomic level as a direct response to hypoosmolarity were shown. Furthermore, the microRNA miR-141-3p was identified as an osmotically sensitive microRNA. By binding to the 3'UTR of the mRNA of specific genes, such as *cyclin-dependent kinase 8* (*Cdk8*), miR-141-3p exerts an antagonistic effect on processes such as cell proliferation. An examination of isolated primary hepatocytes also showed upregulation of miR-141-3p under hypoosmolarity. Inhibitor perfusions demonstrated that miR-141-3p is regulated via mitogen-activated protein kinases Erk-1/2 and $p38^{MAPK}$. Furthermore, miR-141-3p and its target gene *Cdk8* were shown to be involved in the regenerative process of the liver after partial hepatectomy was conducted.

Taken together, the present study assigns a possible key role to the microRNA miR-141-3p in cell proliferation. The findings revealed here suggest that miR-141-3p induces termination of proliferative effects by modulating its specific target genes to protect the cell from possible hepatocellular carcinoma (HCC) development.

1. Introduction

The liver forms the main organ for the metabolism in mammalian organisms. Numerous physiological processes take place in the liver, including macronutrient metabolism, immune system support, blood volume regulation and the detoxification of compounds by removing xenobiotics through metabolic conversion and biliary excretion [1,2]. The liver is also a main regulator of metabolic homeostasis, since it is responsible for the synthesis, storage and redistribution of nutrients, carbohydrates, fats and vitamins [2]. The ability of the liver to store glucose in the form of glycogen and to recover glucose back via the gluconeogenic pathway is one critical function which provides the energy for the aforementioned processes [3]. Oxidizing and storing of excess lipids in other tissues, such as adipose, is also an important function which is controlled by the liver [4,5]. The cell types residing in the liver are of different embryological origin and include hepatocytes, which make up 60% to 70% of the liver cell population, and 90% of total liver mass [6]. Non-parenchymal cells, like endothelial cells, Kupffer cells, biliary epithelial cells (cholangiocytes), lymphocytes and hepatic stellate cells account for 25% to 40% of the total liver cell population, or 10% of total liver mass [7]. The second most abundant cell population of the liver represent cholangiocytes, as they form the lining in the lumen of the bile ducts [8]. Hepatic stellate cells constitute a dynamic cell population, which exist in an activated or quiescent state. In their quiescent state, stellate cells store vitamin A in lipid droplets and are located on a basement membrane-like structure in the so called ‘space of Disse’ [9,10]. Each of these aforementioned cell types have unique functions, which cooperatively regulate hepatic functions. A broad range of metabolic functions are directly affected by cell volume changes, e.g. glycogen synthesis [11–14], glycolysis [15], proteolysis [16–18], glutamine breakdown [19], urea synthesis [19–21] and lipogenesis [14]. Hepatocellular hydration state also affects protein synthesis, whereas cell shrinkage inhibits, but cell swelling stimulates protein synthesis [22,23]. Cell swelling is considered as an anabolic signal, while cell shrinkage leads to a catabolic signal, stimulating protein breakdown under the premise that the proteolytic activity is not already at full capacity [16,24–26]. There is a close relationship between hepatocellular hydration and autophagic proteolysis in the liver, whereas an increase in cellular hydration by 1% inhibits proteolysis by roughly 2% [25,27].

1.1.1 Mechanisms of cell volume control

Cell volume is determined by intracellular osmolarity and extracellular tonicity, whereas changes in cell volume are usually initiated by fluctuation in intracellular or extracellular osmolarity. These changes are always associated with diffusion of water molecules across the

cell membrane (J_v), which in turn is driven by a hydrostatic (Δp) and osmotic ($\Delta\pi$) pressure gradient.

Both pressure gradients depend on the hydraulic conductivity of the cell membrane (L_p):

$$J_v = L_p(\Delta p - \Delta\pi)$$

Most cells can counteract volume perturbations. This behavior is characterized by a regulatory cell volume decrease (RVD), or a regulatory volume increase (RVI), as shown in Figure 1.1. However, the hydration state of cells controlled by RVD or RVI may not completely reconstitute the original hydration state. Therefore, cells are left in a slightly swollen or shrunken state [28].

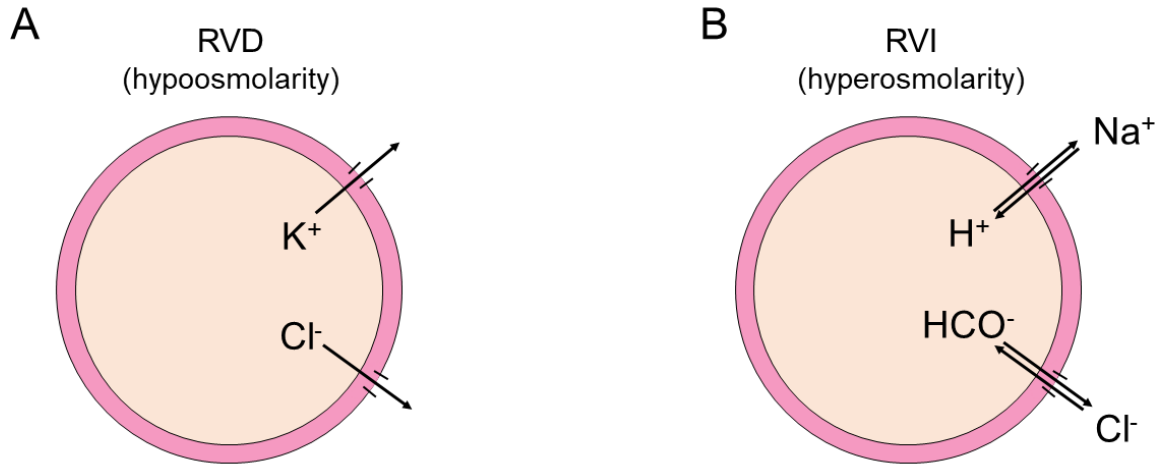

Figure 1.1 Mechanisms underlying regulatory cell volume decrease (RVD) and regulatory cell volume increase (RVI) following hypoosmotic and hyperosmotic exposure in hepatocytes. (**A**) Mechanism of RVD: activation of both K^+ and Cl^- channels resulting in K^+/Cl^- symport out of the cell. (**B**) Mechanism of RVI: parallel activation of Na^+/H^+ exchange and Cl^-/HCO_3^- antiport. Activation of RVI results in a net export of H^+ and HCO^- ions, while Na^+ and Cl^- are imported. (Modified and adapted from [28]).

Responsible mechanisms for RVD and RVI differ among cell types and species, but generally involve the recruitment of ion transport systems into the plasma membrane [28–30]. RVD in rat liver is mainly accomplished by the release of cellular potassium, chloride and bicarbonate ions into the extracellular space [31–35], followed by an activation of K^+ channels together with anion channels [36]. Rat hepatocytes under the influence of cell swelling open non-selective cation channels, which allow a cellular intake of for instance Ca^{2+} ions [37], that results in an activation of Ca^{2+}-sensitive K^+ channels [38]. However, it is still under debate if hypoosmotic hepatocyte swelling increases intracellular Ca^{2+} ion concentrations [25], since Ca^{2+}-activated K^+ channels are not solely responsible for RVD. In contrast, in human lymphocytes, cell swelling is not associated with an intracellular accumulation of Ca^{2+} ion concentrations [39].

There are also K^+ channels in isolated hepatocytes which do not require an enrichment of intracellular Ca^{2+} [40], but are rather activated by cell membrane stretching [41].

Under hyperosmotic conditions, RVI is initiated by simultaneous activation of Na^+/H^+ and Cl^-/HCO_3^- exchangers. In an experimental model of perfused rat livers, hyperosmotic exposure leads to a cellular K^+ uptake which leads to RVI [33,35]. Besides cell volume regulation by ionic mechanisms, some cell types release or accumulate organic compounds in response to cell swelling or cell shrinkage. These organic compounds, so-called 'organic osmolytes', do not interfere with protein function even at high intracellular concentrations [42–44], e.g. inositol and sorbitol [45,46], methylamines (betaine and a-glycerophosphocholine [47,48]), and certain amino acids (taurines [49,50]). These osmolytes are able to create osmotic gradients in the extracellular fluid of up to 1000 mmol/L [43].

1.1.2 Liver cell hydration

Changes in ambient osmolarity, increased amino acid uptake, hormone-induced or toxin-induced ion fluxes across the plasma membrane have a direct impact on the liver cell hydration [28,51,52]. The diffusion of water molecules across the cell membrane is largely dictated by the osmotic pressure gradients [53–56], whereas an imbalance of intracellular and extracellular osmolarity is compensated by diffusion of water molecules across cell membranes. These changes in cell hydration, when inside a narrow physiological range, occur within minutes and directly affect protein and carbohydrate metabolism and gene expression. Despite the activity of cellular volume regulation mechanisms, these regulations are not designed to maintain absolute cell volume constancy, but are rather intended to dampen the effect of hazardous cell volume deviations which would result from cumulative substrate uptake [57] or as a result of diseases [58–60]. Hormones, e.g. insulin, are potent modulators of liver cell volume and impact volume-regulatory mechanisms, while creating a strong signal for cellular metabolism and gene expression [15,28]. For instance, insulin can stimulate the mitogen activated protein (MAP) kinase cascade through a tyrosine receptor-activated signaling cascade. Following a series of protein phosphorylation, membrane ion transporters such as Na^+/H^+ antiporter and the basolateral Na/K-2Cl symporter (solute carrier family 12 member 2 (Slc10a2)) are activated which, subsequently, results in hepatocyte swelling as described in section 1.1.1 [61].

1.1.3 Cell hydration modulates cell signaling function

Detection of changes in cell volume (the so called "osmosensing") and how this information is transmitted and finally results in altered hepatocyte function (known as "osmosignaling"), have been in the spotlight of research for many years. In the past, macromolecular crowding

(meaning the accumulation of proteins) [62,63], stretch-activated ion channels [64], and histidine kinases were investigated, that might act as potential osmosensors [65]. In hepatocytes, $\alpha_5\beta_1$-integrins were identified as osmosensors [66]. The $\alpha_5\beta_1$-integrins are predominantly localized in the plasma membrane and are activated in response to hypoosmotic or insulin-induced hepatocyte swelling [67–69]. $\alpha_5\beta_1$-integrins mediate cell-cell and cell-extracellular matrix interactions. The integrin-mediated activation of downstream MAP kinases can be fully inhibited by the addition of integrin-inhibitory peptides [70]. Subsequent downstream metabolic events, like the stimulation of bile formation or the inhibition of proteolysis, which are otherwise triggered by hypoosmotic cell swelling, remain inactive in presence of integrin-inhibitory peptides. Studies confirmed that these peptides prevent integrins from binding to tripeptide Arg-Gly-Asp attachment sites (RGD) of extracellular matrix proteins, such as fibronectin, laminin, and collagen [71–73]. This impairment prevents the dynamics of integrin/matrix interactions, which are needed for effective osmosensing and the conversion of mechanical force into biochemical signals, called ‘mechanotransduction’ [74]. Downstream osmosignaling involves the activation of the focal adhesion kinase $p125^{FAK}$ (FAK) [75,76], c-Src, the epidermal growth factor receptor (EGFR), and the mitogen-activated protein kinases Erk (Erk-1 and Erk-2) and $p38^{MAPK}$ [66,77,78], as depicted in Figure 1.2. This signaling pathway mediates RVD and inhibits proteolysis, while $p38^{MAPK}$ activation is required for choleresis [66,79–81]. Cell proliferation has also been shown to correlate with an increase in cell volume [68,82]. Hepatocyte shrinkage, however, leads to an accumulation of reactive oxygen species (ROS) and triggers proapoptotic signaling via a short-term activation of the CD95 death receptor as illustrated in Figure 1.2 [28,51]. In hepatocytes, cell shrinkage induced by hyperosmolarity triggers an increase of the intracellular chloride concentration and a volume-regulatory uptake of K^+, Na^+, Cl^- into the cell [52,83]. Accumulation of chloride ions in the cytosol directly activates the vacuolar H^+-ATPase, which results in an endosomal acidification [84]. This acidification leads to an activation of acidic sphingomyelinase, paralleled by a ceramide formation which increases the activation of NADPH oxidase (NOX) [85]. As a byproduct of NOX activity, ROS were identified to trigger activation of c-Jun N-terminal kinase (JNK) and the Src family kinase members Fyn and Yes [86,87]. This signaling pathway also induces the proapoptotic microRNA family 15/107 [88]. Cholestasis is triggered by hyperosmotic activation of Fyn due to retrieval of the bile salt export pump (Bsep) and multidrug resistance associated protein 2 (Mrp2) from the canalicular membrane [86], while sodium/taurocholate co-transporting polypeptide (NTCP) is recovered from the sinusoidal membrane [87]. The proapoptotic state of the hepatocyte is triggered by the activation of Yes and JNK and downstream CD95 activation [89,90].

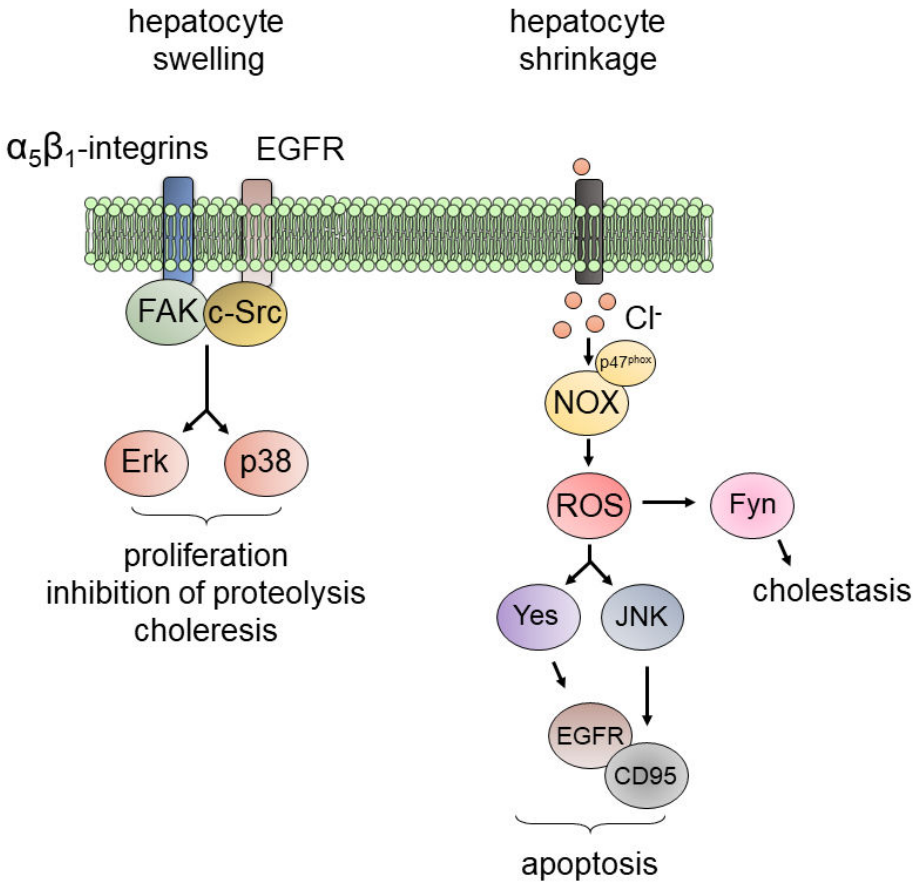

Figure 1.2 Osmosignaling in response to hypoosmotic cell swelling and hyperosmotic cell shrinkage in hepatocytes. (**Left**) Cell swelling in hepatocytes is sensed by transmembrane adhesion receptor $\alpha_5\beta_1$-integrins through a mechanical stimulus. Signaling is transduced via focal adhesion kinase (FAK) and c-Src into $p38^{MAPK}$ activation, which results in proliferation, inhibition of proteolysis and choleresis. (**Right**) Cell shrinkage is accompanied by increase of the intracellular Cl^- ion concentration. Activation of the vacuolar H^+-ATPase triggers a cytosolic acidification, enabling phosphorylation of $p47^{phox}$, a regulatory subunit of NADPH oxidase (NOX). This results in the formation of reactive oxygen species (ROS), which triggers JNK and downstream epithelial growth factor receptor (EGFR) activation. Cell death 95 (CD95) tyrosine phosphorylation by EGFR activates the death-inducing signaling complex leading to apoptosis. (Modified from [91,92]).

1.1.4 Cell swelling and proliferation

Osmotic cell swelling is linked to an accelerated cell proliferation [93], whereas hypertonic shrinkage inhibits cell proliferation [94–97]. In fibroblasts, *Ras* oncogene expression is accompanied by accumulation of intracellular Na^+ ions and export of H^+ ions out of the cell which ultimately leads to an increased cell volume [98–100]. This increase in cell volume is related to fluctuations of intracellular Ca^{2+} ion concentrations [101]. These fluctuations in intracellular Ca^{2+} ion concentration cause a transient shrinkage, due to the activation of Ca^{2+}-sensitive potassium channels [102,103].

However, this process is followed by a sustained increase of cellular volume, due to a depolymerization of actin filaments, since the end of actin filaments are modified by

Ca^{2+}-dependent gelsolin complex [101,104,105]. Na^+/H^+ ion exchange accelerates *Ras* oncogene expression, which in turn initiates cell proliferation [100,106,107]. However, in certain cases, inhibition of the Na^+/H^+ exchanger was not found to impede with cell proliferation, indicating that the activity of ion channels and transporters is not a prerequisite for swelling-induced cell proliferation [108–110]. Erk-1 and Erk-2, are both proteins which are involved in cell cycle regulation and activated by cell swelling [111]. Erk-1 and Erk-2 share a similarity of 84% in their amino acid sequence and also share a functional similarity [112], hence they are usually referred to as Erk-1/2.

1.1.5 Proliferation of hepatocytes in liver regeneration

Adult hepatocytes normally do not undergo cell division but still maintain the ability to proliferate in response injuries or infections. Removal of two thirds of the liver results in the enlargement of the remaining liver until the original liver mass is restored as shown by Higgins and Anderson in 1931 [113]. However, the word ‘regeneration’ can be falsely interpreted, since the severed liver lobes do not grow back, but instead are replaced in a hyperplastic response by the remaining liver cells. Once the original mass of the liver, adjusted and determined by the demands of the organism, is restored, proliferation stops. The three phases of liver regeneration consist of: priming stage, proliferative phase, and termination phase. In rats which were subjected to partial hepatectomy (PHx), the rate of DNA synthesis in hepatocytes is increased after 12 h and peaks around 24 h [114]. During this time point, hepatocytes enter the S phase of the cell cycle, whereas Kupffer and biliary epithelial cells start at around 48 h after PHx. The biggest part of the increase in liver mass occurs 3 days after PHx and is completed after 5 to 7 days [115]. During liver regeneration, liver cells endure both compression and stretching, whereas cell division is accompanied by cell swelling [91,92]. These processes and signal mediations also share the same pathway which are triggered by activation of $\alpha_5\beta_1$-integrins [69,91,116].

1.1.6 Cell hydration affects gene expression

Cell swelling and shrinkage influence the expression of a broad range of genes. In hepatocytes subjected to hypoosmolarity, genes which are relevant for cell structure like *tubulin* (*Tubb*) and *β-actin* (*Actb*) are upregulated, whereas the *tumor necrosis factor* (*TNF-α*) is downregulated [117–119]. The involvement of genes which participate in the structural integrity of cells, point towards an involvement of the cytoskeleton in the molecular response to cellular hydration [120]. A variety of genes encoding for heat shock proteins, that serve to stabilize other proteins and that counteract the effects of increased extracellular salt concentrations, are upregulated under cell shrinkage, e.g. genes encoding for *heat-shock protein 70* (*Hsp70*) and *heat-shock transcription factor 1* (*Hsf1*) [121–123].

1.1.7 Metabolic pathways affected by cell volume

Hormones can serve as mediators, which trigger volume regulatory mechanisms to exert their sustained effects on cellular metabolism. For example, insulin and glucagon can impact the cellular volume, thereby influence cell metabolism. Insulin has a direct effect on liver cell volume and triggers a variety of metabolic functions, i.e. protein and glycogen synthesis, while protein and glycogen degradation are inhibited [15,66,78]. In perfused rat livers, insulin-induced cell swelling can be counteracted by the addition of glucagon. As a major hormonal regulator of glucose metabolism, glucagon decreases cellular K^+, Na^+, and Cl^- ion concentrations by opening responsible ion channels and, thus, leading to cell shrinkage [124,125]. However, glucagon and other Ca^{2+}-mobilizing hormones also act as modulators of mitochondrial matrix volume, whereas cytosolic and mitochondrial water spaces are inversely affected. For example, liver cells exposed to glucagon undergo cell shrinkage but simultaneously have swollen mitochondria [126].

Nutrients were also shown to impact cellular hydration state, resulting in the alteration of protein, glycogen, and lipid metabolism. For instance, addition of glutamine and glycine to rat liver perfusion media resulted in cell swelling to the same extent as under the influence of hypotonic media, whereas both conditions resulted in an inhibition of proteolysis [16]. Other amino acids, e.g. phenylalanine, proline, alanine, and serine also exert an anti-proteolytic effect which is accompanied by cell swelling [127–129]. For example, in rat hepatocytes uptake of L-alanine occurs through a secondary active transport system coupled with Na^+ ions [130]. Cellular accumulation of the Na^+ ions and alanine concentrations result in an osmotic driving force which causes cell swelling [131]. However, macromolecular synthesis and breakdown are not the only processes that are affected by the alteration of cell volume. In hepatocytes, the information on metabolic effects, which originated by modifications of cellular volume, have also been studied extensively [132–135].

1.1.8 Effect of cellular hydration on bile acid secretion

Several cellular functions, such as bile acid secretion, are controlled by the hepatocellular hydration state. Conjugated bile acids are transported across the canalicular membrane by Na^+-dependent transporters (e.g. sodium-dependent bile salt transporter (Asbt, Slc10a2)) [136,137]. The canalicular excretion is predominantly accomplished by an ATP-dependent transport system and is thought to be the overall rate-controlling step for transcellular bile acid transport. In perfused rat livers, the rate of transcellular taurocholate transport critically dependents on the hydration state of the hepatocyte [138,139]. Regardless of whether cellular volume is altered by ambient osmolarity or influenced by amino acid uptake, taurocholate excretion is inhibited by cell shrinkage but stimulated by cell swelling [138]. Here, an increase

of the hepatocellular hydration of 10% roughly doubles the bile salt excretory capacity within minutes [140]. However, this increase is not tied to changes in cellular ATP content, but can be extinguished in the presence of colchicine which induces the disassembly of α-tubulin [24]. This effect ultimately leads to the depolymerization of the microtubule network. This points towards a requirement for intact microtubules and suggests that the microtubule network is required for the interaction between cellular hydration and taurocholate excretion into bile and can be disrupted by colchicine [31,51,141]. Rapid changes in taurocholate secretion can be partially explained by a microtubule-dependent insertion or retrieval of canalicular bile acid molecules into or from the canalicular membrane [31,136,138,141].

1.2 The discovery of microRNAs

As a revolutionary discovery in the field of molecular biology, the first microRNA (miRNA) lin-4 was discovered in 1993 in *Caenorhabditis elegans* by the groups of Ambros and Ruvkun [142,143]. Several years earlier, *lin-4* gene was already characterized by the Horvitz's lab, where they discovered *lin-4* as one of the genes that regulate temporal development of *C. elegans* larvae [144]. In 1987, Horvitz's lab discovered a mutation in *lin-4*, that had an opposite phenotype to a mutation in another gene, called *lin-14* [145,146]. Ambros and Ruvkun later discovered that lin-4 is not a protein-coding RNA, but rather a small so called 'non-coding RNA' [147,148]. It was discovered that *lin-14* is downregulated post-transcriptionally through its 3' untranslated region (UTR) and that lin-4 has a complementary sequence to that of the 3'UTR of *lin-14* mRNA [149]. It was then proposed that *lin-14* is regulated by lin-4 at the post-transcriptional level [150]. Since then, new miRNAs are still being discovered [151] and have been detected in nearly all animal model systems, while some were also shown to be highly conserved across species [152–154]. Being recognized as regulators of gene expression, miRNAs are short non-coding RNAs, with roughly 22 nucleotides in length. miRNAs are transcribed from DNA sequences into primary miRNAs transcripts (pri-miRNAs), are then processed into precursor miRNAs (pre-miRNAs), and finally into mature miRNAs. In most cases, interaction with the 3'UTR of target mRNAs is established and results in a post-transcriptionally suppressed mRNA [155]. It has also been reported, that interaction of miRNAs occur with other regions, including the 5'UTR, coding sequence and even with gene promoters [156]. Under certain conditions, miRNAs were also shown to activate gene expression [157]. Furthermore, recent studies have suggested that miRNAs are conveyed between different subcellular compartments to control the rate of translation and even transcription [158]. Many studies also detected extracellular miRNAs in biological fluids such as plasma/serum [159,160], cerebrospinal fluid [161], saliva [162], and breast milk [163]. However, the exact functions of extracellular miRNAs are still awaiting further analyses.

1.2.1 Biogenesis of miRNAs

The miRNA biogenesis starts with the synthesis of the transcripts by RNA polymerase II or III [164]. Depending on their genomic position, miRNAs can be classified into intragenic and intergenic miRNAs [165,166]. For example, intragenic miRNAs, embedded within exons or introns of protein coding genes on the same strand, are believed to be co-regulated with their host genes by RNA polymerase II. Intergenic miRNAs, which are located between genes, have their own RNA polymerase II or III promoters. However, recent studies revealed that intragenic and even intronic miRNAs are not always co-transcribed with their host genes [167,168]. Some miRNAs are also co-transcribed from a single, long transcript, called clusters. These clusters may have similar 'seed regions' (between nucleotides 2-8 from the miRNA 5'-end), and in this case they are considered as a family [169].

1.2.2 The canonical pathway

The canonical pathway, as illustrated in Figure 1.3, is the dominant pathway by which miRNAs are processed. The pri-miRNAs are processed into pre-miRNAs by the microprocessor complex. Main components of the microprocessor complex consist of an RNA binding protein DiGeorge Syndrome Critical Region 8 (DGCR8) and a ribonuclease III enzyme, Drosha [170]. DGCR8 is responsible for the recognition of N6-methyladenylated GGAC and other motifs within the pri-miRNA [171], while the pri-miRNA duplex is cleaved by Drosha at the base of the unpaired RNA loop, a secondary structure which constitutes a hairpin [172]. This cleavage results in a 2-nucleotide overhang at the 3'-end of the pre-miRNA which is necessary for the binding to the nuclear transporter protein exportin-5 (XPO5)/RanGTP complex. Once the pre-miRNA is exported out of the nucleus, it is processed by the RNAse III endonuclease Dicer in the cytoplasm [170,173,174]. During this process the terminal loop is removed, resulting in a mature miRNA duplex [175]. Depending on the orientation of the mature miRNA strand relative to the position within the pri-miRNA transcript, the name of the mature miRNA is determined. The 5p strand is located near the 5' end of the pri-miRNA hairpin and the 3p strand near the 3' end. Both strands can be recruited into the Argonaute (AGO) family of proteins, which requires the assistance of heat shock proteins such as HSP90 or HSP70, in an ATP-dependent manner [176,177]. The mechanisms behind the selection of the mature miRNA is different among AGO proteins, while the strand which is loaded into AGO is referred to as the 'guide strand'. The unloaded strand, which is called the 'passenger strand', is unwound. AGO2 may cleave passenger strands of miRNAs which contain no mismatches to the guide strands and initiate the degradation of the passenger strand by the cellular machinery. miRNA duplexes with central mismatches or non-AGO2 loaded miRNAs may be unwound and further degraded [164].

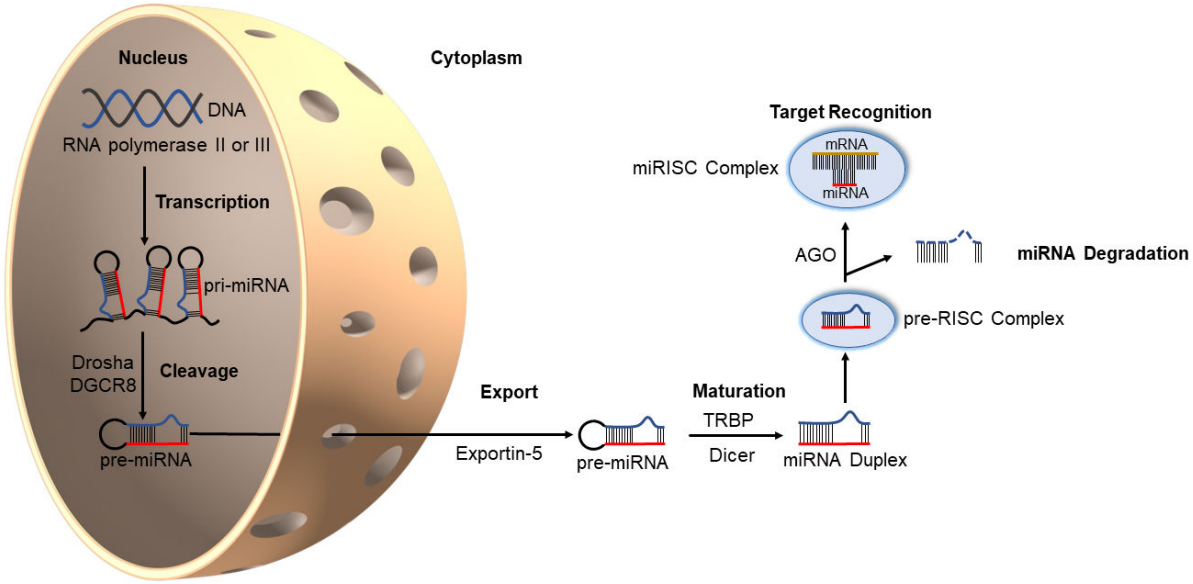

Figure 1.3 MicroRNA biogenesis and mechanisms of action. Canonical miRNA biogenesis starts with the pri-miRNA transcription by RNA polyemrase II or III. The microprocessor complex, consisting of Drosha and DGCR8 produces the precursor-miRNA (pre-miRNA) by cleaving the stem sequence of the pri-miRNA. The pre-miRNA is then exported into the cytoplasm via exportin-5 and processed by the RNase Dicer to produce the mature miRNA duplex. Afterwards, the 5p or 3p strands of the mature miRNA duplex may be loaded into Argonaute (AGO) family proteins to form the miRNA-induced silencing complex (miRISC).

1.3 miRNA-mediated gene silencing

The guide strand of the mature miRNA and AGO proteins form the minimal miRNA-induced silencing complex (miRISC) [178]. Due to its interaction with the complementary sequences on target mRNA, the target specificity of miRISC is determined. The target site on the mRNA which is recognized by the miRNA is called miRNA response elements (MREs). In most cases, a functional miRNA-MRE interaction is established by formation of hydrogen bound between the 5' sequence of the miRNA, the so called 'seed region' (between nucleotides 2-8) and the mRNA [179,180]. Aiding the stability, additional paring at the 3'-end of the miRNA increase the binding capacity of the miRNA target interaction [156]. Depending on the degree of MRE complementarity to the miRNA, a miRISC-mediated translational inhibition with further target mRNA decay or an AGO2-dependent slicing of target mRNA is determined [181]. Target mRNA cleavage is induced by AGO2 endonuclease activity when a nearly complementary miRNA-MRE interaction is present [181]. The remaining fragments are bound to be further degraded by exosomes, a multi-protein complex, or by the activity of 5'-to-3' exonucleases, e.g. XRN4 [182,183]. In animal cells, a multitude of not fully complementary miRNA-MRE interactions were discovered [184]. Usually, the majority of MREs contain central mismatches to their guide miRNA, preventing AGO2 endonuclease activity, but enable the binding of other AGO proteins, e.g. AGO1, AGO3, AGO4 [185]. Here, the formation of the silencing miRISC

complex is followed by the recruitment of the GW182 family of proteins at the GW182 C-terminal region [186]. GW182 contains multiple glycine-tryptophan (GW)-repeats [187,188] and provides the framework needed for the recruitment of other effector proteins [189], including the poly(A)-deadenylase complexes PAN2-PAN3 and CCR4-NOT [190]. The target mRNA poly(A)-deadenylation is initiated by PAN2-PAN3 and finished by the CCR4-NOT complex. Efficient deadenylation is supported by the interaction between the tryptophan (W)-repeats of GW182 and poly(A)-binding protein C (PABPC) [184]. Decapping proteins such as decapping protein 2 (DCP2) are responsible for the removal of the mRNA cap structure [189], followed by an 5' - 3' degradation by exoribonuclease 1 (XRN1) [191].

1.3.1 Translational activation mediated by miRNAs

While most studies are focussing on the inhibitory effects of miRNAs on their targets, recently, few studies reported that miRNAs may up-regulate the level of target mRNAs under certain circumstances. AGO2 and other proteins related to the miRNA-protein complex (microRNPs) were found to be associated with AU-rich elements (AREs) at 3'UTR, resulting in an enhanced translation [192]. For instance, let-7 and several other miRNAs were associated with AGO2 and Fragile-x-mental retardation related protein 1 (FXR1) to activate translation during cell cycle arrest, but also found to inhibit translational process in proliferating cells [192]. These effects were also observed in quiescent cells such as oocytes [193,194]. Here, translational activation by miRNAs is mediated by AGO2 and FXR1 as cofactor instead of GW182 [193]. During amino acid starvation, it was observed that miRNAs bind to the 5'UTR of mRNAs encoding for ribosomal proteins [195], suggesting that under specific conditions miRNAs are able to mediate translational upregulation.

1.4 miRNAs in cellular compartments

Multiple subcellular compartments have been identified to harbor miRISC and target mRNA, including rough endoplasmic reticulum (rER) [196], the trans-Golgi network (TGN) [197], stress granules (SG) [198], processing (P)-bodies [199], early/late endosomes [197], multivesicular bodies (MVB) [200], lysosomes [200], mitochondria [201,202], and the nucleus [203,204]. Depending on the localization of miRISC-mRNA complexes, cofactors that facilitate miRNA-mediated target regulation are accumulated. These effects result in a spatial enrichment of mRNA and miRISC concentrations promoting efficient post-transcriptional regulation [196]. Early on, P-bodies were identified as possible sites for messenger ribonucleoproteins (mRNP), containing mRNAs which were involved in miRNA-mediated suppressive activity [205]. As cytoplasmic foci, they are depleted of ribosomes [205] and accumulated with components of the enzymatic mRNA degradation machinery, e.g. mRNA decapping proteins, the CCR4-NOT complex, XRN1 and GW182 family proteins [206]. Recent

studies observed that P-bodies enriched with active miRISC are associated with SYNE1 (nesprin-1) which helps binding Argonaute and other P-bodies components to microtubules [207]. Mutation or interference through small interfering RNA (siRNA) of nesprin-1, leads to disruption and significant decrease of miRNA suppression of target mRNA and P-body formation. Whereas, stabilization of microtubules through Taxol leads to translational inhibition of *hypoxia inducible factor 1 subunit alpha* (*HIF1A*) mRNA with no mRNA decay, followed by an accumulation of P-bodies [208]. It is still unknown to which degree P-bodies are necessary for efficient miRNA-mediated suppression as mRNA degradation machinery exists diffusely throughout the cytoplasm. It was also discovered that formations of miRISC fuse with polysomes, which are complexes of mRNA with multiple translating ribosomes. These miRISC-polysome formations are found heterogeneously distributed in the cytoplasm or bound to the cytoskeleton [209]. A recent study showed that miRISC formations may be bound to membranous subcellular organelles, such as the rER [196]. The same group also reported that rER-bound mRNA, destined for miRNA-dependent degradation, is processed by deadenylation and degradation inside of endosomes and later may be recycled back into the cytoplasm by miRISC [197].

1.5 Involvement of microRNAs in osmosensing and osmosignaling

Several studies showed that miRNAs also play a role in the modulation of the response to alterations of cellular hydration. Santosa *et al.* demonstrated that miR-15a, miR-15b, and miR-16 levels were significantly upregulated in hyperosmotic perfused rat livers [88]. Known as tumor suppressor miRNAs, miR-15a, miR-15b, and miR-16 are members of the miR-15/107 family and serve key functions for repressing the expression of genes which are involved in cell division and metabolism [210]. Interestingly, miR-15a, miR-15b, and miR-16 are anticipated to regulate apoptosis by the inhibition of the anti-apoptotic genes *Bcl2 apoptosis regulator* (*Bcl2*) and *cyclin D1* (*Ccnd1*), as their interaction between the 3'UTRs of both *Bcl2* and *Ccnd1* was already confirmed in rat, mouse, and human [211–213]. These data underline the effects of hyperosmolarity in hepatocytes, which are known to induce a ligand-independent CD95 death receptor activation, ultimately leading to apoptosis [90,214,215]. Furthermore, it was shown that miRNAs play a role in the maintenance of osmotic homeostasis by participating in the regulation of osmotic stress in zebrafish [216]. Flynt *et al.* demonstrated that miR-8 family miRNAs modulate the expression of *solute carrier family 9 member A3* (*Slc9a3*) mRNA, which regulates Na^+/H^+ ion exchange activity [217]. Additionally, miR-666 and miR-708, two miRNAs induced by hyperosmolarity, were identified to regulate the expression of aquaporin-1 expression in mice [218]. As identified by Zhao *et al.*, high salinity induced miR-196g and miR-196o levels which transiently inhibited *nuclear transcription factor Y subunit alpha*

(*NF-YA*). Altogether, these data indicate that miRNAs can act as a crucial stress response and enable a sensitive control of gene expression which is caused by environmental changes in osmolarity.

1.6 Aim of the thesis

The present study was performed to gain further insight on hepatic miRNAs and to clarify their potential physiological role in liver homeostasis, tissue development, and regeneration. For this purpose, the role and involvement of miRNAs and their potential target gene candidates were investigated in perfused rat livers under hypoosmotic conditions to further elucidate the participation of miRNAs in osmosensing and osmosignaling. Previously, it was shown that hyperosmotic exposure leads to an upregulation of members of the proapoptotic miR-15/107 family and subsequently to a downregulation of anti-apoptotic genes in perfused rat liver [88]. Therefore, for this study hypoosmotic perfused rat livers were investigated via Affymetrix gene chip analysis. Genome-wide transcriptomic data sets were screened for dysregulated mRNAs and based on these results, target prediction analysis was conducted to identify potential upstream miRNA regulators. Potential interaction of miRNAs with mRNAs, for which binding motifs on dysregulated mRNAs could be identified, were validated by qPCR. Selected mRNAs were further evaluated by stimulation experiments using isolated primary rat hepatocytes transfected with specific miRNA mimic to test the responsiveness of mRNAs to miRNA overexpression. To address the involvement of miRNAs in the osmosignaling cascade, inhibitor studies were performed. Altogether this thesis aimed to provide new insights into the role of miRNAs and their target mRNAs in osmosignaling under hypoosmotic exposure to the liver.

2. Materials and Methods

In the following sections the materials and methods used for the experiments presented in this thesis are listed and explained. Reagents and chemicals that were used in the work for this thesis are listed in the following sections, e.g. enzymes (Table 2.1.1), miRNA mimics and transfection reagents (Table 2.1.2), cell culture media and supplements (Table 2.1.4), bacteria and plasmids (Table 2.1.6). Standard laboratory chemicals were purchased from the companies Carl Roth (Karlsruhe, Germany), Thermo Fisher Scientific (Schwerte, Germany), Merck (Darmstadt, Germany), Biomol (Hamburg, Germany), or J.T. Baker (Deventer, Netherlands), unless otherwise stated. Cell culture dishes were obtained from Eppendorf (Hamburg, Germany) or Thermo Fisher Scientific (Schwerte, Germany). Sequences for primer used in qPCR and molecular cloning are given in Table 2.1.8, Table 2.1.9 and Table 2.1.10.

2.1 Materials

Table 2.1.1 Enzymes for PCR, cDNA synthesis and cloning

Takyon™ qPCR Mastermix blue	UF-NSMT-B0710	Kaneka Eurogentec S.A., Seraing, Belgium
NheI-HF®	R3142S	New England BioLabs GmbH, Frankfurt a.M., Germany
SacI-HF®	R3156S	New England BioLabs GmbH, Frankfurt a.M., Germany
Primescript™ Reverse Transcriptase	2680B	Takara Bio Europe S.A.S, Saint-Germain-en-Laye, France
Recombinant RNasin® – RNase Inhibitor	N2515	Promega GmbH, Mannheim, Germany
T4 RNA Ligase, truncated K227Q	M0351L	New England BioLabs GmbH, Frankfurt a.M., Germany
0.05% Trypsin/ 0.02% EDTA (Invitrogen)	25300054	Thermo Fisher Scientific Inc, Schwerte, Germany

Table 2.1.2 Transfection reagents and miRNA mimics

Ambion pre-miR™-141 miRNA precursor	MC10860 miR-141-3p mimic	Thermo Fisher Scientific Inc, Schwerte, Germany
Lipofectamin™ RNAiMax	13778-150	Thermo Fisher Scientific Inc, Schwerte, Germany
Lipofectamin™ 3000	L3000008	Thermo Fisher Scientific Inc, Schwerte, Germany

Table 2.1.3 Molecular biology kits

Dual-Luciferase© Reporter Assay	E1960	Promega GmbH, Mannheim, Germany
Fast-n-Easy Plasmid Mini-Prep Kit	PP-204L	Jena Bioscience GmbH, Jena, Germany
In-Fusion HD Cloning Plus for seamless DNA cloning	638910	Takara Bio Europe S.A.S, Saint-Germain-en-Laye, France
QIAgen miRNeasy Kit	217004	Qiagen GmbH, Hilden, Germany
QIAgen Plasmid Midi Kit	12145	Qiagen GmbH, Hilden, Germany
QIAquick Gel Extraction Kit	28704	Qiagen GmbH, Hilden, Germany
QIAquick PCR Purification Kit	28104	Qiagen GmbH, Hilden, Germany

Table 2.1.4 Cell lines, media, and supplements

Cell lines:		
Human embryonic kidney 293 cell (HEK293)		Provided by Prof. Dr. Verena Keitel (Clinic of Gastroenterology, Hepatology and Infectious Diseases, Düsseldorf, Germany). Purchased from ATCC (CRL-1573™).
Media and supplements:		
Dexamethasone	D8893	Sigma-Aldrich Chemie GmbH, Taufkirchen, Germany
DMEM (w/o sodium chloride)	41966029	Thermo Fisher Scientific Inc, Schwerte, Germany
DMEM/ Ham's F-12	31331093	Thermo Fisher Scientific Inc, Schwerte, Germany
Fetal calf serum (FCS)	S0615	Sigma-Aldrich Chemie GmbH, Taufkirchen, Germany
L-Glutamine solution	59202C	Sigma-Aldrich Chemie GmbH, Taufkirchen, Germany
Insulin solution (human)	I9278	Sigma-Aldrich Chemie GmbH, Taufkirchen, Germany
Penicillin-Streptomycin	15140122	Thermo Fisher Scientific Inc, Schwerte, Germany
William's Medium E	F1115	Biochrom GmbH, Berlin, Germany
Opti-MEM™	31985062	Thermo Fisher Scientific Inc, Schwerte, Germany

Table 2.1.5 Inhibitors and supplements for liver perfusion experiments

Colchicine	C-9754	Sigma-Aldrich Chemie GmbH, Taufkirchen, Germany
PD098059	513000	Merck, Darmstadt, Germany
PD169316	SC-204168B	Santa Cruz Biotechnology, Dallas, USA
PP-2	529576	Merck, Darmstadt, Germany
Heparin	A11726	AdooQ Bioscience, Irvine, USA
Rompun® (2%)	Zu.-Nr. # 6293841.00.00	Bayer AG, Leverkusen, Germany
Ketavet® (100 mg/mL)	Zu.-Nr. # 6187926.00.00	Pfizer Pharma GmbH, Berlin, Germany

Table 2.1.6 Bacteria and plasmids

Stellar™ Competent Cells (provided with In-Fusion HD Cloning Kit)	638920	Takara Bio Europe S.A.S, Saint-Germain-en-Laye, France
pGL3 Promoter Vector	E1751	Promega GmbH, Mannheim, Germany
pRL-SV40	E2231	Promega GmbH, Mannheim, Germany

Table 2.1.7 Media, buffer, and solutions

Krebs-Henseleit buffer (Perfusion medium)	115 mM NaCl 25 mM $NaHCO_3$ 5.90 mM KCl 1.18 mM $MgCl_2$ 1.23 mM NaH_2PO_4 1.20 mM Na_2SO_4 1.25 mM $CaCl_2$ 0.30 mM Pyruvate 2.10 mM Lactate
William's E Medium (Biochrom, Berlin, Germany)	**supplemented with:** 5 mM L-Glutamine 100 U/ml Penicillin 0.1 mg/ml Streptomycin 100 nM Dexamethasone 100 nM Insulin 10 % FCS
Collagenase solution	Perfusion medium 1.0 mg/ml Bovine serum albumin 0.2 mg/ml Collagenase 1.5 mM $CaCl_2$

Table 2.1.8 Oligonucleotide sequences for miRNA profiling using miQPCR

miRNA Primer	Primer	Sequence 5' – 3'
rno-miR-141-3p	Forward	acactgtctggtaaagatggg
Upm2A	Reverse	cccagttatggccgttta

2.1.9 Primers for quantitative *real-time* PCR

Table 2.1.9 Oligonucleotide sequences of qPCR primers for rat mRNA

mRNA Primer	Primer	Sequence 5' – 3'
Camsap1	Forward	tgggtcagcagagtgaaaga
	Reverse	caaaaagaaatgtgcaaaactacg
Cdc25a	Forward	ggatgatggcttcatagacctt
	Reverse	ggggtctcctcatcattcttc
Cdk8	Forward	gctcatcatgacctccgact
	Reverse	tgtgtctgatgtgagtactgtgga
Dmxl1	Forward	gaggctttggcagtacttgg
	Reverse	ccaggatatcccagatctgact
Dstyk	Forward	caaatcctgcatccgacag
	Reverse	gccactgcctggttaagtct
Duoxa2	Forward	ggctggagggcgttaatatc
	Reverse	ttgtagtcaatggtctcgttcag
Eml4	Forward	gcagacaccagttcaaccaa
	Reverse	gttacacagcctggcgtttt
Gucy2c	Forward	accacagactccctaatgacg
	Reverse	aagacggcaatcatcagga
Luc7l3	Forward	aattgctaagatctacaacctcgac
	Reverse	aaaagctccgcacacttcac
Msantd2	Forward	tgccagtttcaaagagaacg
	Reverse	caatattctgcatggtgtctcg
Nags	Forward	tcgatctatgtctctgaggggta
	Reverse	cggctggagctcactacaa
Prmt1	Forward	tgtcaaagccaataagttagacca
	Reverse	tgatgtccaccttctccaca
Rab30	Forward	cctagtccgacgattcactca
	Reverse	gggtgatggagcgaaatct
Rps6	Forward	ggaagcgcaagtctgtccga
	Reverse	aggtcccaaccgacgaggca
Scnn1a	Forward	actgtctgcacccttaatcctt
	Reverse	gtgatgcggtccagctct
Slc39a10	Forward	catcatcgagcactgcatcc
	Reverse	cttgagttgcagccagtcag
Tfeb	Forward	ccgaaatgcagatgcctaa
	Reverse	gggtcaccactgtacacgttc
Timp1	Forward	cagcaaaaggccttcgtaaa
	Reverse	tggctgaacagggaaacact
Zmpste24	Forward	ttcagcttctggtcaggactc
	Reverse	cagagtgggttggctgtcat

2.1.10 Primer sequences for molecular cloning

Oligonucleotide sequences include recognition sequences for restriction enzymes and were cloned using the In-Fusion recombinase system, which require a sequence homology between the insert and the vector (blue font).

Table 2.1.10 Oligonucleotide sequences for cloning miR-141-3p target gene 3'UTRs

Amplified sequence	Primer	Sequence 5' – 3'
miR-141-3p (original sense) binding-site	Forward	aatcgataggtaccgccatctttaccagacagtgttactagcccgggctcga
	Reverse	tcgagcccgggctagtaacactgtctggtaaagatggcggtacctatcgatt
miR-141-3p (antisense) binding-site	Forward	aatcgataggtaccgtaacactgtctggtaaagatggctagcccgggctcga
	Reverse	tcgagcccgggctagccatctttaccagacagtgttacggtacctatcgatt
Cdk8 (original sense) 3'UTR	Forward	aatcgataggtaccggctgtgctggagtctgtc
	Reverse	tcgagcccgggctagattcagaatacttgtgtcattcatg
Cdk8 (antisense) 3'UTR	Forward	aatcgataggtaccgattcagaatacttgtgtcattcatg
	Reverse	tcgagcccgggctaggctgtgctggagtctgtc

2.2 Methods

2.2.1 Animal models

This study and all experimental protocols were approved by the local authorities and the methods were carried out in accordance with the guidelines of the Institutional Animal Care and Use Committee of the University Hospital Düsseldorf. Techniques that involve living animals were approved by local officials (LANUV, Landesamt für Natur, Umwelt- und Verbraucherschutz, Recklinghausen, Nordrhein-Westfalen, AZ 84-02.04.2015.A287 and AZ 9.93.2.10.34.07.163) and all animals received care according to the German animal welfare act by indicated persons (see below).

2.2.2 Rat liver perfusion

Male Wistar rats with a body weight of 160 -180 g were anesthetized with 0.1 mL xylazin (Rompun® - 2%) and 0.4 mL ketamine (Ketavet® - 100 mg/mL) by intraperitoneal injection. A dose of 50 U of heparin was injected intravenously in the femoral vein of the hind leg to prevent clotting during the preparation. The vena cava inferior, the hepatic portal vein and the splenic vein were fixed by loose ligatures and a small incision was made, roughly the size at one third of the portal vein was made with microscissors, to insert a small cannula. After insertion of the cannula, the loose ligatures were tied up and the liver was flushed by perfusion medium (Table 2.1.7) with an estimated flow rate of 4 mL/min per g liver weight. To prevent the liver from overflow-induced swelling the abdominal aorta and vena cava were cut through to create a

drainage via the suprahepatic inferior caval vein right below the ligature, while the ligature of the intrahepatic vena cava inferior was closed tightly. A cannula was placed into the suprahepatic part of the vena cava via the right atrium, so the flow was drained via the suprahepatic inferior caval vein. After preparation of the liver, the system was preperfused for an initial 20 min with perfusion medium. Afterwards, the perfusion medium was either continued with normoosmotic (305 mosm/L) medium or replaced by hypoosmotic perfusion medium (225 mosm/L). Hypoosmotic perfusion medium was prepared by lowering the NaCl concentration of the Krebs-Henseleit buffer to 75 mM. For inhibitor studies, addition of inhibitors to the influent perfusate was performed by dissolution of the compounds in Krebs-Henseleit buffer. Following the preperfusion, normoosmotic medium or hypoosmotic medium was supplemented with 500 nM PD098059 (Calbiochem, Darmstadt, Germany), 250 nM PP-2 (Calbiochem, Darmstadt, Germany), 250 nM PD169316 (Santa Cruz Biotechnology, Heidelberg, Germany) or 500 nM colchicine (Thermo Fisher Scientific, Darmstadt, Germany), respectively. Over a time course of up to 180 min, liver tissue was dissected in a fractionated manner and snap frozen in liquid nitrogen.

2.2.3 RNA isolation from rat liver tissue and cells

Total RNA from liver tissue and primary rat hepatocytes was isolated by phenol/chloroform extraction, followed by spin column clean up. For this purpose, snap frozen liver tissue was mortarized and lysed by addition of 1 mL Qiazol Lysis Reagent (79306, Qiagen) for 3 min by constant vortexing. For RNA isolation from cultured primary rat hepatocytes, cells were washed and rinsed with PBS (Pan Biotech) and exposed to 800 µL of Qiazol Lysis Reagent for 3 min. Afterwards, 600 µL of Qiazol was transferred into clean reaction tubes. To separate and extract the RNA from protein and genomic DNA 200 µL of chloroform were added. Following a short vortex procedure, the samples were centrifuged at 10.000 g for 10 min at 4 °C. Afterwards, the aqueous phase containing the RNA was separated and transferred into clean reaction tubes. By adding 1.5x volumes of 100% ethanol the RNA was precipitated, and RNA purification was performed using the miRNeasy Mini Kit (Qiagen, Hilden, Germany) according to the manufacturer's instructions. The RNA amounts and quality were measured photometrically by using the DropSense16 spectrometer (Trinean, Gentbrugge, Belgium).

2.2.4 mRNA and miRNA expression analysis by microarray

The extracted and purified RNA samples from rat liver perfusion tissue were sent to the Biologisch-Medizinisches Forschungszentrum (BMFZ) of the Heinrich Heine University in Düsseldorf for transcriptome analysis by gene expression microarray (Affymetrix Rat GeneChip 1.0 ST) and miRNA expression microarray (Rat GeneChip™ miRNA 4.0 Array and Flashtag™ Biotin HSR Labeling, Thermo Fisher Scientific). For this purpose, RNA samples

from normoosmotic and hypoosmotic condition of time points t= 0' and t= 180' were prepared from 4 independent experiments. The array data were processed by *Transcriptome Analysis Console 4.0* (Thermo Fisher Scientific).

2.2.5 Cell isolation and culture

Primary rat hepatocytes were kindly isolated by Vanessa Herbertz and Nicole Eichhorst. For this, male Wistar rats with a body weight of approximately 200 g were used for isolation of hepatocytes by utilizing a collagenase perfusion technique in an adapted version as described by Meijer *et al.* [219]. Isolated rat hepatocytes were plated on collagen-coated culture plates (Falcon, New York, USA) and maintained in an atmosphere of 5% CO_2 at 37 °C in Krebs-Henseleit medium (Table 2.1.7) supplemented with 6 mM glucose for 4 h. After the initial incubation, medium was removed, and cells were washed with PBS (Pan Biotech) and cultured in William's E Medium supplemented with 5 mM L-glutamine, 100 U/mL penicillin, 0.1 mg/mL streptomycin, 100 nM dexamethasone, 100 nM insulin, and 10% FCS (Table 2.1.7) for 24 h. Normoosmotic (305 mosm/L) and hypoosmotic cell culture media (225 mosm/L) were generated by addition of raffinose to NaCl-free Williams's E culturing media (Table 2.1.7). The adjusted osmolarity was verified using an Osmomat 3000 (Gonotec, Berlin, Germany). Primary rat hepatocytes were either treated with normoosmotic or hypoosmotic medium for 30 min up to 24 h.

Cell swelling was verified microscopically after 5 min and 3 h of hypoosmotic exposure. For this purpose, cell nucleus diameters of isolated primary hepatocytes were measured and analyzed using the software tools of *cellSens Dimensions* (version 1.16, Olympus, Tokyo, Japan). Images were acquired using an Olympus IX 50 microscope equipped with a DP71 camera (Olympus, Tokyo, Japan). For RNA isolation, cells were treated as described in section 2.2.3.

Human embryonic kidney 293 (HEK293) cells were generously provided by Prof. Dr. Verena Keitel (Clinic of Gastroenterology, Hepatology and Infectious Diseases, Düsseldorf, Germany). Primary rat hepatocytes were cultured in William's Medium E (Table 2.1.7), while HEK293 were maintained in Dulbecco's Modified Eagle Medium (DMEM) supplemented with 10% (v/v) FCS, respectively. HEK293 cell line was grown in sterile T75 cell culture flasks (Cellstar®, Greiner Bio-One GmbH), while primary rat hepatocytes were plated on collagen-coated culture plates at 37 °C in a humidified atmosphere containing 5% CO_2.

2.2.6 Overexpression of miR-141-3p in primary rat hepatocytes

Hepatocytes were isolated from male Wistar rats as described in section 2.2.5. Primary rat hepatocytes were transfected with miR-141-3p mimic (Ambion pre-miR™-141-3p miRNA

precursor, Thermo Fisher Scientific) using the transfection reagent Lipofectamin™ RNAiMAX (Thermo Fisher Scientific). At approximately 80% confluency, cells were transfected according to the manufacturer's instructions. Cells were washed and rinsed with PBS (Pan Biotech) and kept in 5 mL FCS-free cell culture medium. Transfection was performed with 25 pmoles miR-141-3p mimic per well. The miRNA mimic was diluted in 125 µL OPTI-MEM. The transfection reagent (7.5 µL per well) was first diluted in 125 µL OPTI-MEM and then transferred to the diluted miRNA mimic. After an incubation time of 5 min at room temperature (RT), 250 µL transfection solution were pipetted dropwise on top of the cells. Five hours after the transfection, cell culture medium was replaced by fresh DMEM/ Ham's F-12 containing FCS and cells were harvested 24 or 48 h post transfection. The RNA was isolated as described in section 2.2.3.

2.2.7 Partial liver hepatectomy

A surgical removal of the median and left lateral liver lobe (about 70% of the liver) was conducted with 8 - 10 weeks old male Wistar rats, weighing approximately 250 g body weight, as described by Higgins *et al.* [113]. Samples were collected for two weeks during regeneration. The animals were sacrificed and liver tissue samples were taken in a fractionated manner after the livers had been perfused with physiologic buffer as described by Kordes *et al*. [220]. RNA isolation, qPCR and miQPCR were performed (n=3-6 per indicated time point). The animal experiments were approved by the Landesamt für Natur, Umwelt und Verbraucherschutz (Recklinghausen, Germany; AZ 9.93.2.10.34.07.163) and carried out by Dr. Claus Kordes and Dr. Iris Sawitza (Clinic of Gastroenterology, Hepatology and Infectious Diseases, Heinrich Heine University Düsseldorf).

2.2.8 Mechanical stimulation of isolated primary rat hepatocytes

Freshly isolated primary rat hepatocytes (Section 2.2.5) were seeded on sterile silicon stretch chambers (STB-100, STREX, San Diego, USA) precoated with Speed Coating Solution (Pelobiotech GmbH, Planegg, Germany). After 24 h, culture supernatant was aspirated, and 1 mL of fresh William's E medium was added. Stretch chambers were elongated by about 30% for up to 3 h or remained unstretched as a control (Fig. 2.1).

Stretching of the cell nucleus was monitored microscopically using an Olympus IX 50 microscope equipped with a DP71 camera and the extent of stretching was calculated by measuring the diameter of the cell nucleus in the direction of elongation, using the software *cellSens Dimensions*. For RNA isolation, cell culture medium was removed, and cells were washed with PBS (Pan Biotech). Using a sterile cell scraper, cells were detached in and transferred into a clean reaction tube, followed by a centrifugation step at 10.000 g for 5 min at 4 °C. The supernatant was discarded, and pelleted cells were lysed by addition of 500 µL of

Qiazol Lysis Reagent for 3 min. Phenol/chloroform extraction was performed as described in section 2.2.3.

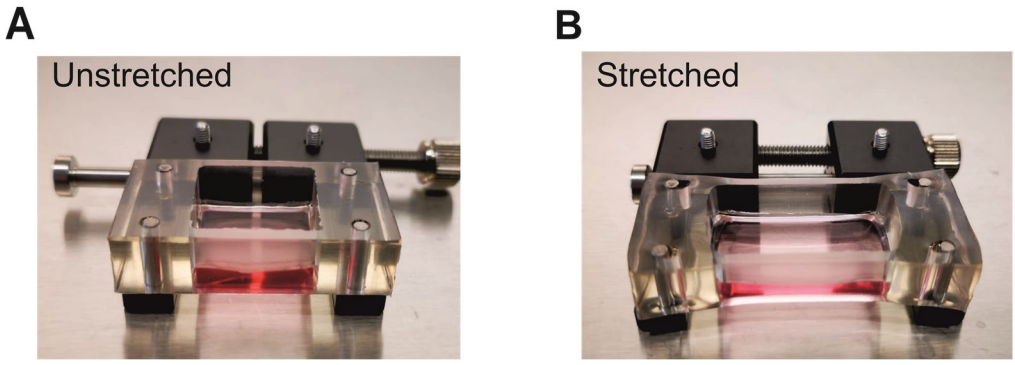

Figure 2.1 Images of cell stretch chambers in their unstretched or stretched state. STB-100 silicone stretch chambers in their unstretched (**A**) and stretched (**B**) state. Cell stretching is conducted by screwing in a bolt in the back of the metal frame.

2.2.9 Primer design for polymerase chain reaction (PCR)

Oligonucleotide primers were designed for PCR amplification of miR-141-3p target gene 3'UTR using genomic sequences obtained from Ensembl Genome Browser (v93 www.ensembl.org/index.html). Melting temperatures for mRNA and miRNA primers were calculated by use of the tool *Oligo Analyzer* 1.1.2 (www.genelink.com/tools/gl-oe.asp). For cloning procedures with the In-Fusion Cloning system, the Cloning Primer Design Tool of Takara Bio Europe (www.takarabio.com/learning-centers/cloning/primer-design-and-other-tools) was used.

The design and assessment of mRNA primers for qPCR was performed by the Roche ProbeLibrary (lifescience.roche.com/en_de/brands/universal-probe-library.html#assay-design-center) with respect to their secondary structure, possible self-dimerization and primer duplexes. The miRNA sequences were obtained from www.mirbase.org (Version 22.1, release October 2018). The oligonucleotides were purchased from Eurofins MWG Synthesis GmbH (Ebersberg, Germany) or Eurogentec Deutschland GmbH (Cologne, Germany).

2.2.10 cDNA synthesis from mRNA.

For mRNA analysis, total RNA from tissue samples and cells was purified (miRNeasy Mini Kit, Qiagen), measured with DropSense16 micro-volume spectrophotometer (2.2.3), and finally taken for cDNA synthesis using the Revert Aid H Minus First Strand cDNA Synthesis Kit (K1632, Thermo Fisher Scientific). For this purpose, 1 µg total RNA in a volume of 20 µL reaction buffer was used according to manufacturer's recommendations using the reaction mixture indicated in the Table 2.2.1:

Table 2.2.1 Reaction mixture for cDNA synthesis

Components	**Volumes [µL]**
5x Reaction Buffer	4.0
RiboLock RNase Inhibitor (20 U/µL)	1.0
dNTP Mix (10 mM)	2.0
RevertAid H Minus Transcriptase (200 U/µL)	1.0
Random Primer (0.2 µg/µL)	1.0
OligoDT (0.5 µg/µL)	1.0
RNA (1 µg/µL)	1.0
Nuclease-free water	9.0
Total reaction volume	**20.0**

The cDNA was synthesized using the reaction mixture displayed in Table 2.2.1 in a thermal cycler at 65 °C for 5 min, 25 °C for 15 min, and 42 °C for 60 min, followed by heat inactivation at 70 °C for 15 min. Synthesized cDNA was diluted to 1 ng/µL with nuclease free water and used as template for qPCR.

2.2.10 Quantitative real-time PCR

Quantitative PCR (qPCR) was performed in a qTower^3 (Analytik Jena AG, Jena, Germany) with Takyon™ qPCR Mastermix (UF-NSMT-B0710, Eurogentec) using the reaction mixture indicated in the Table 2.2.2:

Table 2.2.2 Reaction mixture for qPCR of mRNA

Components	Volumes [µL]
2x Takyon™ qPCR Mastermix	7.5
Forward primer (10 µM)	2.1
Reverse primer (10 µM)	2.1
cDNA (1 ng/µL)	2.5
Nuclease-free water	0.8
Total reaction volume	**15.0**

To analyze each gene of interest, one master mix containing 2x Takyon™ qPCR Mastermix, nuclease-free water and the gene-specific primers was mixed and 12.5 µL of Master Mix were transferred in appropriate 96-well plates (4titude® Ltd, Berlin, Germany). Next, 2.5 µL (2.5 ng) of the respective cDNA was added, whereby each sample was measured in at least two technical replicates. qPCR was performed using the settings depicted in Table 2.2.3:

Table 2.2.3 qPCR program for relative quantification of mRNA

Step	Temperature [°C]	Time [s]	Cycles
Heat-activation	95	300	x45
Denaturation	95	15	
Elongation	72	20	
Melting curve analysis			1x

The melting curve was assessed between 60 °C to 95 °C with a temperature increase of 1 °C per 15 seconds. For relative mRNA quantifications, amplifications curves were analyzed using qPCRsoft 3.2 (Analytik Jena) and a signal intensity threshold within the linear range was set. The threshold cycles (C_t-values) were exported and mRNA quantities were calculated by utilizing *qBase* software v 1.3.5 [221] based on the delta-delta C_t ($\Delta\Delta C_t$) method [222]. The raw data were normalized to the C_t values of the reference gene ribosomal protein S6 (*Rps6*). Statistical analysis was conducted by unpaired student's t-test or one-way analysis of variance (ANOVA) with a significance level of $p < 0.05$ as appropriate.

2.2.12 Synthesis of cDNA for quantitative miRNA analysis

In order to calculate the relative quantity of miRNAs in liver tissue and cells, miQPCR [223] was performed. Due to their short length and a lack of a poly(A) tail, miRNAs require a method which utilizes the activity of T4 RNA Ligase, to uniformly elongate the 3'-ends of small RNAs to a short oligonucleotide adaptor, called miLINKER. Next, PrimeScript™ RTase and reverse-transcription primer (mQ-RT) that specifically hybridizes to the miLINKER adaptor sequence are used to reverse-transcribe the elongated RNA sequences. This method allows for a quantification of various miRNAs of interest, without the need to specifically generate individual cDNAs for each miRNA of interest. The miQPCR was performed in PTC-200 thermal cyclers (MJ research) with 10 ng of diluted RNA and 6 µL of elongation mix (Table 2.2.4), incubated at 25 °C for 30 min and afterwards cooled down to 10 °C. The elongated RNA samples were mixed with 7 µL cDNA Mix 1 (Table 2.2.4) and heated up to 85 °C for 2 min to allow mQ-RT primer annealing. Afterwards, the samples were cooled down to 46 °C, and 5 µL of cDNA Mix 2 (Table 2.2.4) were added. Samples were incubated at 46 °C for 30 min, to complete the first strand reverse transcription. In the final step, samples were heat-inactivated at 85 °C for 2 min and cooled down to 10 °C. A working cDNA stock solution (0.05 ng/µL) was created by diluting to a total volume of 200 µL with nuclease-free water.

Table 2.2.4 Composition of master mixes required for cDNA synthesis by miQPCR (Benes *et al.* 2015)

Components	Volumes [µL]
1) Elongation Mix	
10x T4 Rnl2 Buffer (New England BioLabs)	0.90
$MgCl_2$ (450 mM)	0.10
PEG 8000 (50%)	3.10
miLINKER (5 mM)	0.10
RNase inhibitor (40 U/µL, Roche)	0.10
Truncated T4 RNA Ligase (K227Q) (New England BioLabs)	0.20
Nuclease-free water	3.10
2) cDNA Mix 2	
dNTPs (10 mM)	0.05
mQ-RT primer (10 mM)	0.25
Nuclease-free water	7.00
3) cDNA Mix 3	
5x RT Buffer (Takara Bio Europe)	4.40
PrimeScript™ RTase (Takara Bio Europe)	0.14
Nuclease-free water	0.85

Relative miRNA quantification was then carried out by qPCR with miRNA-specific forward primers and the universal reverse primer Upm2A. The qPCR assays for miRNAs were typically conducted with 2.5 µL cDNA (i.e. 125 pg cDNA) in a total volume of 15 µL as follows:

Table 2.2.5 Reaction mixture for qPCR quantification of miRNAs

Components	Volumes [µL]
2x Takyon™ qPCR Mastermix	7.5
Forward primer (10 µM)	2.1
Reverse primer (10 µM)	2.1
cDNA (50 pg/µL)	2.5
Nuclease-free water	0.8
Total reaction volume	**15.0**

A Master mix containing miRNA-specific, universal Upm2A primer, 2x Takyon™ qPCR Mastermix and nuclease-free water was prepared and aliquoted into a 96-well plate together with 2.5 µL of cDNA as described earlier (Section 2.2.9). All samples were measured in at least two technical replicates and qPCR was carried out with the following protocol:

Table 2.2.6 qPCR program for relative quantification of miRNAs

Step	Temperature [°C]	Time [s]	Cycles
Heat-activation	95	300	x50
Denaturation	95	10	
Elongation	60	35	
Melting curve analysis			1x

The melting curve was assessed between 60 °C and 95 °C with a temperature gradient of 1 °C per 15 seconds. Data were analyzed using *qPCRsoft* 3.2 and *qBase* 1.3.5 [221] as described earlier (Section 2.2.11).

2.2.13 Cloning of *Cdk8* 3'UTR into pMir(+) promoter vector

The full length of the rat *Cdk8* 3'UTR was cloned into pMir(+) *Firefly* luciferase plasmid, which derived from pGL3 promoter vector (Promega), as described by Castoldi *et al*. [224] utilizing the In-Fusion Cloning Plus system (Takara Bio Europe). The desired sequence was analyzed, using the In-Fusion Cloning Primer Design Tool, which generates primers that allow the amplification of the 3'UTR with homologous termini to the linearized target vectors (Table 2.1.10). As shown in Table 2.1.10, sequence-specific primers were designed with a NheI recognition site at the 5'-end, serving as a forward primer, and a SacI recognition site at the 5'-end of the reverse primer, which allowed for the site-directed insertion of the desired

sequence between the NheI and SacI recognition sites within the multiple-cloning site (MCS) of the reporter plasmids. By switching of the NheI and the SacI recognition sites in forward and reverse directions, two plasmids were generated, one with the 3'UTR in its original orientation (+) and the other with the 3'UTR in antisense orientation (-), used as a control vector.

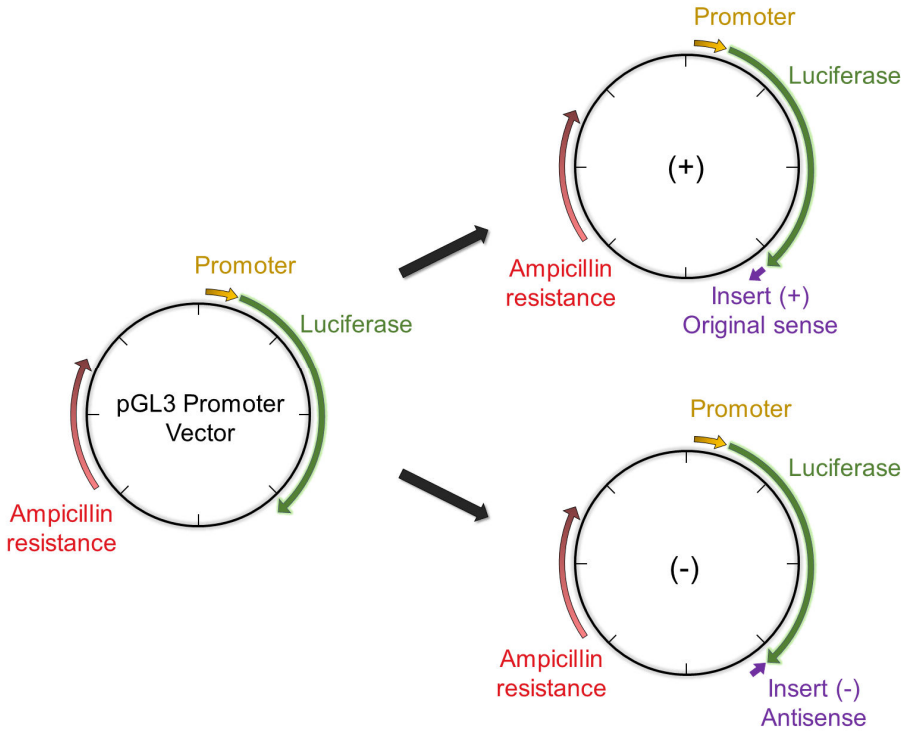

Figure 2.2 Cloning of pMir(+) *Firefly* luciferase plasmid for miR-141-3p target gene validation. Schematic illustration of the generation of two plasmids, one with the insert in its original sense orientation and the other with the insert in its antisense orientation, serving as a negative control.

Amplification of the desired sequence was performed via PCR using a total of 30 ng genomic rat DNA (gDNA) serving as template using CloneAmp HiFi PCR Premix (Takara Bio Europe) according to the manufacturer's instructions. The amplified PCR product was purified with QIAquick PCR Purification Kit (Qiagen). pMir(+) *Firefly* luciferase plasmid was linearized by digestion with 40 U of the restriction enzymes NheI-HF and SacI-HF in 1x CutSmart buffer (New England BioLabs) at 37 °C overnight. Vector and amplified inserts were quantified using DropSense16 spectrometer as described above (Section 2.2.3). For the fusion of vector and insert in a total volume of 10 µL, a total of 50 ng linearized pMir(+) *Firefly* luciferase plasmid and a 2-fold molecular excess of inserts were used together with 1x In-Fusion HD Enzyme Premix. The reaction was performed at 50 °C for 15 min and terminated by cooling on ice. Out of 10 µL reaction mixture, an aliquot of 2.5 µL was transformed in Stellar™ Competent Cells according to the manufacturer's instructions. Transformed bacteria suspensions were plated

out on LB-agar plates, supplemented with 100 µg/mL ampicillin (Sigma Aldrich), and bacteria were incubated overnight at 37 °C. Bacterial colonies were picked using a sterile pipet tip and inoculated into 2 mL for small-scale or into 50 mL of ampicillin-containing LB-medium for large-scale plasmid preparation. The isolation and preparation of plasmid DNA was conducted with the use of Fast-n-Easy Plasmid Mini-Prep Kit (Qiagen) for small-scale and QIAGEN Plasmid Midi Kit (Qiagen) for large-scale preparation according to the manufacturer's protocol. The recombinant plasmids were sequenced by the Genomics and Transcriptomics Laboratory (GTL) at the Heinrich Heine University (Düsseldorf) using Sanger-Sequencing technique.

2.2.14 Validation of miR-141-3p target-genes by Dual-Luciferase® Reporter Assay

To validate the binding site of miR-141-3p onto the *Cdk8* 3'UTR, which was cloned into luciferase reporter plasmids (2.2.13), a Dual-Luciferase® Reporter Assay was performed. The Dual-Luciferase® Reporter Assay is based on the detection of a chemi-luminescent signal, which is measured from the lysates of cells. This technique allows to evaluate whether a cloned fragment may encode for a functional MRE. If a functional MRE for miR-141-3p is present, treatment with miR-141-3p mimic should result in the binding of miR-141-3p to the fragment, and thus inhibit the expression of luciferase. The luciferase plasmids used in this thesis are the *Firefly* luciferase plasmid, which serve as the actual reporter plasmid and the *Renilla* luciferase plasmid, which were co-transfected for data normalization. These two luciferase plasmids differ in their substrate specificity and their optimal enzyme reaction catalyzation based on the adherent pH. The co-transfection of the recombinant *Firefly* plasmid and pRL-SV40 (*Renilla* plasmid) was conducted in HEK293 cells in sterile 12-well plates with an estimated confluency of 60% (~70.000 cells/well). The transfection was performed using Lipofectamin™ 3000 (Thermo Fisher Scientific) with 300 ng *Firefly* plasmid DNA, 6.25 ng pRL-SV40 *Renilla* luciferase plasmid in either the presence or the absence of 25 pmoles of miR-141-3p mimic according to the manufacturer's instructions. After 5 hours the transfection medium was replaced by fresh culture medium and the cells were incubated for 24 hours. Afterwards, the cells were washed and lysed in 150 µL 1x Passive Lysis Buffer (Promega) for 15 min at RT. Cell lysates were transferred into reaction tubes and centrifuged at 10,000 g for 2 min at 4 °C. Next, 50 µL of the supernatant was transferred into white opaque 96-well plates. The chemiluminescence assay was performed in a GloMax® Multi Plus Multiplate reader (Promega) with an integrity time of 10 seconds for each individual read. Data were normalized by calculating ratios of *Firefly/Renilla* activities to correct for variations in transfection efficiencies.

2.2.15 Online databases and bioinformatic tools

miRNA sequences were acquired from *miRBASE* (Version 22.1, release October 2018, www.mirbase.org). Sequences of 3'UTRs were downloaded from *Ensembl Genome Browser* (release: Ensembl Gene database 93 at www.ensembl.org/index.html and mRNA primers for qPCR were designed using *Universal ProbeLibrary Assay Design Center* (lifescience.roche.com/en_de/brands/universal-probe-library.html#assay-design-center). Melting temperatures for all miRNA and mRNA primers were calculated by use of the tool *Oligo Analyzer* 1.1.2 (www.genelink.com/tools/gl-oe.asp).

For target gene prediction, the online database *miRWalk* 3.0 (mirwalk.umm.uni-heidelberg.de), *TargetScan* 7.2 (www.targetscan.org), and *RNA22* (cm.jefferson.edu/rna22/) were used. *CLC Genomics Workbench* (Version 3.6.5) was utilized for virtual cloning and analysis of nucleic acids sequences received from Sanger-Sequencing. Primers for the In-Fusion Cloning Plus system were designed using Takaras web-based *In-Fusion Cloning Primer Design Tool* (www.takarabio.com/learning-centers/cloning/in-fusion-cloning-tools). QPCR data were analyzed using *qBase* software v1.3.5 and the reference gene *Rps6* was selected based on the *GeNorm* algorithm [221]. Microarray raw data were analyzed using the software *Transcriptome Analysis Console* 4.0 (Thermo Fisher Scientific). Data from luciferase assays were exported using *Instinct*® Software 3.1.3 (Promega).

2.2.16 Statistics

Statistical analyses were carried out with values from at least 3 independent experiments or from at least 3 different rats and are presented as means. Variations are indicated as standard error of the mean (±SEM). Statistical analyses for the comparisons between two groups were performed by using *GraphPad Prism* 5.03 (GraphPad Software, San Diego, USA) software, applying unpaired, two-tailed student's t-test (parametric test). For comparisons between three or more groups, the one-way ANOVA (parametric test) was applied and *p*-values smaller than 0.05 were considered significant. For comparisons between different conditions and timepoints, the two-way ANOVA (parametric test) was applied and *p*-values smaller than 0.05 were considered significant. For statistical evaluation of the GeneChip™ miRNA 4.0 Array and Flashtag™ Biotin HSR Labeling for miRNAs and Affymetrix GeneChip 1.0 ST, multiple t-test was applied with a false discovery rate (FDR) of 0.5% (p-value < 0.05).

3. Results

3.1 miRNA and mRNA expression changes in rat livers under hypoosmolarity

Previous studies by Santosa *et al*. [88] demonstrated that members of the miR-15/107 family are induced by hyperosmolarity, inducing apoptosis through the inhibition of anti-apoptotic genes in rat liver [211,225]. However, the role of miRNAs in the liver regarding the maintenance of osmotic homeostasis and osmosignaling under hypoosmolarity is largely unknown. To identify hypoosmolarity-responsive miRNAs, transcriptome-wide microarray chip analysis of hypoosmotic perfused rat liver tissue was conducted. Therefore, RNA of rat livers perfused with normoosmotic and hypoosmotic perfusion media for up to 180 min was isolated and hybridized to an Affymetrix array (GeneChip™ miRNA 4.0 Array and Flashtag™ Biotin HSR Labeling) and analyzed via *Transcriptome Analysis Console* software. Microarray analyses identified several of significantly regulated miRNAs, as depicted in Figure 3.1. When comparing miRNA levels from livers perfused with hypoosmotic medium for 180 min to normoosmotic medium, 728 miRNAs were identified, out of which 12 were downregulated, 16 were upregulated and 700 remained unchanged (Fig. 3.1 C). For instance, the following miRNAs were found to be significantly downregulated under hypoosmolarity compared to normoosmotic control after 180 min of liver perfusion:

- miR-874-3p
- miR-770-3p
- miR-541-5p.

Subsequent miRNAs were downregulated under hypoosmotic condition with a fold change of more than 2:

- miR-184
- miR-92a-5p
- miR-101b-3p.

Among 16 upregulated miRNAs under hypoosmolarity, miR-18a-5p was upregulated with a fold change of 2.1, miR-503-5p with a fold change of 2.45, and miR-350 with a fold change of 2.08. Several other miRNAs, were also upregulated under hypoosmotic condition compared to normoosmotic control, including:

- miR-155-3p
- miR-338-5p
- miR-141-3p
- miR-212-3p.

Altogether, these data point towards an involvement of miRNAs in the cellular response to hypoosmolarity in the experimental setup of *ex vivo* liver perfusion.

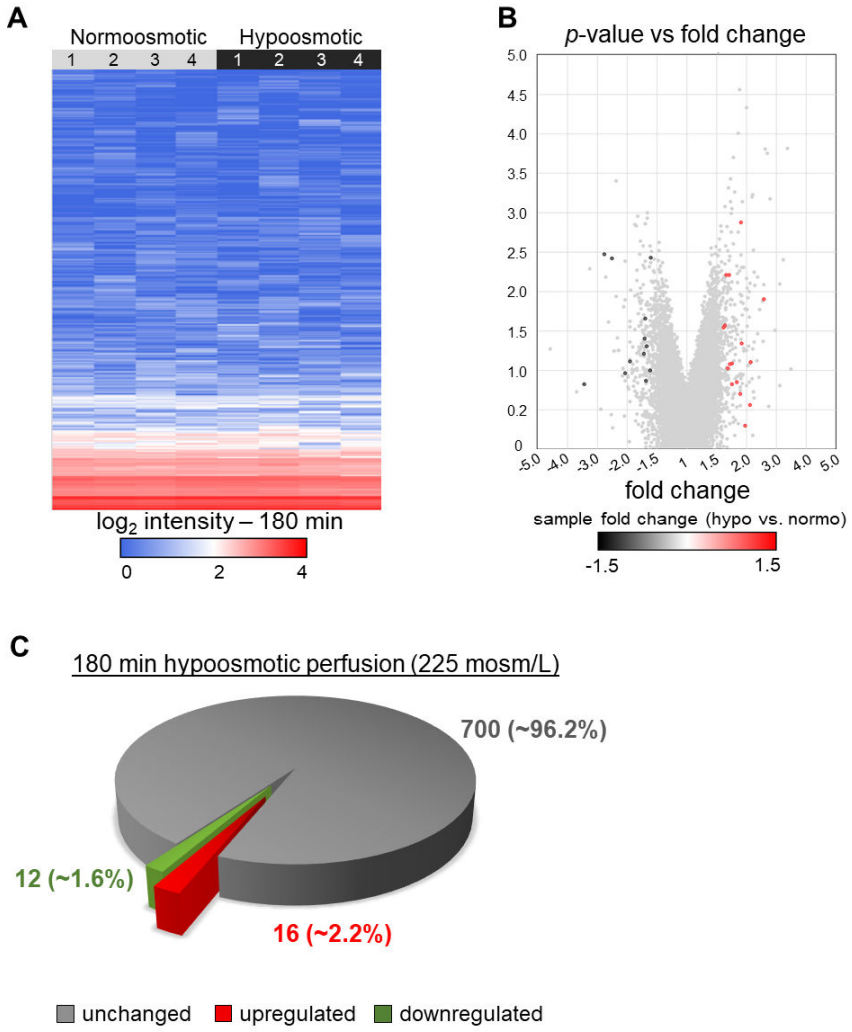

Figure 3.1 Microarray analysis of miRNAs from rat liver tissue perfused with normo- or hypoosmotic medium. Rat livers were perfused with normo- (305 mosm/L) or hypoosmotic medium (225 mosm/L) for 180 min. Livers were dissected and RNA was isolated. RNA was then hybridized to Affymetrix array (GeneChip™ miRNA 4.0 Array and Flashtag™ Biotin HSR Labeling, n=4). *Transcriptome Analysis Console* was used for data analysis by applying a cut-off of 1.5-fold change and a significance level of $p<0.05$ (one-way ANOVA). (**A**) Heat map representing the hierarchical clustering of differential expressed miRNAs under normo- or hypoosmotic condition. (**B**) Volcano blot demonstrating differential miRNA levels after 180 min in perfused rat liver under normo- or hypoosmotic condition. A 1.5-fold change cut-off was applied with a statistical significance level of $p<0.05$. Significantly upregulated mRNAs are labeled in red and significantly downregulated mRNAs are indicated in black, while mRNAs with non-significant changes are displayed in grey (**C**). Pie charts representing the number of regulated miRNAs found in rat livers after 180 min of hypoosmotic perfusion compared to normoosmotic perfusion.

To investigate the impact of hypoosmolarity on gene expression changes in rat liver perfusion, a transcriptome-wide analysis of the mRNA expression profile was conducted with normoosmotic and hypoosmotic perfused rat liver tissue. Microarray analysis revealed that after 180 min of hypoosmotic exposure, 534 mRNAs were upregulated, while 609 were

downregulated compared to normoosmotic perfused control livers, whereas a total of 21406 mRNA remained unchanged (Fig. 3.2 C). To explore the impact of hypoosmolarity on signaling pathways via alterations in gene expression, a pathway analysis was conducted for significant upregulated mRNA using *Transcriptome Analysis Console* software. Several pathways, including the *TGF-β* signaling pathway, the $\alpha_6\beta_4$-integrin signaling pathway, and the MAPK signaling pathway were affected by upregulated mRNA levels. Among upregulated mRNA, c*yclin B2* (*Ccnb2*), *caveolin 1* (*Cav1*), *exportin 1* (*Xp1*), and *cyclin dependent kinase inhibitor 1*a (*Cdkn1a*) are involved in the *TGF-β* signaling pathway, whereas *laminin subunit gamma 2* (*Lamc2*) and *vimentin* (*Vim*) are involved in the $\alpha_6\beta_4$-integrin signaling pathway. Altered MAPK signaling pathway was indicated by the upregulation of *fos proto-oncogene* (*Fos*), *heat shock protein family A member* (*Hspa1a*), and *heat shock protein family B member 1* (*Hspb1*) mRNA.

These data suggest, that hypoosmotic exposure of rat livers has a pronounced effect on the levels of cellular mRNA.

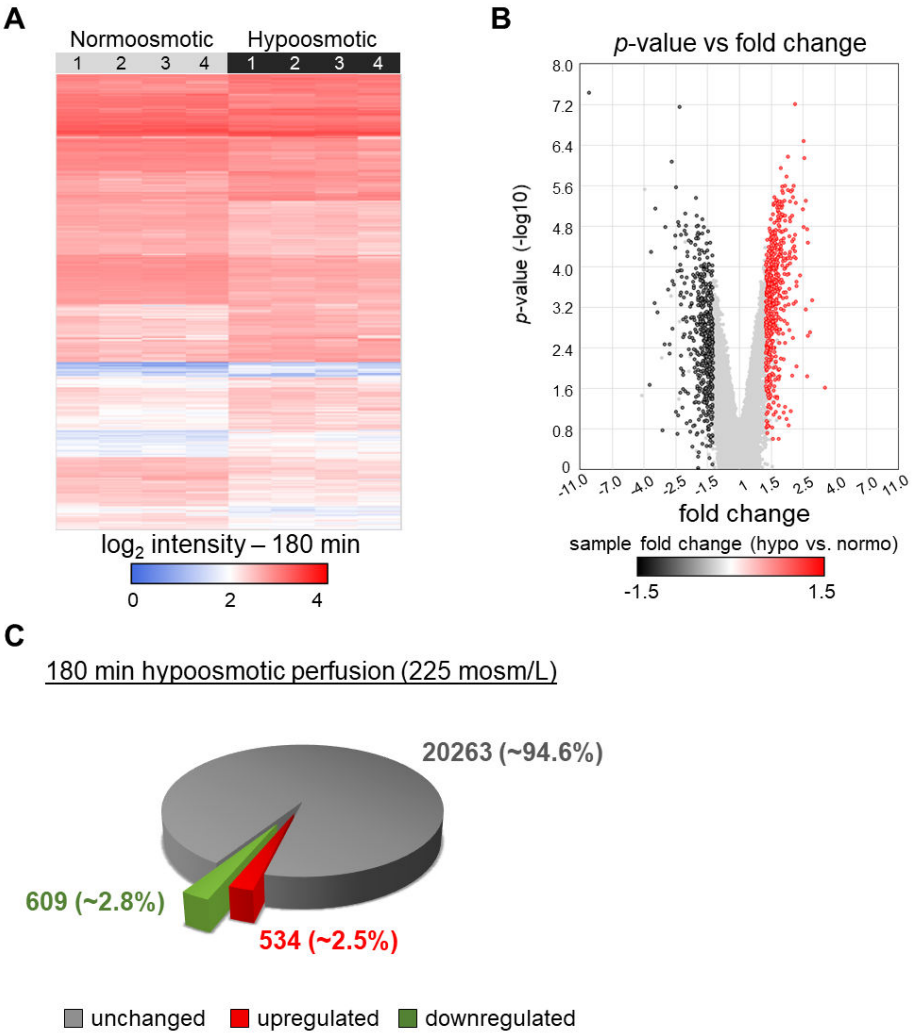

Figure 3.2 Microarray analysis of mRNA from rat livers perfused with normo- or hypoosmotic medium. Rat livers were perfused with normo- (305 mosm/L) or hypoosmotic medium (225 mosm/L) for 180 min. Livers were dissected and RNA was isolated. RNA was then hybridized to Affymetrix array (GeneChip™ mRNA 1.0 Array, n=4). *Transcriptome Analysis Console* was used for data analysis by applying a cut-off of 1.5-fold change and a significance level of $p<0.05$ (one-way ANOVA). (**A**) Heat map representing the hierarchical clustering of differential expressed mRNAs under normo- or hypoosmotic condition. (**B**) Volcano blot demonstrating differential mRNA levels after 180 min in perfused rat livers under normo- or hypoosmotic condition. A 1.5-fold change cut-off was applied with a statistical significance of $p<0.05$. Significantly upregulated mRNAs are labeled in red and significantly downregulated mRNAs are displayed in black, while mRNAs with non-significant changes are indicated in grey. (**C**) Pie charts representing the number of regulated mRNA found in rat livers upon 180 min of hypoosmotic perfusion compared to normoosmotic perfusion.

3.2 Connection of miRNA and mRNA expression changes

To identify a correlation between downregulated mRNA and upregulated miRNA levels, possible binding sites for miRNAs in the sequence of the 609 downregulated mRNAs were compared with previous upregulated miRNAs found by microarray analysis. Because a single miRNA can target tens to hundreds of mRNAs, we utilized *TargetScan* 7.2 and *miRWalk* 3.0 for prediction of possible target gene candidates to anticipate downstream target genes. Our

bioinformatics analyses revealed that among all of the 609 downregulated mRNAs were many miRNA target gene candidates for several miRNAs, including miR-18a-5p, miR-141-3p, miR-127-3p, miR-483-5p, and miR-338-5p. Strikingly, target prediction revealed that miR-141-3p putatively targets 249 (40.9%) out of 609 downregulated mRNAs, which were found by microarray chip analysis (Fig. 3.3 A). These data strongly point towards an involvement of miR-141-3p in the regulation of the cellular response to hypoosmolarity.

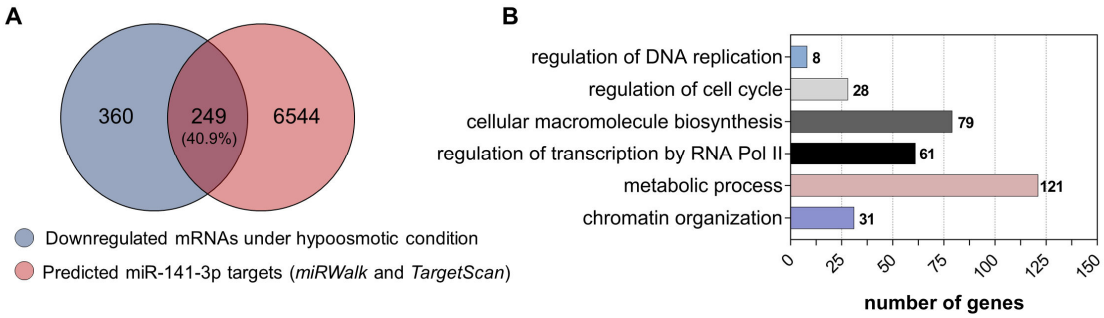

Figure 3.3 miR-141-3p target prediction analysis of significantly downregulated mRNAs under hypoosmotic conditions. (**A**) Venn diagram illustrating the number of downregulated mRNAs under hypoosmotic condition which identified as putative miR-141-3p target, by the target prediction algorithms *miRWalk* and *TargetScan*. (**B**) *Gorilla Gene Ontology enrichment* tool was utilized to analyze the predicted target gene candidates of miR-141-3p. Numbers of genes associated with given GO terms are indicated next to the bars.

To gain a better insight of the functions of miR-141-3p and the possible out-turn associated with miR-141-3p deregulation, Gene ontology enrichment analysis was conducted. All 249 identified miR-141-target gene candidates were included in this study, independent of the fold change. Gene ontology enrichment analysis revealed that the 249 miR-141-3p target gene candidates are enriched in processes such as metabolic processes, regulation of cell cycle, regulation of transcription by RNA polymerase II, cellular macromolecule biosynthesis, and chromatin organization. Thus, gene ontology enrichment analysis is indicative for an involvement of miR-141-3p in a broad spectrum of cellular mechanisms and regulations mediated via its target gene candidates. This refers to processes associated with metabolism and biosynthesis of macromolecules, e.g. proteins.

3.3 miQPCR and qPCR validation of hypoosmotically-regulated miR-141-3p

To independently validate the observed expression changes of miR-141-3p, miQPCR was carried out on RNA isolated from rat livers perfused with normo- or hypoosmotic medium over a time course of up to 180 min. As illustrated in Figure 3.4, miR-141-3p expression was increased to 1.82-fold (± 0.26, p=0.027) under hypoosmotic conditions after 180 min of rat liver perfusion. Under normoosmotic conditions miR-141-3p levels presented a stable expression during rat liver perfusion.

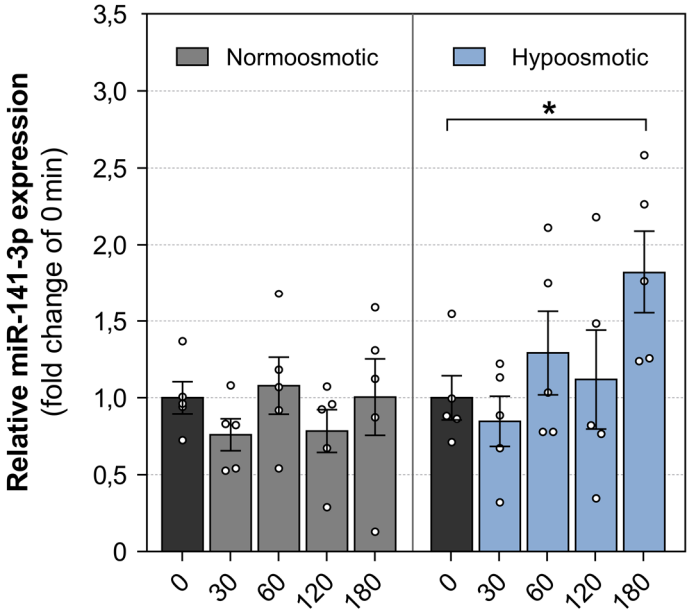

Figure 3.4 Relative quantification of miR-141-3p in perfused rat livers in response to normo- and hypoosmotic exposure. Rat livers were perfused with normo- (305 mosm/L) or hypoosmotic medium (225 mosm/L) over a time course of 180 min. After initialization of perfusion, liver lobes were dissected at the indicated time points, RNA was isolated and miRNA expression was analyzed using miQPCR (n=5). miRNA levels were median normalized by scaling the samples to their median value [226]. Statistical analysis was carried out by one-way ANOVA. Data are shown as average ± standard error of the mean (SEM) with * p<0.05.

As a member of the miR-200 family, miR-141-3p is shown to be involved in many cellular processes, e.g. proliferation, migration, invasion, and drug resistance [227–230]. Cell swelling, induced by hypoosmotic condition in perfused rat liver is known to enhance cell proliferation [68]. For this purpose, miR-141-3p and its putative target mRNAs were picked for further investigation to investigate a possible connection with cell proliferation. For this purpose, qPCR was carried out on isolated RNA from rat livers perfused with normoosmotic or hypoosmotic medium for 180 min and mRNA levels of selected miR-141-3p target gene candidates were assessed. Specifically, putative target mRNAs associated with biological processes like proliferation, cell cycle progression, and transcriptional activity were chosen for

qPCR analyses. These included mRNAs encoding for *Cdk8*, *zinc metallopeptidase STE24* (*Zmpste24*), *cell division cycle 25A* (*Cdc25a*), and *nuclear factor of activated t cells 5* (*Nfat5*).

As presented in Figure 3.5, qPCR analysis of potential target gene candidates of miR-141-3p revealed differentially expressed mRNA under hypoosmotic exposure in rat liver perfusion compared to normoosmotic control.

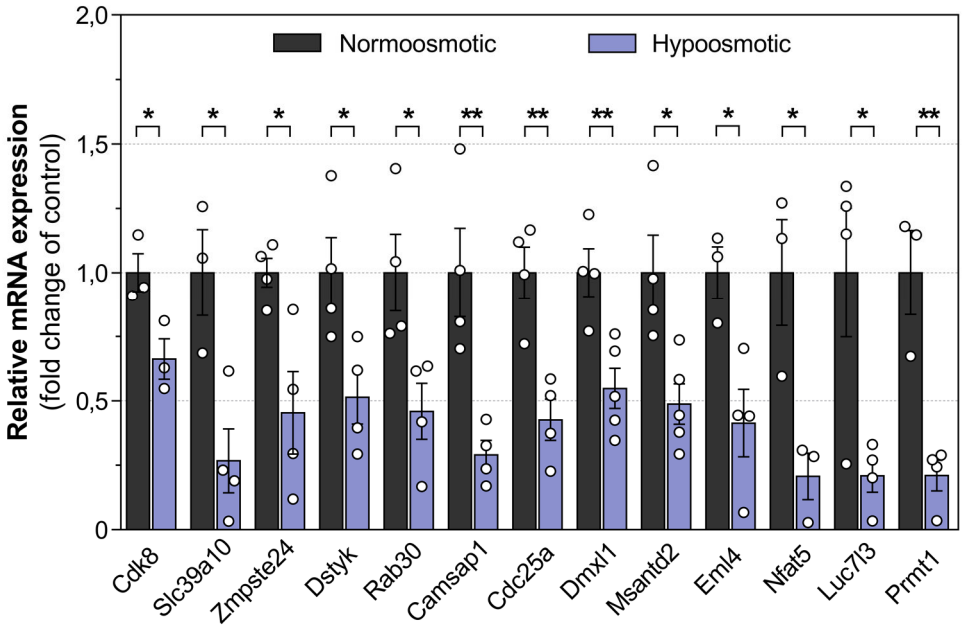

Figure 3.5 Quantitative analysis of putative target mRNA of miR-141-3p in perfused rat livers in response to normo- and hypoosmotic exposure. Rat livers were perfused with normo- (305 mosm/L) or hypoosmotic medium (225 mosm/L) for 180 min. Livers were dissected, RNA was isolated, and miRNA expression was analyzed using qPCR (n=3-5). qPCR values were normalized to *Rps6* mRNA levels. Statistical analysis was carried out by student's t-test. Data are shown as average ± SEM with * $p<0.05$ and ** $p<0.01$.

Under hypoosmotic exposure selected mRNA levels of putative miR-141-3p target genes were significantly downregulated compared to normoosmotic control as displayed in Table 3.3.1:

Table 3.3.1 mRNA levels of putative target mRNA of miR-141-3p

Name	Identifier	downregulated to	*p*-value
Cyclin dependent kinase 8	*Cdk8*	0.66-fold ± 0.07	0.035
Solute carrier family 39 member 10	*Slc39a10*	0.26-fold ± 0.12	0.015
Zinc metallopeptidase STE24	*Zmpste24*	0.45-fold ± 0.15	0.018
Dual serine/threonine and tyrosine protein kinase	*Dstyk*	0.51-fold ± 0.10	0.029
Member ras oncogene family	*Rab30*	0.45-fold ± 0.05	0.026
Calmodulin regulated spectrin associated protein 1	*Camsap1*	0.29-fold ± 0.07	0.007
Cell division cycle 25A	*Cdc25a*	0.42-fold ± 0.07	0.004
Dmx like 1	*Dmxl1*	0.54-fold ± 0.07	0.007
Myb/SANT DNA binding domain containing 2	*Msantd2*	0.48-fold ± 0.07	0.013
EMAP like 4	*Eml4*	0.41-fold ± 0.13	0.020

Table 3.3.1 mRNA levels of putative target mRNA of miR-141-3p (continued)

Nuclear factor of activated t cells 5	*Nfat5*	0.20-fold ± 0.09	0.024
LUC7 like 3 pre-mRNA splicing factor	*Luc7l3*	0.20-fold ± 0.06	0.024
Protein arginine methyltransferase 1	*Prmt1*	0.21-fold ± 0.05	0.003

As illustrated in Figure 3.5 and shown in Table 3.3.1, all selected mRNA were significantly downregulated after 180 min of hypoosmotic rat liver perfusion.

Table 3.3.2 shows several genes which are not affected on their mRNA level by hypoosmotic exposure in rat liver perfusion, to emphasize the distinct effect of hypoosmolarity on specific mRNA.

Table 3.3.2 mRNA not affected by hypoosmotic exposure

Name	Identifier	Fold-change	*p*-value
Solute carrier family 22 member 5	*Slc22a5*	0.99 ± 0.01	0.9888
Regulator of G-protein signaling 20	*Rgs20*	1.00 ± 0.01	0.9276
Microtubule-associated protein 1 light chain 3 beta	*Map1lc3b*	0.99 ± 0.01	0.9094
Solute carrier family 1 member 7	*Slc1a7*	0.97 ± 0.03	0.8153
Gap junction protein alpha 1	*Gja1*	0.97 ± 0.05	0.9155
Acyl-CoA dehydrogenase	*Acadl*	0.99 ± 0.01	0.8671
Zinc finger protein 18	*Zfp18*	0.99 ± 0.03	0.9956
Mitochondrial elongation factor 1	*Mief1*	0.99 ± 0.01	0.7222

3.4 Analysis of miR-141-3p in isolated primary rat hepatocytes.

To investigate whether changes in miR-141-3p levels and its putative target gene mRNA levels can be mimicked *in vitro*, exposure of primary rat hepatocytes to hypoosmotic medium was performed, since hepatic parenchymal cells constitute about 70% of all liver cells and represent the basic structural component of the liver [231]. Figure 3.6 A and B display microscopical images of isolated primary rat hepatocytes exposed to normo- and hypoosmotic medium. Hypoosmotic exposure resulted in an increased cell surface and swelling of the cell nucleus. To assess the extent of cell swelling, cell nucleus diameters were measured and compared between the two conditions (Fig. 3.6 C). Isolated primary rat hepatocytes, which were exposed to normoosmotic medium for 5 min, had an average cell nucleus diameter of 9.7 µm (± 1.2 µm). Hypoosmotic exposure led to an average cell nucleus diameter of 13.1 µm (± 2.0 µm) after 5 min, resulting in a diameter increase by about 35% (p=0.001, Fig. 3.6 D). After 3 h of hypoosmotic exposure, the average cell nucleus diameter decreased back to 10.4 µm (± 1.3 µm). This resulted in an increased diameter by about 7% compared to normoosmotic control, due to counteractive volume regulatory mechanisms (RVD).

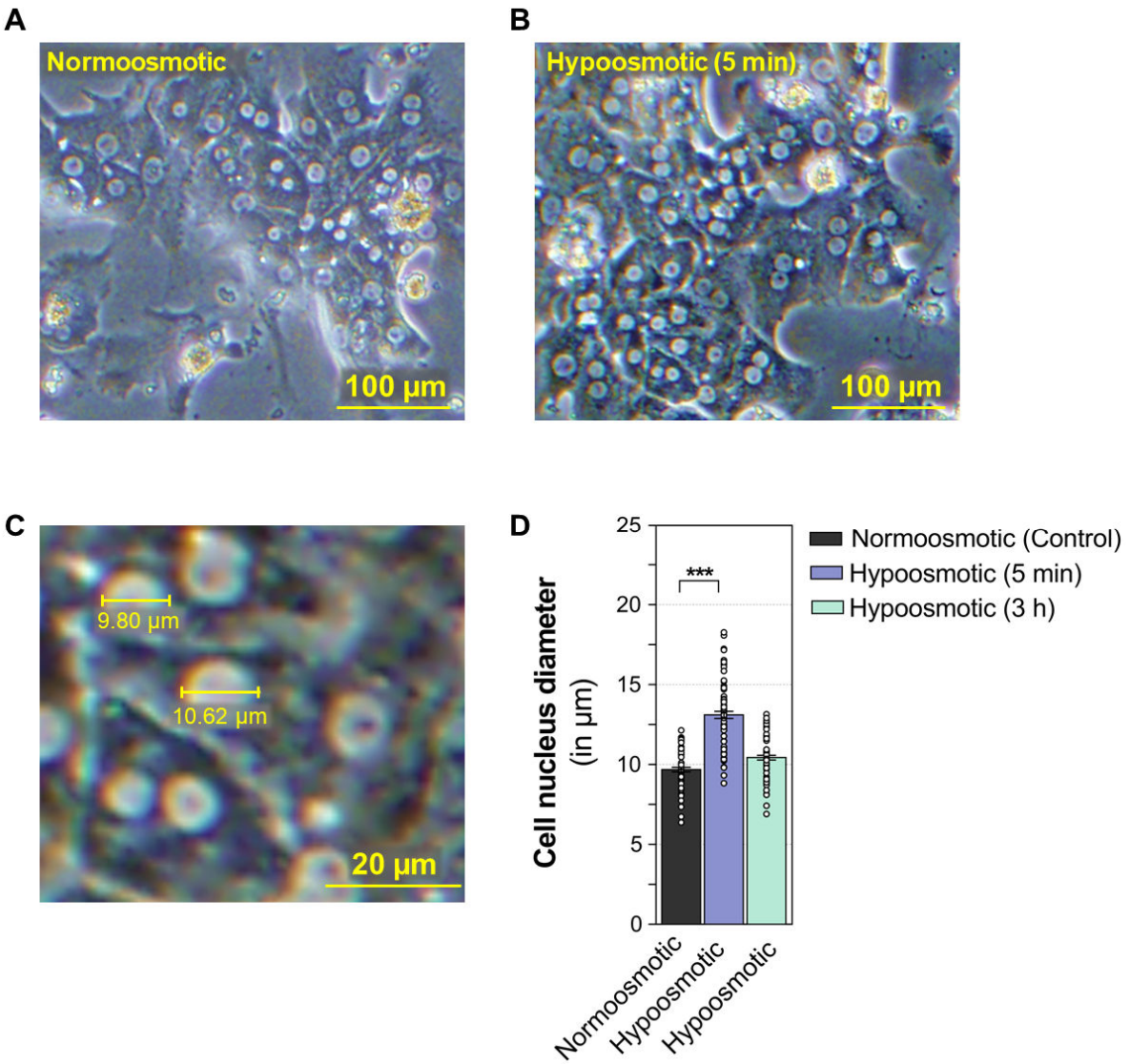

Figure 3.6 Effect of normo- and hypoosmotic exposure on the cell nucleus of rat primary hepatocytes. To determine the extent of cell swelling on rat primary hepatocytes cell nucleus diameters were measured in rat primary hepatocytes, which were exposed to (**A**) normo- (305 mosm/L) or (**B**) hypoosmotic medium (225 mosm/L) over a duration of 5 min. (**C**) Example of measurement of the cell nucleus diameter. (**D**) Mean cell nucleus diameters were compared between normo- and hypoosmotic condition using *cellSens Dimension* software. For statistical analysis, the diameters of a total of 80 nuclei were assessed. Statistical analysis was carried out by unpaired student's t-test. Data are shown as average ± SEM with *** $p<0.001$.

With the aim to investigate whether hypoosmotic-induced overexpression of miR-141-3p can be mimicked in isolated primary rat hepatocytes, miQPCR was conducted for the relative quantification of miR-141-3p levels. As depicted in Figure 3.7, miR-141-3p levels remained stable within 3 h of normo- and hypoosmotic exposure. However, after 24 h of hypoosmotic exposure miR-141-3p expression levels increased to 2.17-fold (± 0.27, p=0.006), while it remained stable under normoosmotic exposure.

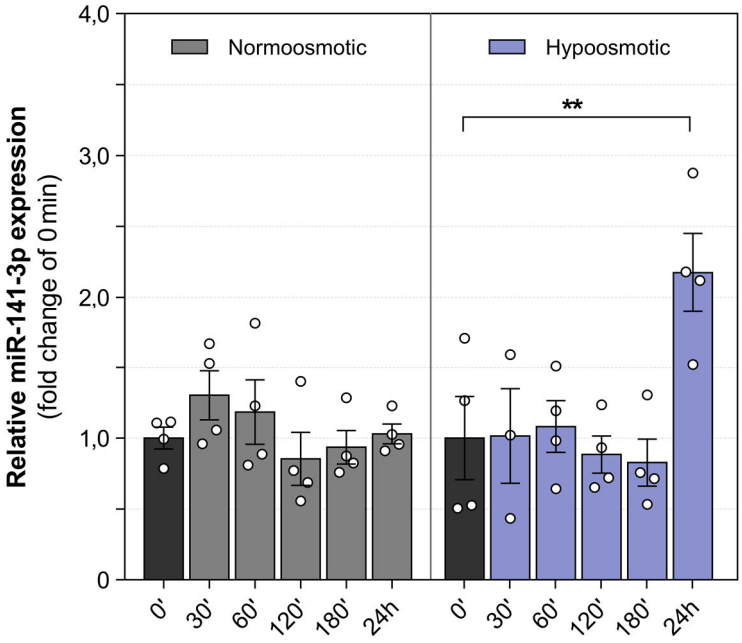

Figure 3.7 Quantitative qPCR analysis of miRNA miR-141-3p in primary rat hepatocytes in response to normo- and hypoosmotic exposure. Isolated primary rat hepatocytes were treated with normo- (305 mosm/L) or hypoosmotic medium (225 mosm/L) for up to 24 h. Following RNA isolation, miRNA expression was analyzed using miQPCR (n=3-4). miRNA levels were median normalized by scaling the samples to their median value [226]. Statistical analysis was carried out by one-way ANOVA. Data are shown as average ± SEM with ** $p<0.01$.

Next, qPCR was conducted to assess whether the selected putative target mRNAs of miR-141-3p shown in Figure 3.5 are inversely related to miR-141-3p levels in isolated primary rat hepatocytes as well (Fig. 3.8). After 24 h of hypoosmotic exposure to primary rat hepatocytes *Slc39a10* were significantly downregulated to 0.40-fold (± 0.03, $p=0.006$), *Dstyk* to 0.68-fold (± 0.06, $p=0.016$), *Rab30* to 0.75-fold (± 0.06, $p=0.042$), *Cdc25a* to 0.58-fold (± 0.04, $p=0.022$), *Dmxl1* to 0.64-fold (± 0.03, $p=0.041$), and *Nfat5* to 0.38-fold (± 0.02, $p=0.002$) as compared to normoosmotic control.

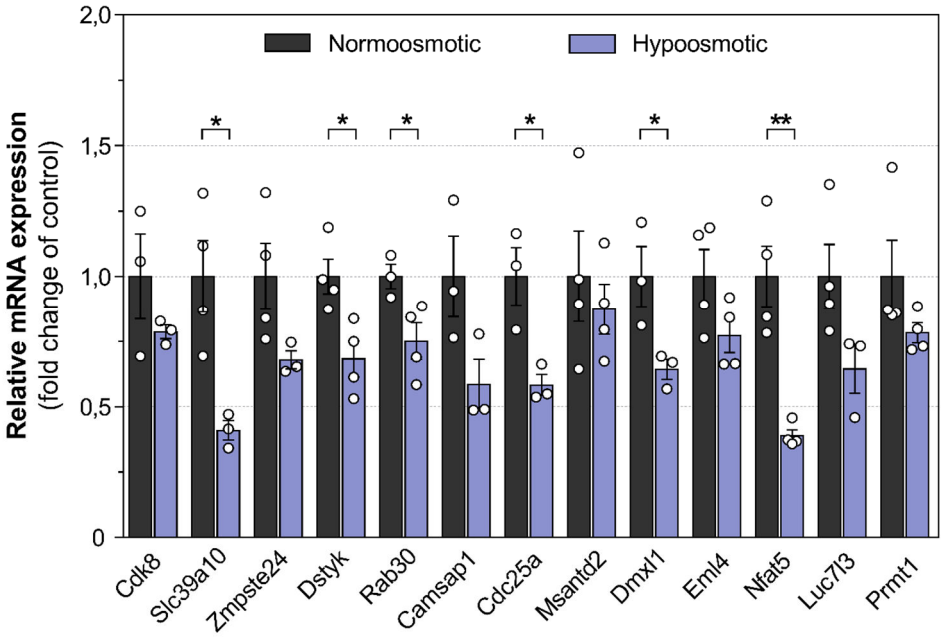

Figure 3.8 Quantitative qPCR analysis of putative target mRNA of miR-141-3p in primary rat hepatocytes in response to normo- and hypoosmotic exposure. Isolated primary rat hepatocytes were treated with normo- (305 mosm/L) or hypoosmotic medium (225 mosm/L) over a time course of up to 24 h. Following RNA isolation, mRNA expression was analyzed using qPCR (n=3-4). qPCR runs were normalized to *Rps6* mRNA levels. Statistical analysis was carried out by student's t-test. Data are shown as average ± SEM with * $p<0.05$.

Cdk8, *Zmpste24*, *Camsap1*, *Msantd2*, *Eml4*, *Luc7l3*, and *Pmrt1* mRNA levels showed a tendency towards downregulation, without reaching significance. Overall, all selected putative target mRNAs of miR-141-3p showed decreased mRNA levels after 24 h of hypoosmotic exposure in comparison with normoosmotic controls. Collectively, these data indicate that the effect of hypoosmotic exposure in rat liver perfusions can be mimicked in isolated primary rat hepatocytes, resulting in enriched miR-141-3p levels and decreased mRNA levels of selected putative target genes.

3.5 Overexpression of miR-141-3p in primary rat hepatocytes

To evaluate whether overexpression of miR-141-3p is sufficient to induce downregulation of putative target mRNAs, miR-141-3p mimic transfections were conducted in isolated primary rat hepatocytes. Figure 3.9 displays the successful overexpression of miR-141-3p in isolated primary rat hepatocytes. Cellular levels of miR-141-3p were enriched by 2,033-fold (p=0.004) at 24 h and by 6,800-fold (p=0.001) at 48 h post transfection, indicating a successful overexpression of miR-141-3p in the target cells.

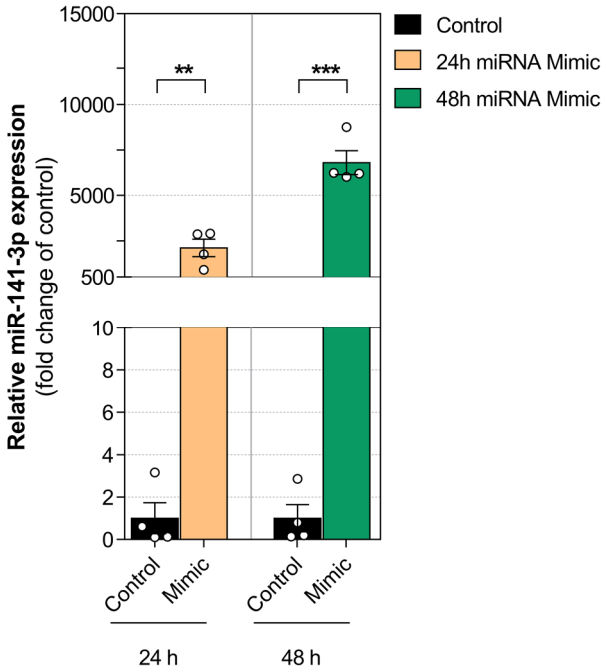

Figure 3.9 Quantitative qPCR analysis of cellular miR-141-3p levels in miR-141-3p mimic transfected primary rat hepatocytes. Primary rat hepatocytes were transfected with miR-141-3p mimic for 24 or 48 h. Control groups were mock-transfected in absence of miR-141-3p mimic. Cells were washed, lysed, RNA was isolated, and miRNAs were quantified using miQPCR. miRNA levels were median normalized by scaling the samples to their median value [226] and statistical analysis was carried out by student's t-test (n=3). Data are shown as average ± SEM with ** $p<0.01$ and *** $p<0.001$.

In the next step, levels of selected target mRNA candidates were investigated via qPCR. Figure 3.10 shows the relative amount of selected mRNA levels after 24 h (A) and 48 h (B) post mimic transfection. A tendency for downregulation after 24 h post transfection was observed for the putative target mRNA *Nfat5* ($p=0.067$), however without reaching significance (Fig. 3.10 A).

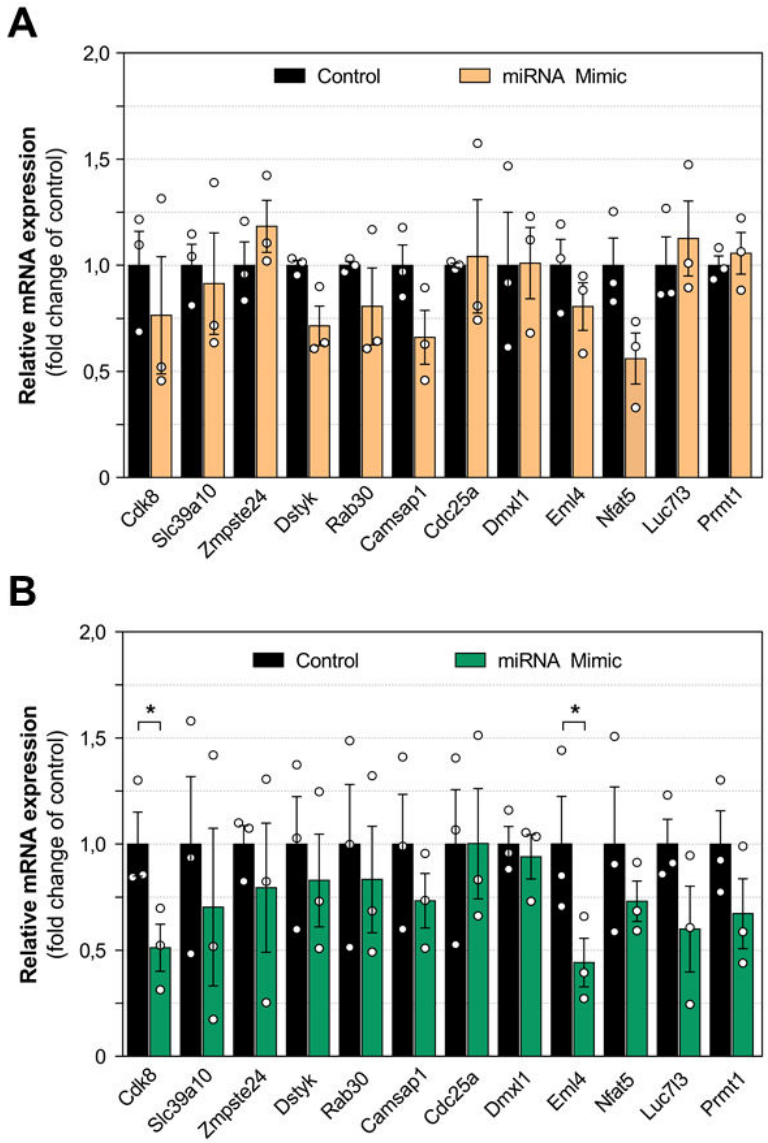

Figure 3.10 Relative mRNA levels of putative miR-141-3p target mRNAs in primary rat hepatocytes transfected with miR-141-3p mimic. Primary rat hepatocytes were transfected with miR-141-3p mimic for 24 h (**A**) or 48 h (**B**). Control groups were mock-transfected in absence of miR-141-3p mimic. Cells were washed, lysed, RNA was isolated, and mRNAs were quantified using qPCR. qPCR runs were normalized to *Rps6* mRNA levels. Data represent average ± SEM of 3 independent experiments. Statistical analysis was carried out by student's t-test with * $p<0.05$.

After 48 h, however, a significant downregulation of *Cdk8* mRNA by 0.49-fold (± 0.11, $p=0.047$) and *Eml4* mRNA by 0.56-fold (± 0.11, $p=0.026$) was observed in cells transfected with miR-141-3p mimic in comparison to control cells. *Nfat5* mRNA levels ($p=0.078$) showed a tendency for downregulation, although the effects did not match statistical significance.

3.6 Validation of *Cdk8* as a target gene of miR-141-3p

As an important regulator of cell cycle progression, *Cdk8* was selected for further target validation. For this purpose, binding site analysis was conducted using the miRNA target discovery algorithm *RNA22*. *RNA22* identifies binding sites by screening the complementarity of the selected miRNA and the transcript and the folding energy which is released upon formation of the miRNA-mRNA heteroduplex [232]. This bioinformatic approach revealed that the 3'UTR of *Cdk8* mRNA harbors two potential binding sites (miRNA response elements - MREs) for miR-141-3p, as depicted in Figure 3.11.

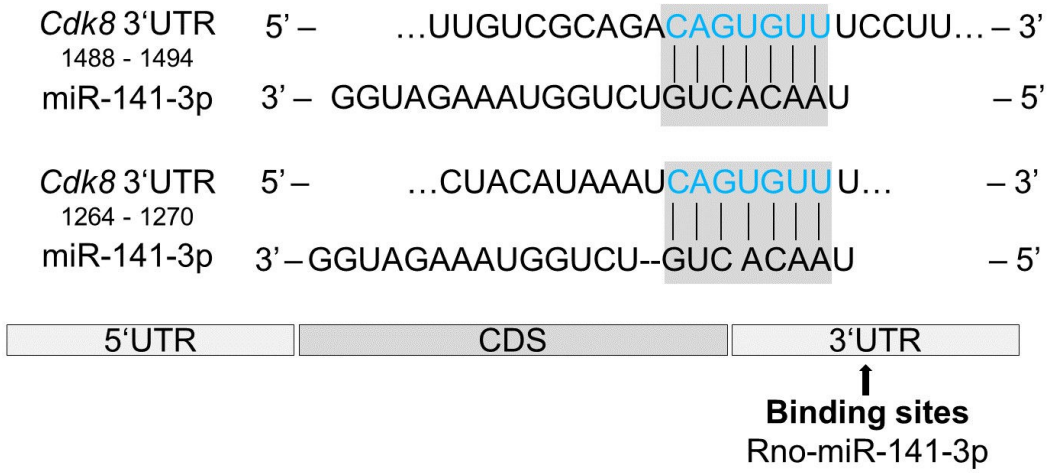

Figure 3.11 Putative miR-141-3p binding sites on the 3'UTR of rat *Cdk8* mRNA. *RNA22* predicted two binding sites for miR-141-3p in the 3'UTR of rat *Cdk8* mRNA. Black lines indicate predicted base pairing between miR-141-3p and target sequence. The seed sequence of miR-141-3p is indicated in grey boxes and corresponding nucleic acids are displayed in blue font.

The miRNA target discovery algorithm *RNA22* suggests that *Cdk8* mRNA may be directly targeted by miR-141-3p on two different binding sites encoded in the 3'UTR. Previous analyses presented in this study displayed that upregulation of miR-141-3p decreased the mRNA levels of *Cdk8* (Fig. 3.5, Fig. 3.8, and Fig. 3.10 B). To further assess and verify the direct interaction between miR-141-3p and *Cdk8* mRNA, a luciferase-based reporter assay was performed (Section 2.2.14). For this purpose, the full-length sequence of *Cdk8* 3'UTR was cloned into pMir(+) and pMir(-) reporter plasmids, whereas pMir(-) serves as a negative control plasmid. The recombinant luciferase plasmids were transfected into HEK293 in presence or absence of miR-141-3p mimic, respectively.

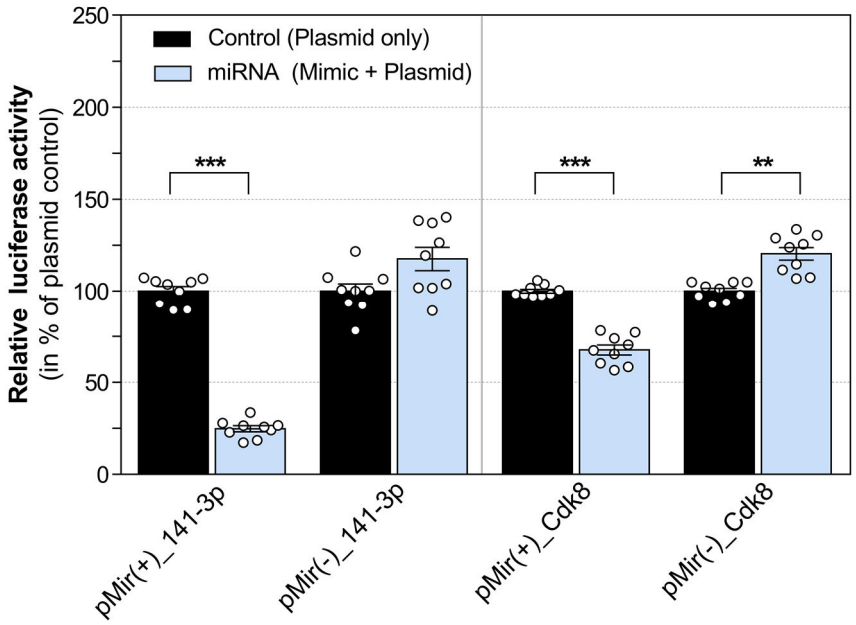

Figure 3.12 Validation of rat *Cdk8* 3'UTR as a direct target site for miR-141-3p. HEK293 cells were transfected with recombinant plasmids either in absence (black) or in presence of miR-141-3p mimic (light blue). Luciferase activity was measured from cell lysates 24 h post transfection. Data are represented as percentage ± SEM of 3 independent experiments. As control, luciferase activity in absence of miR-141-3p was set to 100%. Asterisks indicate significant differences between groups, student´s t-test with significance level ** $p<0.01$, *** $p<0.001$.

Figure 3.12 displays the luciferase activity of pMir(+)_141-3p transfected cells which were co-transfected with miR-141-3p mimic or mock transfected. In presence of miR-141-3p mimic luciferase activity was significantly decreased to 24.7% (± 1.6%, p=0.001) after 24 h post transfection. These data indicated that the product of pMir(+)_141-3p vector harbors a perfect miR-141-3p MRE. Luciferase activity from cells transfected with pMir(-)_141-3p, which harbored the perfect miR-141-3p binding site in its inverse orientation (negative control), was not inhibited by the co-transfection with miR-141-3p mimic (Fig. 3.12). A significant change in luciferase activity was observed in cells transfected with pMir(+)_Cdk8. In presence of miR-141-3p mimic luciferase activity was decreased to 67.5% (± 2.6%, p=0.001) in comparison to cells transfected with plasmid in absence of miR-141-3p mimic. In cells transfected with pMir(-)_Cdk8, luciferase activity was increased by 20.3% (± 3.4%, p=0.005) in presence of miR-141-3p mimic. To summarize, the observed changes in luciferase activity can be ascribed to the binding of miR-141-3p to the luciferase transcript, resulting in a miRNA-mediated repression, thus leading to decreased luciferase protein levels. Therefore, these data provided the evidence for a direct interaction between miR-141-3p and the cloned 3'UTR of *Cdk8* mRNA as illustrated in Figure 3.11.

3.7 Expression of miR-141-3p and *Cdk8* mRNA after partial hepatectomy (PHx).

Studies from Gao *et al.* showed that miR-141-3p plays a role in cell proliferation in different types of tissues [233], but whether miR-141-3p and *Cdk8* may also be involved in proliferative processes in the liver is not yet confirmed. To investigate an involvement of miR-141-3p and *Cdk8* in proliferative processes like liver regeneration, quantitative PCR analysis of miR-141-3p and *Cdk8* mRNA expression levels was conducted with tissue from livers of 10 weeks old rats, in whom PHx had been performed and who recovered from this drastic surgical measure for a period of up to 14 days (Fig. 3.13).

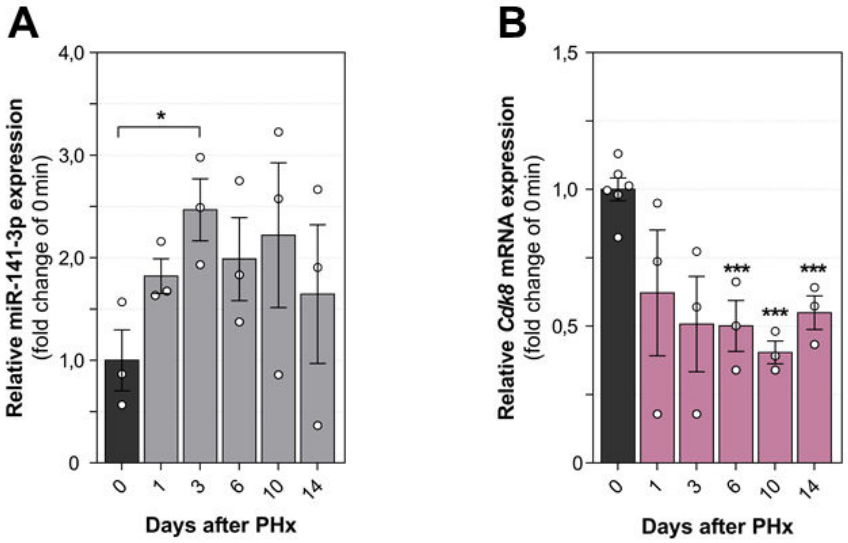

Figure 3.13 Effects of partial hepatectomy on levels of miR-141-3p and *Cdk8* mRNA in rat livers. Rats at the age of 10 weeks were subjected to partial hepatectomy (PHx) as described by Higgins *et al.* [113]. Rats were sacrificed after 0-14 days as indicated. Hepatic RNA was isolated and levels of miR-141-3p and *Cdk8* were analyzed by qPCR. (**A**) Levels of miR-141-3p in the livers of partial hepatectomized rat. miRNA levels were median normalized by scaling the samples to their median value [226]. (**B**) Relative *Cdk8* levels in the liver of rat subjected to PHx. qPCR runs were normalized to *Rps6* mRNA levels. Statistical analysis was carried out by one-way ANOVA (n=3-6, data are shown as average ± SEM with * $p<0.05$ and *** $p<0.001$).

As illustrated in Figure 3.13 A, the levels of miR-141-3p transiently increased by 1.82-fold (± 0.16, $p=0.07$) after 1 day and 2.46-fold (± 0.3, $p=0.02$) after 3 days after PHx, when parenchymal and non-parenchymal cells proliferate to reconstitute the liver mass. At later time points during liver regeneration, no significant upregulation of miR-141-3p was observed. In contrast, *Cdk8* mRNA levels decreased, showing the lowest values 10 days after PHx (0.4-fold ± 0.04, $p=0.001$, Fig. 3.13 B). These findings suggest that miR-141-3p and its target gene *Cdk8* might be involved in liver regeneration and associated with cell proliferation.

3.7 Mechanical stimulation of isolated primary rat hepatocytes

The stretching of liver cells occurs during hypoosmotic induced cell swelling, cell division, and liver regeneration [114,234]. Mechanical stimulation of cells is sensed by several mechanisms that also include integrins resulting in Src-, Erk-, and $p38^{MAPK}$ signaling [235]. This process is referred to as 'mechanotransduction' [116]. To gain further insights into potential factors which enable the upregulation of miR-141-3p, rat primary hepatocytes exposed to a mechanical stimulation were investigated. For this reason, isolated rat primary hepatocytes were seeded on flexible thin silica membrane chambers (STB-100, STREX), which allows the appliance of a tractive force.

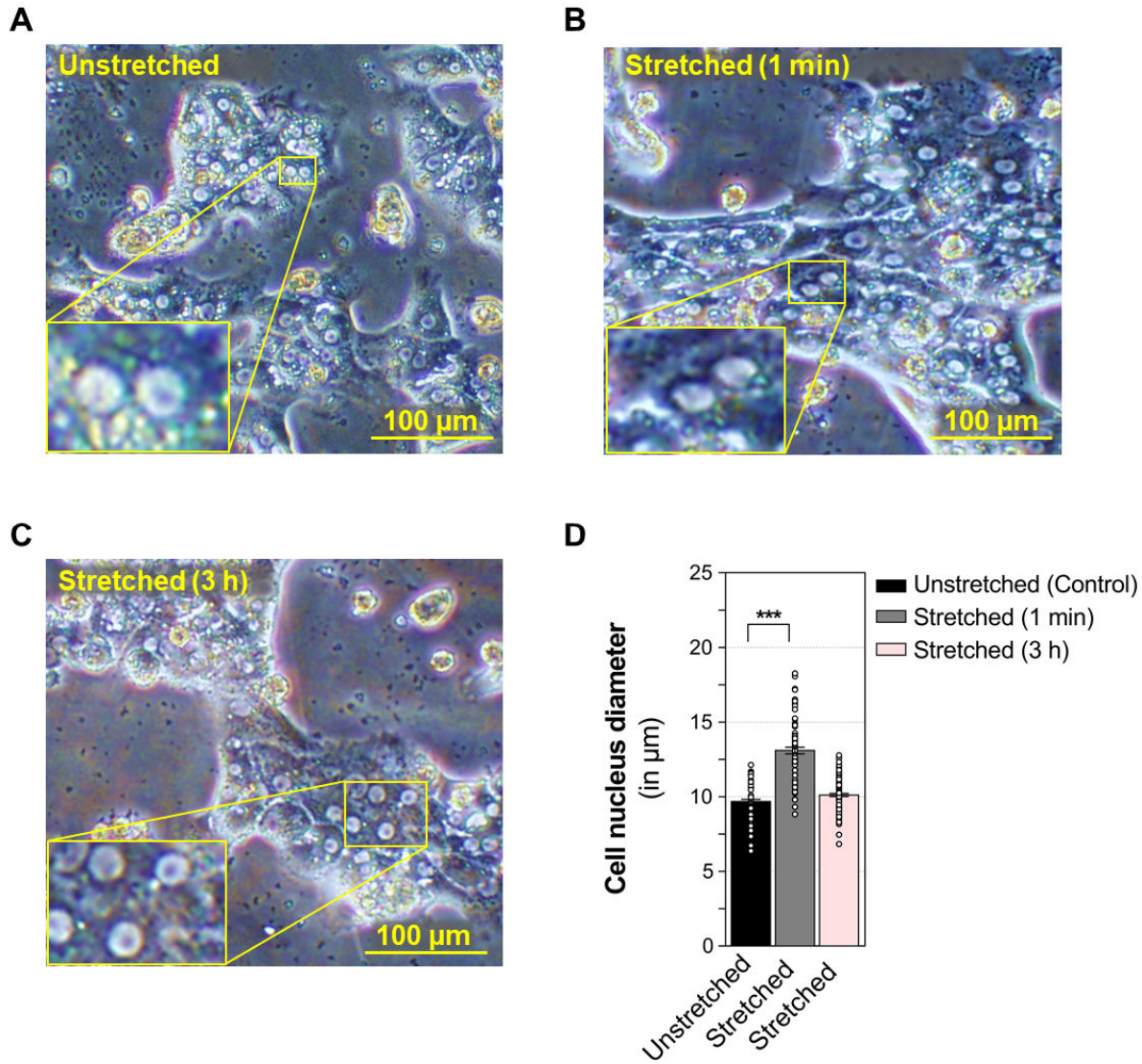

Figure 3.14 Effect of mechanical stimulation on cell nucleus diameters of primary rat hepatocytes. Primary rat hepatocytes were seeded on silicone stretch chambers and remained unstretched (**A**) or were stretched (**B** and **C**). Representative images of groups of nuclei are displayed in 2-3-fold magnification in the left lower corner. (**D**) Mean cell nucleus diameters were compared between stretched and unstretched primary rat hepatocytes using *cellSens Dimension* software. For statistical analysis, the diameters of a total of 80 nuclei were assessed. Statistical analysis was carried out by unpaired student's t-test. Data are shown as average ± SEM with *** $p<0.001$.

Figure 3.14 depicts microscopical images on isolated primary rat hepatocytes seeded on silicone stretch chambers which remained unstretched (Fig. 3.14 A) or which were subjected to stretching (Fig. 3.14 B and C). Cell nucleus diameters were measured and the average unstretched cell nucleus showed a diameter of 9.7 µm (± 1.2 µm), whereas stretched cells exhibited an increased diameter of 12.8 µm (± 2.1 µm). The mechanical stimulation resulted in an increased cell nucleus diameter by 31.6% (p=0.001). After 3 h of stretching the cells reshaped back to their initial size and their cell nucleus turned back to an average of 10.0 µm (± 1.3 µm). All measurements were taken immediately after the stretching of the cells. The effect of mechanical stretching on the relative levels of miR-141-3p and *Cdk8* mRNA in hepatocytes was investigated by miQPCR and qPCR, respectively.

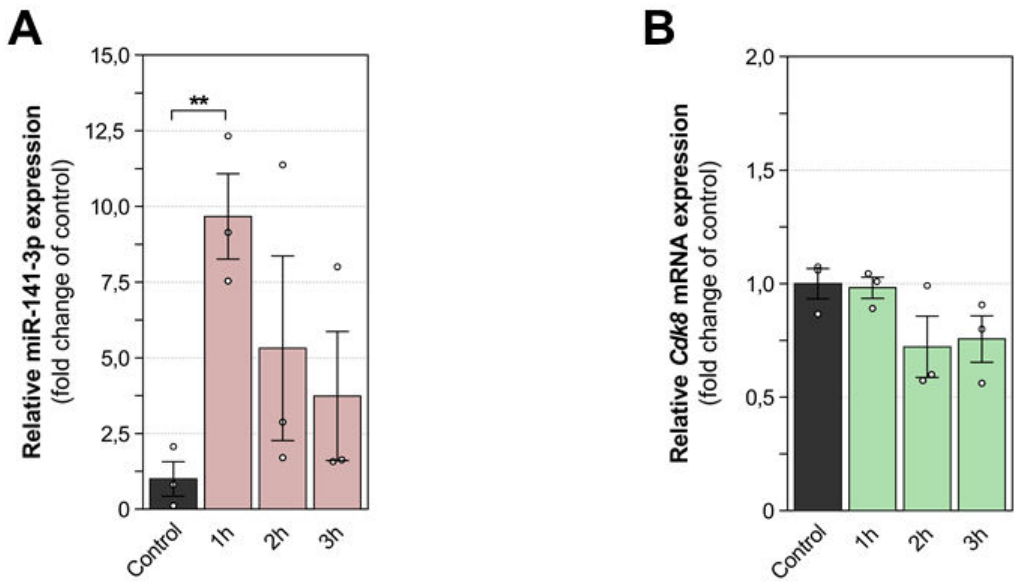

Figure 3.15 Effect of mechanical stimulation on miR-141-3p and *Cdk8* mRNA expression in primary hepatocytes. Primary rat hepatocytes were seeded on silicone stretch chambers and either stretched by roughly 30% or remained unstretched as a control. **A**) Levels of miR-141-3p in primary rat hepatocytes during cell stretching at indicated time points. **B**) *Cdk8* mRNA amount in primary rat hepatocytes during stretching. The cells were washed, lysed, and RNA was isolated. Levels of miR-141-3p were analyzed by miQPCR, *Cdk8* mRNA amounts were analyzed by qPCR, and values were normalized to *Rps6* mRNA levels. miQPCR data were median normalized by scaling the samples to their median value [226]. Statistical analysis was carried out by one-way ANOVA (n=3, data are shown as average ± SEM with ** p<0.01).

Expression of miR-141-3p was increased to 9.67-fold (± 1.4, p=0.004) 1 h after stretching of hepatocytes. miR-141-3p expression was increased to 5.31-fold (± 3.0) after 2 h, and to 3.72-fold (± 2.1) after 3 h, but without reaching significance as illustrated in Figure 3.15 A. In contrast, *Cdk8* mRNA levels remained stable for 1 h after cell stretching and showed a tendency towards downregulation after 2 h (0.72-fold ± 0.1) and 3 h (0.75-fold ± 0.1), without reaching significance (Fig. 3.15 B).

Altogether, the cell stretching accompanied by an enrichment in miR-141-3p levels did not influence *Cdk8* mRNA levels on the same level as seen after hypoosmotic exposure (Fig. 3.5 and Fig. 3.8), mimic transfection (Fig. 3.10 B), and PHx (Fig. 3.13 B). It is therefore conceivable that *Cdk8* mRNA expression levels may also be influenced by other factors such as growth factors released by neighboring cells of hepatocytes or ion channels which may not be responsive to the application of a mechanical stimulus.

3.8 Rat liver perfusions with Src-, Erk-, and p38^{MAPK} inhibitors

Hypoosmotic exposure results in an activation of $\alpha_5\beta_1$- integrins signaling and a subsequent activation of Src-, Erk-1/Erk-2, and p38^{MAPK} kinases [235]. To investigate the potential role of these osmosensing and osmosignaling pathways in the observed upregulation of miR-141-3p, rat liver perfusion were conducted in presence of Src (PP-2), Erk-1/2 (PD098059), and p38^{MAPK} (PD169316) inhibitors.

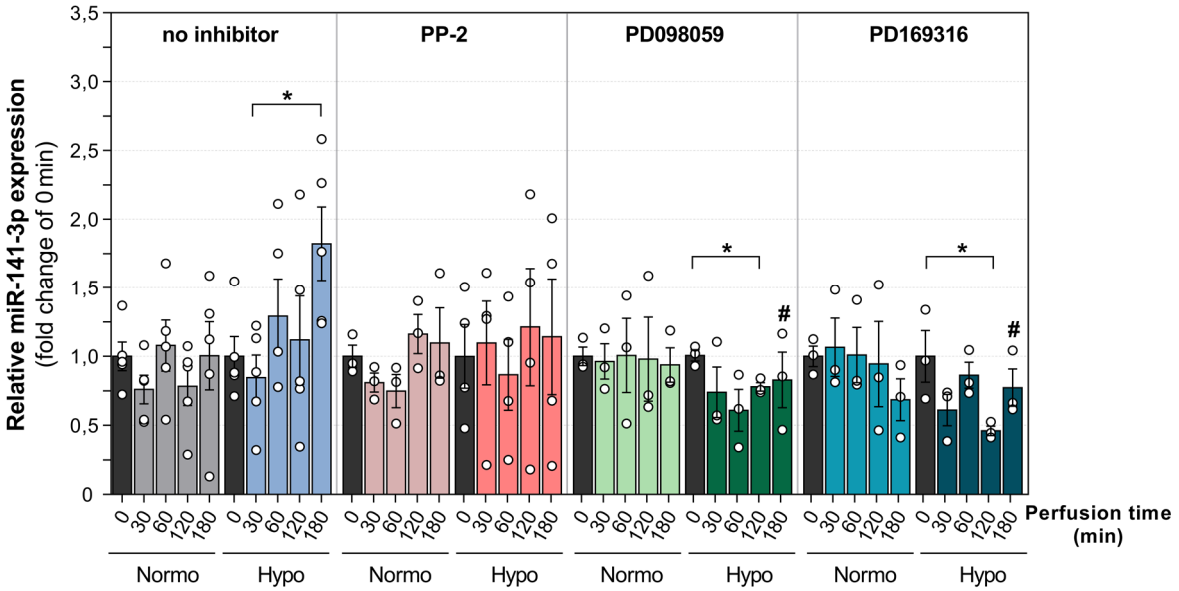

Figure 3.16 Analysis of miR-141-3p levels by hypoosmolarity in presence of Src-, Erk-, and p38^{MAPK}-inhibitiors. Rat livers were perfused with normo- (305 mosm/L) or hypoosmotic (225 mosm/L) medium for 0-180 min. Inhibitors of Src (PP-2, 250 nM), Erk (PD098059, 500 nM) and p38 (PD169316, 250 nM) were added to the perfusate as indicated. After initialization of perfusion, liver lobes were dissected at the indicated time points, RNA was isolated, and miR-141-3p expression was quantified by miQPCR. Data represent the relative levels of miR-141-3p as percentage to the preperfusion state (0 min). miRNA levels were median normalized by scaling the samples to their median value [226]. Statistical analysis was carried out by two-way ANOVA. (n=3-4, data are shown as average ± SEM with * p<0.05 for significance against 0 min of the respective condition, # indicates p<0.05 against 180 min of hypoosmotic perfusion with no inhibitors).

Addition of Src inhibitor PP-2 to the perfusate had no significant effect on miR-141-3p expression levels under normo- or hypoosmotic condition but prevented a miR-141-3p upregulation as observed in absence of PP-2 inhibitor (Fig. 3.16 left). Supplementation of the

Erk inhibitor PD098059 to the hypoosmotic perfusion buffer resulted in a transient downregulation of miR-141-3p levels after 60 min with a significant reduction after 120 min to 0.77-fold (± 0.03, p=0.011) in comparison to the preperfusion state (0 min). Addition of Erk inhibitor to hypoosmotic perfusion resulted in a significant lower miR-141-3p level after 180 min of perfusion compared to 180 min of hypoosmotic perfusion with no supplemented inhibitors (# indicates p=0.042). In contrast, normoosmotic controls containing PD098059 in the perfusion buffer remained stable (Fig. 3.16 middle).

Addition of $p38^{MAPK}$ inhibitor PD169316 resulted in a transient downregulation under hypoosmolarity compared to the normoosmotic condition. Expression levels of miR-141-3p decreased after 30 min to 0.61-fold (± 0.11, p=0.149) and after 120 min significant to 0.46-fold (± 0.03, p=0.046, Fig. 3.16 right). Addition of $p38^{MAPK}$ inhibitor to hypoosmotic perfusion resulted in significant lower miR-141-3p levels compared to 180 min of hypoosmotic perfusion without supplemented inhibitors (# indicates p=0.030). Overall, inhibitor perfusion studies revealed that hypoosmotic-induced miR-141-3p upregulation was abolished under hypoosmotic exposure through addition of Src-, Erk-, and $p38^{MAPK}$ kinases inhibitors. Collectively, these data indicate that miR-141-3p expression levels are dependent on Src-, Erk-, and $p38^{MAPK}$ signaling.

3.9 Rat liver perfusion with colchicine

Hypoosmotic induced osmosignaling and downstream activation of $p38^{MAPK}$ kinase is known to inhibit proteolysis [18]. However, this inhibitory effect resulting from hypoosmotic exposure can be abolished by the addition of colchicine to the perfusate [236]. Colchicine is a well-known microtubule inhibitor, which prevents microtubule assembly and therefore inhibits the microtubule- and $p38^{MAPK}$-dependent autophagic proteolysis [237]. To further investigate the involvement of $p38^{MAPK}$ in hypoosmolarity-induced effects on miR-141-3p levels in liver cells (e.g. involvement in metabolic processes), rat liver perfusions in presence of colchicine were conducted.

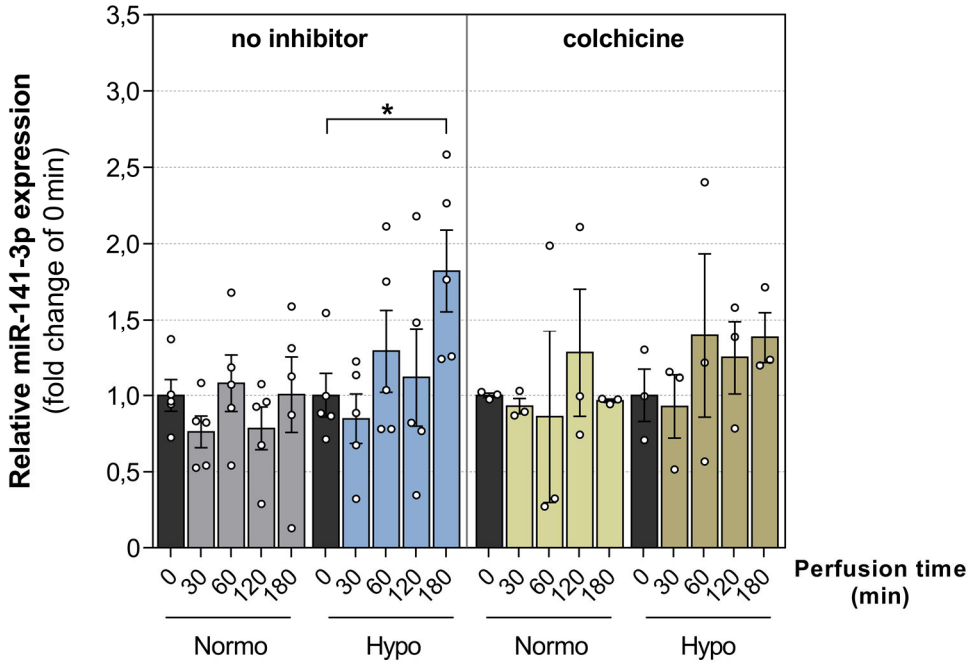

Figure 3.17 Analysis of miR-141-3p levels by hypoosmolarity in presence of colchicine. Rat livers were perfused with normo- (305 mosm/L) or hypoosmotic (225 mosm/L) medium for 0-180 min. Colchicine (500 nM) was added to the perfusate as indicated. After initialization of perfusion, liver lobes were dissected at the indicated time points, RNA was isolated and miR-141-3p expression was quantified by miQPCR. Data represent the relative expression of miR-141-3p as percentage to the preperfusion state (0 min). miRNA levels were median normalized by scaling the samples to their median value [226]. Statistical analysis was carried out by two-way ANOVA (n=3, data are shown as average ± SEM with * $p<0.05$).

Addition of colchicine to the perfusate resulted in lower miR-141-3p expression levels under hypoosmolarity compared to hypoosmotic perfusion without the addition of colchicine. Under hypoosmotic condition the addition of colchicine to the perfusate induced a moderate miR-141-upregulation to 1.38-fold (± 0.16) after 180 min of perfusion compared to normoosmotic control (Fig. 3.17 right). No significant changes in miR-141-3p levels were observed in comparison with rat liver perfusion in absence of colchicine (Fig. 3.17 left). Altogether, these data indicate that the addition of colchicine to the perfusate prevented miR-141-3p increase in perfused rat liver under hypoosmolarity.

4. Discussion

Liver cells face constant challenges to their cellular volume either through extracellular osmolarity or changes in intracellular solute content. These volume perturbations are counteracted by activation of specific membrane transporters and/or metabolic processes, which result in net solute loss or gain. Osmosensing and osmosignaling pathways are known which couple cellular volume to gene expression, proliferation, and apoptosis. However, the role of miRNAs regarding liver cell environment and the downstream osmosignaling pathways, which are coupled to hypoosmotic exposure, is largely unknown. This study aimed to analyze miRNA and mRNA expression differences during hypoosmotic exposure in perfused rat liver, and to identify miRNAs which are involved in the osmosignaling pathway. Based on bioinformatic approaches, 249 osmosensitive mRNAs were identified to be putatively targeted by a single miRNA, miR-141-3p. Using quantitative PCR analysis, miR-141-3p was found to be significantly upregulated under hypoosmotic condition in perfused rat liver, while selected putative target mRNAs were significantly downregulated. This effect was also observed in isolated primary rat hepatocytes, where individual mRNAs were also found to be downregulated after miR-141-3p upregulation. A luciferase reporter-based assay was performed to validate *Cdk8* mRNA*,* which is involved in critical cellular processes, such as transcription or cell cycle, as a direct target of miR-141-3p [238]. The role of miR-141-3p in the osmosignaling pathway under hypoosmolarity was investigated by inhibitor perfusion studies. This approach revealed that miR-141-3p levels were significantly affected by Erk and $p38^{MAPK}$ inhibition. Inhibition of Erk and 38^{MAPK} led to a significant downregulation of miR-141-3p under hypoosmotic condition. In addition, miR-141-3p and *Cdk8* mRNA levels were analyzed after partial hepatectomy (PHx), a condition exposing liver cells to persistent mechanical stress due to hyperperfusion. Primary rat hepatocytes were subjected to mechanical stimuli, to assess their potential role in proliferation and liver regeneration, since PHx also subjects the liver cells to increased mechanical forces due to the increasing blood volume passing through the blood vessels [234].

4.1 Hypoosmolarity leads to differential miRNA and mRNA levels

Microarray chip analysis of miRNA and mRNA levels of hypoosmotic perfused rat livers revealed differentially expressed miRNAs and mRNAs after 180 min of perfusion. Only 9 (1.2%) of 728 miRNAs were found to be significantly downregulated, and 22 (3.0%) miRNAs being significantly upregulated. Thus, the number of differentially expressed miRNAs under hypoosmolarity compared to the normoosmotic controls seems to trigger very specific changes in miRNA levels. Several upregulated miRNAs found by microarray analysis, such as miR-338-5p, miR-18a-5p, and miR-155-3p were already identified by other studies to promote

cell proliferation and/or inhibit apoptosis [239]. For example, miR-18a-5p was found to promote proliferation, migration, and invasion by targeting *fructose-bisphosphatase 1* (*FBP1*) in liver cells [240], whereas Tang *et al.* discovered that miR-155-3p promotes proliferation by suppressing *f-box and wd repeat domain containing 7* (*FBXW7*) expression in the liver [241]. These results underline the effects facilitated by hypoosmotic exposure to liver cells, since cell swelling was shown to correlative with enhanced cell proliferation [68,82].

Gene chip analysis of hypoosmotic perfused rat liver revealed 609 (2.8%) significantly downregulated and 534 (2.5%) significantly upregulated mRNA compared to normoosmotic control. Interestingly, mRNA encoding for heat-shock protein 70 (Hsp70), which is upregulated in cells exposed to hyperosmolarity [242,243], was also found to be significantly elevated under hypoosmotic condition in the present microarray analysis. Under hyperosmolarity, *Hsp70* gene expression is activated by the denaturation of proteins, which is induced by hyperthermia [244]. Enrichment of *Hsp70* mRNA is known to be accompanied by many types of stress, fulfilling the role of stabilizing native protein structures and prevent harmful accumulation of denatured proteins. Kurz *et al.* also observed higher *Hsp70* mRNA levels in primary rat hepatocytes under hypoosmotic exposure when a heat shock was applied to the cells compared to normoosmotic control [245]. In agreement with previous data by Kurz *et al.*, enriched *Hsp70* mRNA levels in hypoosmotic perfused rat livers compare well to those found in primary rat hepatocytes exposed to a heat shock followed by hypoosmotic condition [245]. These findings may indicate that increased *Hsp70* mRNA levels under hypoosmolarity assist in the prevention of aggregation and misfolding of proteins.

Moreover, *heat-shock transcription factor 1* (*Hsf1*) is induced by hypertonic shock with the same intensity which can be found by the activation via application of a heat shock [121]. *Hsf1* is a stress-induced transcription factor, that binds to the promoter region of heat-shock proteins (HSPs) to regulate their transcription [246]. Microarray analysis of perfused rat liver exposed to hypoosmolarity revealed *Hsf1* and *Hsf2* were both significantly downregulated after 180 min of hypoosmotic exposure compared to normoosmotic control (Fig. 3.2). Thus, hypoosmolarity led to an opposite regulation of *Hsf1* and *Hsf2*. Hypoosmotic and hyperosmotic exposure represent two opposing physical forces - which when applied to the living cell - can result in different physiological responses and functions, including different signaling pathways (Fig. 1.2). Therefore, it is conceivable that the upregulation of *Hsf1* and *Hsf2* mRNA is required only for the cellular response to hyperosmolarity, while other genes may be major players in the cellular response to hypoosmolarity.

In the recent extension of this work, a potential player in nutrient and osmosignaling pathways, *transcription factor EB* (*Tfeb*) was significantly downregulated under hypoosmotic conditions compared to normoosmotic controls (Bardeck *et al.* [247]). *Tfeb* is involved in the function and biogenesis of the endo-lysosomal compartment, which includes membrane trafficking and autophagy [248,249]. During autophagy, which is a catabolic process, *Tfeb* mRNA levels are increased [249]. However, cell swelling is considered as an anabolic signal, leading to the inhibition of proteolysis [16,24–26], which might be the reason for decreased *Tfeb* mRNA levels.

Overall, microarray analysis of differentially expressed mRNAs revealed that the effect of hypoosmolarity on perfused rat livers only affected a small fraction of the liver transcriptome. These changes point towards the specificity of the swelling signal, which were also observed in previous studies performed by Warskulat *et al.* [250]. They discovered that hyperosmotic exposure led to an increase of the mRNA levels of *tyrosine aminotransfer*ase (*Tat*) and *phosphoenolpyruvate carboxykinase* (*Pepck*), whereas hypoosmotic exposure to H4IIE rat hepatoma cells decreased their mRNA levels by about 40%. These data are in accordance with our microarray chip analysis of hypoosmotic perfused rat livers, where *Tat* and *Pepck* mRNA levels were also decreased by similar amounts. This effect may be explained by the increased stimulation of glycolysis and glycogen synthesis, which are both sensitive to cell swelling [15]. As a main control point for the regulation of gluconeogenesis, Pepck catalyzes the formation of phosphoenolpyruvate from oxaloacetate and the expression of the *Pepck* gene can also be affected by insulin and glucagon [251,252]. Both hormones affect the cellular hydration level, allowing the hypothesis that *Pepck* mRNA levels are directly affected by the cellular hydration level. Long-term effects of hypoosmotic exposure to rat livers regarding the mRNA level have already been described in the past. For instance, enriched mRNA levels for *tubulin* [23,237], *β-actin* [35], *ornithine decarboxylase* [253], and *c-jun* [254] were found in rat liver perfusion and primary rat hepatocytes in response to hypoosmolarity. Our microarray analysis also found *actin beta* (*Actb*) and *ornithine decarboxylase* (*Odc1*) at increased levels. Hypoosmotic exposure to liver cells leads to alterations of the cellular shape and can alter cytoskeletal rearrangements, thus leading to changes in the expression patterns of proteins like Actb, which are required for the cytoskeletal structure.

In the next step, downregulated mRNAs were investigated for possible binding sites for miRNAs which were upregulated in rat livers following perfusion wit hypoosmotic medium. Remarkably, *TargetScan* and *miRWalk* revealed that out of 609 downregulated mRNAs, 249 (41%) mRNAs were putatively targeted by miR-141-3p (Fig. 3.3 A). The GO enrichment analysis revealed the involvement of miR-141-3p target gene candidates in various cellular

processes, including the regulation of cell cycle, metabolic processes, and the biosynthesis of cellular macromolecules (Fig. 3.3 B). These findings are in accordance with effects found in cells affected by hypoosmotic exposure (e.g. enhanced proliferation and altered metabolism), thus making miR-141-3p an interesting target for further investigation.

miR-141-3p belongs to the miR-200 family which is composed of five highly conserved miRNAs: miR-200a/200b/200c, miR-141, and miR-429 [255]. It is established, that miR-141-3p is implicated in different types of oncogenesis, but its function in the liver is still not clarified [256–258]. The miR-200 family members are mainly recognized as tumor suppressors, but depending on the cellular context the biological functions of the miR-200 family are subject to change and may also exert tumor promoting effects [259]. However, these long-term effects were not investigated in this thesis. miR-200 family members are associated with the formation of cancer stem cells and the regulation of epithelial-to-mesenchymal transition (EMT), in which cells gain migratory and invasive properties resulting in the transition to mesenchymal stem cells [260–262]. miR-141-3p inhibits cell proliferation and invasion by targeting mitogen-activated protein kinase 4 (*MAP4K4*) [263], but in contrast may also act as an oncogene in ovarian and colon cancers [264,265]. These findings suggest that miR-141-3p has various roles which may depend on its specific target in different cell types or tissues.

4.2 Downregulation of downstream target genes of miR-141-3p

Hepatic miR-141-3p levels were significantly upregulated after 180 min of hypoosmotic perfusion compared to normoosmotic control (Fig. 3.4). Upregulation of miR-141-3p after 180 min of rat liver perfusion is an experimental model for mimicking long-term effects of hypoosmotic exposure, since liver cells regain their original cell volume within minutes with the help of RVD mechanisms.

To elaborate the role and function of miR-141-3p, predicted target gene candidates which play a role in proliferation, cell cycle progression, and cellular metabolism, were selected for further analyses. As shown in Figure 3.5, after 180 min of hypoosmotic perfusion, all selected target gene candidates were significantly or tendentially downregulated on the mRNA level.

Among the downregulated mRNAs, *Nfat5*, also known as a tonicity-responsive enhancer-binding protein, is an important transcription factor involved in the maintenance of cellular homeostasis against hypertonic and hyperosmotic environments [266]. Under hyperosmotic stress the amount and nuclear translocation of *Nfat5* is increased, to accumulate organic osmolytes and restore cell homeostasis [267–269]. *Nfat5* is responsible for the expression of a variety of osmoprotective genes, such as ion transporters, aldose reductase,

and heat shock protein 70 [270]. It was also shown by Zhu *et al.* that *Nfat5* triggers autophagy by the activation of autophagy related protein 5 (*Atg5*) [271]. As presented in Figure 3.5, *Nfat5* mRNA levels were significantly downregulated after 180 min of hypoosmotic exposure. In contrast, Bounedjah *et al.* identified upregulation of *Nfat5* mRNA under hyperosmotic exposure [272].

In this thesis, the opposing regulation of *Nfat5* mRNA under hypoosmolarity could be a direct result of miR-141-3p upregulation. Therefore, miR-141-3p may be in-part responsible for the restoration of cellular homeostasis by directly binding to *Nfat5* mRNA. However, it cannot be excluded that additional mechanisms may also affect *Nfat5* levels, since *Nfat5* activity is regulated through phosphorylation of signal molecules like Fyn [273], $p38^{MAPK}$, and protein kinase A [274,275]. Furthermore, activation of *Nfat5* and downstream activation of autophagy is not required during hypoosmolarity which is an anabolic signal, thus leading to the inhibition of proteolysis [27].

Zmpste24 is another putative miR-141-3p target gene candidate downregulated under hypoosmotic condition in perfused rat livers. This gene encodes for a zinc metallopeptidase that is involved in the two step post-translational proteolytic cleavage of prelamin A to form mature lamin A, which is required for the structure of the cell nucleus membrane [276]. Additionally, in human, *ZMPSTE24* is identified as a direct target of miR-141-3p [277]. Here, *ZMPSTE24* mRNA levels were decreased, while miR-141-3p was found to be upregulated during senescence in mesenchymal stem cells. Decreased levels of *ZMPSTE24* mRNA led to an upregulation of prelamin A mRNA in mesenchymal stem cells. These findings lead to the assumption, that by targeting *Zmpste24*, miR-141-3p can directly affect the formation of lamin A which is required during the S-phase of cell division [278].

Another confirmed target of miR-141-3p is *cell division cycle protein 25A* (*Cdc25a*) mRNA. As a dual-specificity protein phosphatase, it is responsible for the progression from G1 to the S phase of the cell cycle [279]. *Cdc25a* removes the inhibitory phosphorylation in cyclin-dependent kinases (CDKs) such as cyclin-dependent kinase 6 (Cdk6), cyclin-dependent kinase 4 (Cdk4), and cyclin-dependent kinase 2 (Cdk2). Qiu *et al.* demonstrated that high miR-141-3p levels decreased the expression of Cdc25a on the protein level, which results in the arresting of cells at G1 phase without triggering cell apoptosis [279]. In hypoosmotic rat liver perfusion and primary rat hepatocytes exposed to hypoosmotic media, *Cdc25a* mRNA levels were significantly downregulated compared to normoosmotic controls. As an important player in cell cycle progression, the activity of Cdc25A on the protein level must be timely and precisely regulated throughout the whole cell cycle. Previous studies confirmed multiple

mechanisms behind the regulation of Cdc25A expression at the transcriptional [280,281], translational [282,283], and post-translational level [284]. Interestingly, Qiu *et al.* observed that miR-141-3p increased the expression of *CDC25A* on the mRNA level and also decreased its expression on the protein level, showing that miR-141-3p affects gene expression on both transcriptional and post-transcriptional level [285]. Again, by targeting *Cdk25a*, miR-141-3p may be in-part responsible for processes which include cell proliferation in the liver. Furthermore, cyclin-dependent kinase 8, a subunit of the regulatory Cdk module of the transcriptional Mediator complex [286] that couples enhancer-binding transcriptional activators to RNA polymerase II for the initiation of transcription [238], was identified as a putative target of miR-141-3p. Cyclin-dependent kinases are involved in critical cellular processes such as transcription or cell cycle. *Cdk8*, unlike better-known members of the Cdk family (e.g. *cyclin-dependent kinase 1* [287] or *cyclin-dependent kinase 2* [288]), is not required for cell cycle progression [286,289] and instead co-regulates several transcription factors, such as *Wnt/β-catenin* [290], serum response network [291], *TGFβ/SMAD* [292], and *NFκB* [293]. *Cdk8* is amplified or overexpressed in many types of cancers, including colon [290], breast [289,294,295], pancreatic [296], and prostate cancer [297]. Many mechanisms of positive regulation of transcription such as the regulation of RNA-polymerase II by Cdk8 have been elucidated [291,298–300] with fewer known mechanisms of negative regulation by Cdk8 in mammalian cells [301]. As a co-regulator of above-mentioned transcription factors, downregulation of *Cdk8* mRNA under hypoosmolarity may play a role in cell growth, cell differentiation, and/or apoptosis. Furthermore, Cdk8 is linked to lipid and glucose metabolism, as well as to the regulation of the cellular response to the depletion of nutrients [301–303]. Knockdown experiments conducted in mammalian cells revealed that Cdk8 kinase activity upregulates the expression of glycolytic enzymes [304]. These findings underline the role of Cdk8 as an oncogene and for stem cell maintenance [305,306], since metabolic changes can be responsible for the alteration in gene expression or the proteome [307]. Additionally, metabolic changes may drive cell differentiation and cancer, whereas cancer cells are heavily dependent on glycolysis [308,309] and differentiated, non-proliferating cells redirect metabolites towards oxidative phosphorylation [310].

Collectively, these data indicate that miR-141-3p may assist in the modulation of various processes, which may contribute to proliferation, cell differentiation, and cellular metabolism, mediated via its downstream target genes.

4.3 Hypoosmolarity leads to miR-141-3p upregulation in primary rat hepatocytes and restoration of cytoskeleton

Hepatocytes constitute the majority of the liver volume and retain most of their functions after isolation and restoration of the cell cytoskeleton [311–313]. To identify a potential source behind enriched miR-141-3p levels under hypoosmolarity, isolated primary rat hepatocytes were exposed to hypoosmotic medium *in vitro*. To measure the extent of swelling, which cells endure during hypoosmotic exposure, microscopical images were taken after cells were exposed to hypoosmotic medium for 5 min and 3 h (Fig. 3.6). Isolated primary rat hepatocytes showed an increased cell nucleus accompanied by an upregulation of miR-141-3p level after 24 h of hypoosmotic exposure compared to normoosmotic controls. Since ambient osmolarity changes were achieved by the addition of raffinose, enrichment of miR-141-3p levels can be explained by changes in osmolarity or cell volume, and not by alterations of extracellular Na^+ or Cl^- ion concentrations. However, the hypoosmotically-induced effect of miR-141-3p upregulation showed a delay of more than 20 h compared to the observed effect in perfused rat livers. Primary rat hepatocytes retain specific hepatocyte properties close to their physiological level, although the *in vivo* state cannot be maintained for long. Discrepancies in the observed effects may also be explained by the missing biological cell matrix of *in vitro* primary rat hepatocytes, which is still preserved in the perfusion experiments. Interaction of different neighboring cell types may be crucial for relevant short-scale signaling transductions. Furthermore, isolated primary rat hepatocytes lack an intact microtubule network, which is required for the antiproteolytic effect of cell swelling [23,314]. Thus, anti-proteolytic effects cannot be shown in isolated primary rat hepatocytes [315], which are characterized by a disintegrated microtubule network [23,69,117]. Taken altogether, these factors may be responsible for a more timely *in vivo* signaling towards miR-141-3p, which can not be shown *in vitro* at early time points. Quantitative analysis of previous selected target gene candidates showed a significant downregulation for *Slc39a10*, *Dstyk*, *Rab30*, *Cdc25a*, *Dmxl1*, and *Nfat5* on the mRNA level. *Cdk8*, *Zmpste24*, *Camsap1*, *Msantd2*, *Eml4*, *Luc7l3*, and *Prmt1* tended to decrease at the mRNA level (Fig. 3.7), thus, exposure of isolated primary rat hepatocytes to hypoosmolarity showed similar results compared to hypoosmotic liver perfusions. Taken together, these data suggests that hepatocytes, which make up to 70% of the liver cell population, may be the primary source for miR-141-3p expression levels in the liver under hypoosmotic condition. These findings solidify the idea that miR-141-3p might influence the expression of various processes, including cell proliferation, cell differentiation, and cell cycle progression via its downstream target genes in the liver. This leads to the assumption, that upregulation of miR-141-3p may be a direct response to hypoosmotic exposure and ultimately

contributes to the modulation of transcriptional events which are interlinked with liver cell swelling [68,82].

4.4 miR-141-3p transfection leads to downregulation of target gene candidates

To further investigate the effects of miR-141-3p on its downstream target genes, mRNA levels of previous selected target gene candidates were analyzed in response to miR-141-3p overexpression in isolated primary rat hepatocytes (Fig. 3.9). After 24 h of miR-141-3p mimic transfection, several genes tended to decrease at the mRNA level, including *Cdk8*, *Dstyk*, *Camsap1*, *Eml4* and *Nfat5*. However, *Cdk8* and *Eml4* were significantly decreased at the mRNA level after 48 h of miR-141-3p mimic transfection, while *Luc7l3* and *Pmrt1* showed tendentially decreased mRNA levels (Fig. 3.10).

Of note, isolated primary rat hepatocytes are extracted from their natural cell matrix, which might be a decisive prerequisite for the interplay of miR-141-3p and its target genes. The moderately affected mRNA levels raise the hypothesis that besides enriched miR-141-3p levels certain additional mechanisms may control the mRNA levels of selected target gene candidates *in vitro*. However, more work is necessary to further investigate the mediating effects of miR-141-3p on its target genes in response to cellular stimuli.

To provide the evidence for a direct interaction between miR-141-3p and *Cdk8* mRNA, a luciferase reporter gene assay was conducted. As shown in Figure 3.11, two possible binding motifs were determined in the 3'UTR of *Cdk8* mRNA, strengthening the idea that miR-141-3p may be in-part responsible for the downregulation of *Cdk8*. Moreover, miR-141-3p mimic transfection inhibited the expression of luciferase by binding directly to the 3'UTR of *Cdk8* mRNA (Fig. 3.12), certifying the miRNA-MRE interaction of *Cdk8* mRNA and miR-141-3p. These findings are in line with bioinformatic analysis conducted with *TargetScan* software and *RNA22* algorithm which revealed two binding sites for miR-141-3p in the sequence of *Cdk8* 3'UTR. Collectively, the luciferase reporter assay provided evidence that *Cdk8* 3'UTR can be confirmed as a direct target of miR-141-3p.

4.5 Role of miR-141-3p and *Cdk8* in liver regeneration

To investigate a possible role of miR-141-3p and its downstream target gene *Cdk8* in liver regeneration, liver tissue from rats recovering from PHx was analyzed. In normal adult livers, hepatocyte proliferation is rarely seen, as most hepatocytes are in the G0 phase of the cell cycle [316,317]. However, after PHx approximately 95% of hepatic cells rapidly re-enter the cell cycle [114]. Quantitative PCR analysis of rat liver tissue revealed that miR-141-3p levels start to increase after 24 h, reaching a significance 36 h after PHx (Fig. 3.13 A). In rats, the

rate of DNA synthesis in hepatocytes is increased after 12 h and peaks around 24 h after PHx [114]. These findings raise the possibility that miR-141-3p upregulation is tied to the proliferative phase of hepatocytes during rat liver regeneration, since transiently upregulated miR-141-3p levels can be observed during and shortly after (i.e. 24 h and 36 h) hepatocyte proliferation. Simultaneously, *Cdk8* mRNA levels show a decrease after 24 h, reaching a significant downregulation after 6, 10 and 14 days after PHx (Fig. 3.13 B). As a direct target of miR-141-3p, downregulation of *Cdk8* mRNA may be a result of increased miR-141-3p levels. These findings point towards an involvement of miR-141-3p and *Cdk8* in rat liver regeneration. Ko *et al.* also reported the participation of *Cdk8* in the initial steps of liver regeneration in zebrafish [318]. Repression of Cdk8 protein led to an enhanced Notch signaling which induced differentiation of liver progenitor cells (LPC) into hepatocytes [318]. However, future studies are required to elucidate the detailed mechanism behind the upregulation of miR-141-3p and regulation of *Cdk8* in liver regeneration. Furthermore, several other mRNA candidates responsible for proliferation and cell differentiation like *Cdc25a*, *Camsap1*, *and Eml4* mRNA remain to be investigated.

The signals that determine the size of the liver during liver regeneration and the termination phase are still poorly understood, but a few mechanisms like the inhibition of specific growth factor and cytokine-mediated pathways are able to regulate organ size [114]. Suppressors of cytokine signaling (SOCS) are important regulators that prevent tyrosine phosphorylation of signal transducer and activator of transcription (STAT) proteins [319–321]. *Interleukin 6* (*IL-6*) signaling has been shown to directly affect the upregulation of *SOCS3*, which is coupled with the subsequent downregulation of phosphorylated *STAT3*, ultimately terminating *IL-6* signaling [322]. Additionally, SOCS proteins also provide an important mechanism to prevent uncontrolled cytokine signaling [323]. Furthermore, *transforming growth factor β* (*TGFβ*) is upregulated during liver regeneration [324]. *TGFβ* activity can be assessed by SMAD activation, which is located downstream of *TGFβ*. Interestingly, transcriptional activation of SMAD is regulated via phosphorylation by *Cdk8* which subsequently promotes the recruitment of yes associated transcriptional regulator (YAP) to the phosphorylated linker sites [325,326]. Phosphorylation of SMAD by Cdk8 provides an important counterbalance to *TGFβ* signaling [325,327]. Once liver regeneration is terminated, SMAD levels decrease, while the liver is returning to a quiescent state [328]. Therefore, it is conceivable that downregulation of *Cdk8* mRNA via miR-141-3p may be interlinked to processes which determine the termination phase during liver regeneration.

Precise signaling during the termination phase is important, since uncontrolled initiation of cell cycles and uncontrolled proliferation are characteristics of cancer cells. Especially during liver

regeneration, excessive cell proliferation can lead to HCC [329]. In the past, miR-141-3p and the miR-200 family have been demonstrated to be dysregulated in pancreatic ductal adenocarcinoma cells, with a direct enhancement effect on cell proliferation [330]. These effects are in part mediated through miR-141-3p downstream target genes, such as *zinc finger e-box binding homeobox 1* (*ZEB1*) and *zinc finger e-box binding homeobox* 2 (*ZEB2*), both well-known for their EMT regulatory effects [331,332]. Thus, miR-141-3p upregulation and its target downregulation of *Cdk8* mRNA could potentially play an additional role during the termination phase of liver regeneration to prevent the potential emergence of HCC during uncontrolled cell cycle progression. These results further consolidate earlier findings, where upregulation of miR-141-3p in hypoosmotic perfused rat liver was observed after 180 min, possible functioning as a time delayed 'signal' to cease cell proliferation. This hypothesis can be further substantiated by the fact, that during hypoosmolarity enhanced cell proliferation in rat liver perfusion can be observed [68,250,333,334].

4.6 Regulation of miR-141-3p is sensitive to mechanical stimulation

During liver regeneration and/or hypoosmotic cell swelling the membrane of affected liver cells endure both compression and stretching. As mentioned before, these mechanical stimuli can be sensed by integrins and transmitted into downstream signaling pathways [69,91,116]. An increase in hepatocellular volume leads to an integrin-dependent EGFR and Erk1/-2 activation in hepatocytes, triggering a proliferative response [68,335,336]. In the past, K^+-selective ion channels were discovered which are both activated by membrane stretch and by cell swelling induced by hypoosmotic exposure [337]. As stated earlier, activation of K^+ ion channels in rat liver results in RVD [31–35]. Primary rat hepatocytes, which were subjected to a lateral stretch by roughly 30%, showed a significant increase in miR-141-3p expression levels after 1 h. After 2 h and 3 h, miR-141-3p expression levels are slowly declining, which was accompanied by reshaping of the cells back to their initial size and form. Thus, upregulation of miR-141-3p may be linked to a mechanical stimulus which is probably sensed and transmitted by integrins via a controlled mechanism called mechanotransduction.

Interestingly, Cheng *et al*. discovered that compression along an axis (e.g. horizontal axis) can inhibit cell growth and induce a programmed cell death in tumor spheroids [338]. However, this effect was highly dependent on the cell density. Regions of high cell density are affected by high compressive stress resulting in apoptosis, whereas regions of low cell density allowed proliferation [338]. Because isolated primary rat hepatocytes are highly confluent on the silicone stretch chambers, these findings may further lead to the assumption that miR-141-3p is in-part responsible for anti-proliferative effects in hepatocytes.

Furthermore, *Cdk8* mRNA levels showed a tendency towards decrease 2 h and 3 h after cells were subjected to stretching. However, for an early regulatory effect additional mechanisms may be implicated, since a lateral stretch might impair mechanically gated ion channels. Affected ion channels could be responsible for co-regulation of transcriptional activation for certain mRNAs. Additionally, interaction and communication with neighboring cells via soluble factors and gap junctions may also influence transcription of *Cdk8*. Dolega *et al*. observed that global compression of tumor spheroids decreased the volume of on a larger scale than osmotic compression of single cells [339]. It still remains unclear if cells sense osmotic compression through the same pathways which are implicated through solid stress, including stretch-activated ion channels or involvement of the cytoskeleton and cell-matrix adhesions [339,340].

4.7 Src, Erk, and p38^{MAPK} signal miR-141-3p regulation

Hypoosmotic cell swelling is sensed by the integrin system, resulting in a subsequent activation of c-Src kinase and downstream targets like Erk and p38^{MAPK} [91,92]. To further elucidate the role and the required signal transductions in response to miR-141-3p upregulation in the osmosignaling pathway, inhibitor perfusion studies were conducted. Through the addition of specific Src-, Erk, and p38^{MAPK} inhibitors to rat liver perfusions, hypoosmotic-induced upregulation of miR-141-3p was prevented (Fig. 3.16). Furthermore, inhibition of Erk and p38^{MAPK} signaling resulted in a significant downregulation of miR-141-3p after 120 min of rat liver perfusion, indicating that miR-141-3p may be a feedback mechanism downstream of Src, Erk and p38^{MAPK}. As Src, Erk, and p38^{MAPK} are well-known downstream effectors of the signaling pathways induced by hypoosmolarity [91,92,341,342], this is the first study indicating that miR-141-3p may be directly involved in cellular mechanisms as a response to hypoosmotic condition, mechanical stimulation, and cell swelling.

Addition of colchicine to the perfusate also resulted in the prevention of a significant upregulation of miR-141-3p by hypoosmolarity, although a tendency towards upregulation after 180 min was observed (Fig. 3.17). Colchicine is known to induce depolymerization of the microtubule network by preventing the assembly of α-tubulin leading to an inhibition of mitosis [24,343]. Microtubules are a major component of the cytoskeleton of hepatocytes and play an established role in their physiology [344–346]. The organization of microtubules and the spindle apparatus are mediated via p38^{MAPK} and play an active role in cellular hydration, since microtubules are able to bind different proteins, including ionic channels responsible for the transport of Ca^{2+} ions [347–350]. Furthermore, swelling-mediated effects of hypoosmotic exposure require an intact cytoskeleton and the physiological interaction between extracellular matrix proteins and the integrin system [68,351,352]. Thus, inhibition of microtubules by

depolymerization, resulting in the prevention of miR-141-3p upregulation, may indicate the involvement of miR-141-3p in the osmosignaling pathway triggered by hypoosmotic-induced swelling. Additionally, Wang *et al.* reported that *circular kelch like ECH associated protein 1* (*circKEAP1*) is a direct target of miR-141-3p. Overexpression of *circKEAP1* in human A549 cells led to decreased levels of cell mitosis and lower percentages of proliferation as also seen by the application of colchicine [353,354], further supporting the idea that miR-141-3p is involved in cell proliferation control of the liver.

4.8 Conclusion

In conclusion, the insights gained in the present study identified miR-141-3p as an osmosensitive miRNA which plays a potential role as a modulator in liver cell swelling and proliferation. It is proposed that hypoosmotic conditions lead to an upregulation of miR-141-3p, most likely controlled by $\alpha_5\beta_1$-integrin-, Src-, Erk-, and $p38^{MAPK}$ signaling. As a result, mRNA levels of various genes involved in metabolic processes, macromolecular biosynthesis, and cell cycle progression such as *Cdk8*, *Cdc25a*, *Zmpste24*, *and Nfat5* are directly affected and coherently downregulated. Rat livers subjected to PHx also exhibited elevated miR-141-3p levels, placing miR-141-3p and its target gene *Cdk8* into a regulative signaling network of the regenerative liver, although tension-influenced mechanotransduction seems to differ from signaling events induced by hypoosmoosmotic conditions.

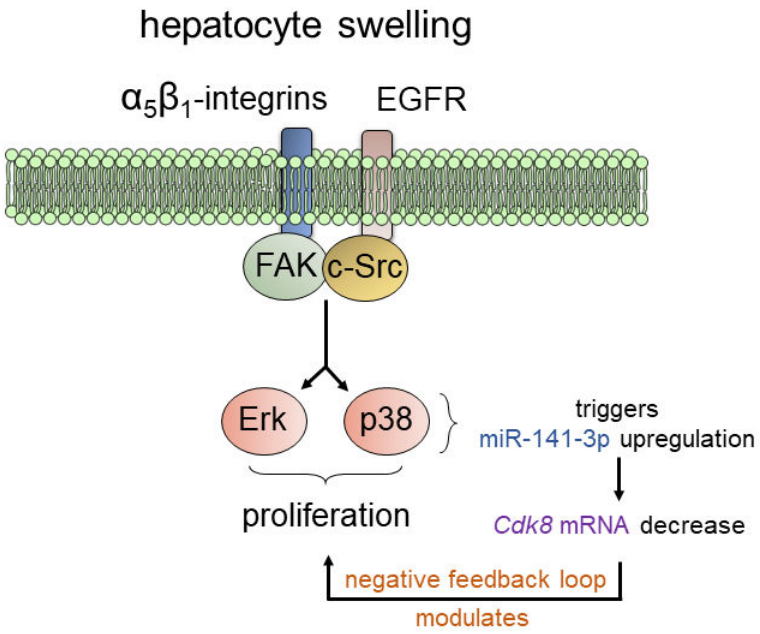

Figure 4.1 Proposed model for the feedback mechanism controlled by miR-141-3p. During hypoosmotic exposure and liver regeneration, cell swelling and deformation is sensed by transmembrane adhesion receptor $\alpha_5\beta_1$-integrins through mechanical stimuli. Following activation, they mediate the Src-, Erk-, and $p38^{MAPK}$-kinase activation which leads to proliferation. Triggered by this event, upregulation of miR-141-3p results in decreased mRNA levels of miR-141-3p target genes, including *Cdk8* mRNA. As a hypothesis of this work, miR-141-3p could be responsible to modulate cell proliferation in the liver, e.g. preventing excessive hepatocyte growth during liver repair.

Furthermore, miR-141-3p overexpression was triggered by a mechanical stimulus, leading to the assumption that mechanosensors such as $\alpha_5\beta_1$-integrins may be in-part responsible for the signaling to mediate miR-141-3p expression. Yet, more work is required to fully understand the role of miR-141-3p in the liver and its potential contribution to osmosensing, osmosignaling as well as cell proliferation during liver regeneration. Future studies must take into

consideration that miR-141-3p has been described to fulfill diverse functions depending on specific targets in different cell types or tissues.

5. References

1. Abumrad, N. A. & Davidson, N. O. Role of the gut in lipid homeostasis. *Physiol. Rev.* **92**, 1061–1085 (2012).

2. Schnabl, B. & Brenner, D. A. Interactions between the intestinal microbiome and liver diseases. *Gastroenterology* **146**, 1513–1524 (2014).

3. Hijmans, B. S., Grefhorst, A., Oosterveer, M. H. & Groen, A. K. Zonation of glucose and fatty acid metabolism in the liver: mechanism and metabolic consequences. *Biochimie* **96**, 121–129 (2014).

4. Guzmán, M. & Castro, J. Zonation of fatty acid metabolism in rat liver. *Biochem. J.* **264**, 107–113 (1989).

5. Jungermann, K. & Thurman, R. G. Hepatocyte heterogeneity in the metabolism of carbohydrates. *Enzyme* **46**, 33–58 (1992).

6. Daoust, R. & Cantero, A. The numerical proportions of cell types in rat liver during carcinogenesis by 4-dimethylaminoazobenzene (DAB). *Cancer Res.* **19**, 757–762 (1959).

7. Alpini, G., Phillips, J. O., Vroman, B. & Larusso, N. F. Recent advances in the isolation of liver cells. *Hepatology* **20**, 494–514 (1994).

8. Tietz, P. S. & LaRusso, N. F. Cholangiocyte biology. *Curr. Opin. Gastroenterol.* **22**, 279–287 (2006).

9. Kordes, C. & Häussinger, D. Hepatic stem cell niches. *J. Clin. Invest.* **123**, 1874–1880 (2013).

10. Kordes, C., Sawitza, I., Götze, S. & Häussinger, D. Hepatic stellate cells support hematopoiesis and are liver-resident mesenchymal stem cells. *Cell. Physiol. Biochem.* **31**, 290–304 (2013).

11. Agius, L., Peak, M., Beresford, G., Al-Habori, M. & Thomas, T. H. The role of ion content and cell volume in insulin action. *Biochem. Soc. Trans.* **22**, 516–522 (1994).

12. Al-Habori, M., Peak, M., Thomas, T. H. & Agius, L. The role of cell swelling in the stimulation of glycogen synthesis by insulin. *Biochem. J.* **282**, 789–796 (1992).

13. Baquet, A., Hue, L., Meijer, A. J., van Woerkom, G. M. & Plomp, P. J. Swelling of rat hepatocytes stimulates glycogen synthesis. *J. Biol. Chem.* **265**, 955–959 (1990).

14. Baquet, A., Lavoinne, A. & Hue, L. Comparison of the effects of various amino acids on glycogen synthesis, lipogenesis and ketogenesis in isolated rat hepatocytes. *Biochem. J.* **273**, 57–62 (1991).

15. Peak, M., Al-Habori, M. & Agius, L. Regulation of glycogen synthesis and glycolysis by insulin, pH and cell volume. Interactions between swelling and alkalinization in mediating the effects of insulin. *Biochem. J.* **282 (Pt 3**, 797–805 (1992).

16. Hallbrucker, C., vom Dahl, S., Lang, F. & Häussinger, D. Control of hepatic proteolysis

by amino acids. The role of cell volume. *Eur. J. Biochem.* **197**, 717–724 (1991).

17. Häussinger, D. *et al.* Cell volume is a major determinant of proteolysis control in liver. *FEBS Lett.* **283**, 70–72 (1991).

18. Häussinger, D., Hallbrucker, C., vom Dahl, S., Lang, F. & Gerok, W. Cell swelling inhibits proteolysis in perfused rat liver. *Biochem. J.* **272**, 239–242 (1990).

19. Häussinger, D., Lang, F., Bauers, K. & Gerok, W. Interactions between glutamine metabolism and cell-volume regulation in perfused rat liver. *Eur. J. Biochem.* **188**, 689–695 (1990).

20. Häussinger, D. & Lang, F. Exposure of perfused liver to hypotonic conditions modifies cellular nitrogen metabolism. *J. Cell. Biochem.* **43**, 355–361 (1990).

21. Häussinger, D. *et al.* Proton magnetic resonance spectroscopy studies on human brain myo-inositol in hypo-osmolarity and hepatic encephalopathy. *Gastroenterology* **107**, 1475–1480 (1994).

22. Kruppa, J. & Clemens, M. J. Differential kinetics of changes in the state of phosphorylation of ribosomal protein S6 and in the rate of protein synthesis in MPC 11 cells during tonicity shifts. *EMBO J.* **3**, 95–100 (1984).

23. vom Dahl, S., Stoll, B., Gerok, W. & Haussinger, D. Inhibition of proteolysis by cell swelling in the liver requires intact microtubular structures. *Biochem. J.* **308**, 529–536 (1995).

24. vom Dahl, S. *et al.* Cell hydration controls autophagosome formation in rat liver in a microtubule-dependent way downstream from p38MAPK activation. *Biochem. J.* **354**, 31–36 (2001).

25. vom Dahl, S. & Häussinger, D. Nutritional state and the swelling-induced inhibition of proteolysis in perfused rat liver. *J. Nutr.* **126**, 395–402 (1996).

26. Hallbrucker, C., vom Dahl, S., Lang, F. & Häussinger, D. Control of hepatic proteolysis by amino acids. The role of cell volume. *Eur. J. Biochem.* **197**, 717–724 (1991).

27. Hallbrucker, C., vom Dahl, S., Lang, F., Gerok, W. & Häussinger, D. Inhibition of hepatic proteolysis by insulin. Role of hormone-induced alterations of the cellular K^+ balance. *Eur. J. Biochem.* **199**, 467–474 (1991).

28. Häussinger, D. The role of cellular hydration in the regulation of cell function. *Biochem. J.* **313**, 697–710 (1996).

29. Chamberlin, M. E. & Strange, K. Anisosmotic cell volume regulation: a comparative view. *Am. J. Physiol. Physiol.* **257**, C159–C173 (1989).

30. Sarkadi, B. & Parker, J. C. Activation of ion transport pathways by changes in cell volume. *Biochim. Biophys. Acta* **1071**, 407–427 (1991).

31. Bruck, R., Haddad, P., Graf, J. & Boyer, J. L. Regulatory volume decrease stimulates bile flow, bile acid excretion, and exocytosis in isolated perfused rat liver. *Am. J. Physiol. Liver Physiol.* **262**, G806–G812 (1992).

32. vom Dahl, S., Hallbrucker, C., Lang, F. & Häussinger, D. Role of eicosanoids, inositol phosphates and extracellular Ca^{2+} in cell-volume regulation of rat liver. *Eur. J. Biochem.* **198**, 73–83 (1991).

33. Haddad, P., Thalhammer, T. & Graf, J. Effect of hypertonic stress on liver cell volume, bile flow, and volume-regulatory K^+ fluxes. *Am. J. Physiol. Liver Physiol.* **256**, 563–569 (1989).

34. vom Dahl, S. *et al.* Release of osmolytes from perfused rat liver on perivascular nerve stimulation: alpha-adrenergic control of osmolyte efflux from parenchymal and nonparenchymal liver cells. *Hepatology* **29**, 195–204 (1999).

35. Schulz, W. A., Eickelmann, P., Hallbrucker, C., Sies, H. & Häussinger, D. Increase of β-actin mRNA upon hypotonic perfusion of perfused rat liver. *FEBS Lett.* **292**, 264–266 (1991).

36. Lau, K. R., Hudson, R. L. & Schultz, S. G. Cell swelling increases a barium-inhibitable potassium conductance in the basolateral membrane of Necturus small intestine. *Proc. Natl. Acad. Sci. U. S. A.* **81**, 3591–3594 (1984).

37. Bear, C. E. & Li, C. H. Calcium-permeable channels in rat hepatoma cells are activated by extracellular nucleotides. *Am. J. Physiol.* **261**, 1018–1024 (1991).

38. Bear, C. E. & Petersen, O. H. L-alanine evokes opening of single Ca^{2+}-activated K^+ channels in rat liver cells. *Pflugers Arch.* **410**, 342–344 (1987).

39. Grinstein, S., Dupre, A. & Rothstein, A. Volume regulation by human lymphocytes. Role of calcium. *J. Gen. Physiol.* **79**, 849–868 (1982).

40. Henderson, R. M., Graf, J. & Boyer, J. L. Inward-rectifying potassium channels in rat hepatocytes. *Am. J. Physiol. Liver Physiol.* **256**, 1028–1035 (1989).

41. Sackin, H. Stretch-activated potassium channels in renal proximal tubule. *Am. J. Physiol. Physiol.* **253**, 1253–1262 (1987).

42. Yancey, P., Clark, M., Hand, S., Bowlus, R. & Somero, G. Living with water stress: evolution of osmolyte systems. *Science.* **217**, 1214–1222 (1982).

43. Garcia-Perez, A. & Burg, M. B. Renal medullary organic osmolytes. *Physiol. Rev.* **71**, 1081–1115 (1991).

44. Burg, M. B. Molecular basis for osmoregulation of organic osmolytes in renal medullary cells. *J. Exp. Zool.* **268**, 171–175 (1994).

45. Warepam, M. *et al.* N-acetylaspartate is an important brain osmolyte. *Biomolecules* **10**, (2020).

46. Ahmadyan, S. *et al.* The osmolyte type affects cartilage associated pathologic marker expression during in vitro mesenchymal stem cell chondrogenesis under hypertonic conditions. *Cell. Mol. Biol. (Noisy-le-grand).* **64**, 56–61 (2018).

47. Lever, M. & Slow, S. The clinical significance of betaine, an osmolyte with a key role in methyl group metabolism. *Clin. Biochem.* **43**, 732–744 (2010).

48. Gallazzini, M., Ferraris, J. D. & Burg, M. B. GDPD5 is a glycerophosphocholine phosphodiesterase that osmotically regulates the osmoprotective organic osmolyte GPC. *Proc. Natl. Acad. Sci. U. S. A.* **105**, 11026–11031 (2008).

49. Dayang, W. & Dongbo, P. Osmolyte taurine induction in UVA exposed human retinal pigment epithelial cells. *Cutan. Ocul. Toxicol.* **37**, 338–343 (2018).

50. Ballatori, N. & Boyer, J. L. ATP regulation of a swelling-activated osmolyte channel in skate hepatocytes. *J. Exp. Zool.* **279**, 471–475 (1997).

51. Lang, F. *et al.* Functional significance of cell volume regulatory mechanisms. *Physiol. Rev.* **78**, 247–306 (1998).

52. Graf, J. & Häussinger, D. Ion transport in hepatocytes: mechanisms and correlations to cell volume, hormone actions and metabolism. *J. Hepatol.* **24 Suppl 1**, 53–77 (1996).

53. Sackin, H. Stretch-activated ion channels. *Kidney Int.* **48**, 1134–1147 (1995).

54. Graf, J., Haddad, P., Häussinger, D. & Lang, F. Cell volume regulation in liver. *Ren. Physiol. Biochem.* **11**, 202–220.

55. Guharay, F. & Sachs, F. Stretch-activated single ion channel currents in tissue-cultured embryonic chick skeletal muscle. *J. Physiol.* **352**, 685–701 (1984).

56. Petrie, R. J. & Koo, H. Direct measurement of intracellular pressure. *Curr. Protoc. cell Biol.* **63**, 1–9 (2014).

57. Häussinger, D., Lang, F. & Gerok, W. Regulation of cell function by the cellular hydration state. *Am. J. Physiol.* **267**, 343–355 (1994).

58. Lemp, M. A. *et al.* Tear osmolarity in the diagnosis and management of dry eye disease. *Am. J. Ophthalmol.* **151**, 792–798 (2011).

59. Brocker, C., Thompson, D. C. & Vasiliou, V. The role of hyperosmotic stress in inflammation and disease. *Biomol. Concepts* **3**, 345–364 (2012).

60. Campbell, H. T., Fincher, M. E. & Sklar, A. H. Severe hyponatremia without severe hypoosmolality following transurethral resection of the prostate (TURP) in end-stage renal disease. *Am. J. Kidney Dis.* **12**, 152–155 (1988).

61. Hotamisligil, G. S. & Davis, R. J. Cell signaling and stress responses. *Cold Spring Harb. Perspect. Biol.* **8**, (2016).

62. Minton, A. P., Colclasure, G. C. & Parker, J. C. Model for the role of macromolecular crowding in regulation of cellular volume. *Proc. Natl. Acad. Sci. U. S. A.* **89**, 10504–10506 (1992).

63. Parker, J. C. & Colclasure, G. C. Macromolecular crowding and volume perception in dog red cells. *Mol. Cell. Biochem.* **114**, 9–11 (1992).

64. Naruse, K. Mechanomedicine. *Biophys. Rev.* **10**, 1257–1262 (2018).

65. Maeda, T., Wurgler-Murphy, S. M. & Saito, H. A two-component system that regulates

an osmosensing MAP kinase cascade in yeast. *Nature* **369**, 242–245 (1994).

66. Häussinger, D. *et al.* Involvement of integrins and Src in tauroursodeoxycholate-induced and swelling-induced choleresis. *Gastroenterology* **124**, 1476–1487 (2003).

67. Gohlke, H., Schmitz, B., Sommerfeld, A., Reinehr, R. & Häussinger, D. $\alpha_5\beta_1$-integrins are sensors for tauroursodeoxycholic acid in hepatocytes. *Hepatology* **57**, 1117–1129 (2013).

68. Reinehr, R., Sommerfeld, A. & Häussinger, D. Insulin induces swelling-dependent activation of the epidermal growth factor receptor in rat liver. *J. Biol. Chem.* **285**, 25904–25912 (2010).

69. vom Dahl, S. *et al.* Involvement of integrins in osmosensing and signaling toward autophagic proteolysis in rat liver. *J. Biol. Chem.* **278**, 27088–27095 (2003).

70. Shiokawa, S. *et al.* Functional role of Arg-Gly-Asp (RGD)-binding sites on β_1 integrin in embryo implantation using mouse blastocysts and human decidua1. *Biol. Reprod.* **60**, 1468–1474 (1999).

71. Elices, M. J. *et al.* VCAM-1 on activated endothelium interacts with the leukocyte integrin VLA-4 at a site distinct from the VLA-4/fibronectin binding site. *Cell* **60**, 577–584 (1990).

72. Carter, W. G., Ryan, M. C. & Gahr, P. J. Epiligrin, a new cell adhesion ligand for integrin alpha 3 beta 1 in epithelial basement membranes. *Cell* **65**, 599–610 (1991).

73. Yamada, K. M. Adhesive recognition sequences. *J. Biol. Chem.* **266**, 12809–12812 (1991).

74. Ingber, D. E. Tensegrity: the architectural basis of cellular mechanotransduction. *Annu. Rev. Physiol.* **59**, 575–599 (1997).

75. Tilly, B. C. *et al.* Activation of the osmo-sensitive chloride conductance involves P21rho and is accompanied by a transient reorganization of the F-actin cytoskeleton. *Mol. Biol. Cell* **7**, 1419–1427 (1996).

76. Tilly, B. C., van den Berghe, N., Tertoolen, L. G., Edixhoven, M. J. & de Jonge, H. R. Protein tyrosine phosphorylation is involved in osmoregulation of ionic conductances. *J. Biol. Chem.* **268**, 19919–19922 (1993).

77. Schliess, F., Reissmann, R., Reinehr, R., vom Dahl, S. & Häussinger, D. Involvement of integrins and Src in insulin signaling toward autophagic proteolysis in rat liver. *J. Biol. Chem.* **279**, 21294–21301 (2004).

78. vom Dahl, S., Hallbrucker, C., Lang, F., Gerok, W. & Häussinger, D. Regulation of liver cell volume and proteolysis by glucagon and insulin. *Biochem. J.* **278**, 771–777 (1991).

79. Kubitz, R., D'Urso, D., Keppler, D. & Häussinger, D. Osmodependent dynamic localization of the multidrug resistance protein 2 in the rat hepatocyte canalicular membrane. *Gastroenterology* **113**, 1438–1442 (1997).

80. Noé, B., Schliess, F., Wettstein, M., Heinrich, S. & Häussinger, D. Regulation of taurocholate excretion by a hypo-osmolarity-activated signal transduction pathway in rat

liver. *Gastroenterology* **110**, 858–865 (1996).

81. Hue, L. Regulation of liver carbohydrate and lipid metabolism by cell volume. *Ann. Endocrinol. (Paris).* **56**, 599–601 (1995).

82. Reinehr, R., Sommerfeld, A. & Häussinger, D. Insulin-induced hepatocyte proliferation involves swelling-dependent activation of the epidermal growth factor receptor. *Z. Gastroenterol.* **49**, (2011).

83. Häussinger, D., Stehle, T. & Lang, F. Volume regulation in liver: further characterization by inhibitors and ionic substitutions. *Hepatology* **11**, 243–254 (1990).

84. Schreiber, R., Stoll, B., Lang, F. & Häussinger, D. Effects of aniso-osmolarity and hydroperoxides on intracellular pH in isolated rat hepatocytes as assessed by (2',7')-bis(carboxyethyl)-5(6)-carboxyfluorescein and fluorescein isothiocyanate-dextran fluorescence. *Biochem. J.* **303**, 113–120 (1994).

85. Reinehr, R. *et al.* Endosomal acidification and activation of NADPH oxidase isoforms are upstream events in hyperosmolarity-induced hepatocyte apoptosis. *J. Biol. Chem.* **281**, 23150–23166 (2006).

86. Cantore, M., Reinehr, R., Sommerfeld, A., Becker, M. & Häussinger, D. The Src family kinase Fyn mediates hyperosmolarity-induced Mrp2 and Bsep retrieval from canalicular membrane. *J. Biol. Chem.* **286**, 45014–45029 (2011).

87. Sommerfeld, A., Mayer, P. G. K., Cantore, M. & Häussinger, D. Regulation of plasma membrane localization of the Na^+-taurocholate cotransporting polypeptide (Ntcp) by hyperosmolarity and tauroursodeoxycholate. *J. Biol. Chem.* **290**, 24237–54 (2015).

88. Santosa, D., Castoldi, M., Paluschinski, M., Sommerfeld, A. & Häussinger, D. Hyperosmotic stress activates the expression of members of the miR-15/107 family and induces downregulation of anti-apoptotic genes in rat liver. *Sci. Rep.* **5**, 1–19 (2015).

89. Reinehr, R., Graf, D., Fischer, R., Schliess, F. & Häussinger, D. Hyperosmolarity triggers CD95 membrane trafficking and sensitizes rat hepatocytes toward CD95L-induced apoptosis. *Hepatology* **36**, 602–614 (2002).

90. Reinehr, R., Schliess, F. & Häussinger, D. Hyperosmolarity and CD95L trigger CD95/EGF receptor association and tyrosine phosphorylation of CD95 as prerequisites for CD95 membrane trafficking and DISC formation. *FASEB J.* **17**, 731–733 (2003).

91. Schliess, F. & Häussinger, D. Osmosensing by integrins in rat liver. *Methods Enzymol.* **428**, 129–144 (2007).

92. Reinehr, R. & Häussinger, D. Hyperosmotic activation of the CD95 system. *Methods Enzymol.* **428**, 145–160 (2007).

93. Anbari, K. & Schultz, R. M. Effect of sodium and betaine in culture media on development and relative rates of protein synthesis in preimplantation mouse embryos in vitro. *Mol. Reprod. Dev.* **35**, 24–28 (1993).

94. Albertyn, J., Hohmann, S., Thevelein, J. M. & Prior, B. A. GPD1, which encodes glycerol-3-phosphate dehydrogenase, is essential for growth under osmotic stress in

Saccharomyces cerevisiae, and its expression is regulated by the high-osmolarity glycerol response pathway. *Mol. Cell. Biol.* **14**, 4135–4144 (1994).

95. Graeme-Cook, K. A., May, G., Bremer, E. & Higgins, C. F. Osmotic regulation of porin expression: a role for DNA supercoiling. *Mol. Microbiol.* **3**, 1287–1294 (1989).

96. Miyoshi, K., Funahashi, H., Okuda, K. & Niwa, K. Development of rat one-cell embryos in a chemically defined medium: effects of glucose, phosphate and osmolarity. *J. Reprod. Fertil.* **100**, 21–26 (1994).

97. Robbins, E., Pederson, T. & Klein, P. Comparison of mitotic phenomena and effects induced by hypertonic solutions in HeLa cells. *J. Cell Biol.* **44**, 400–416 (1970).

98. Meyer, M., Maly, K., Uberall, F., Hoflacher, J. & Grunicke, H. Stimulation of K^+ transport systems by Ha-ras. *J. Biol. Chem.* **266**, 8230–8235 (1991).

99. Lang, F. *et al.* Ion channels in cell proliferation and apoptotic cell death. *J. Membr. Biol.* **205**, 147–157 (2005).

100. Dartsch, P. C., Ritter, M., Häussinger, D. & Lang, F. Cytoskeletal reorganization in NIH 3T3 fibroblasts expressing the ras oncogene. *Eur. J. Cell Biol.* **63**, 316–325 (1994).

101. Dartsch, P. C., Ritter, M., Gschwentner, M., Lang, H. J. & Lang, F. Effects of calcium channel blockers on NIH 3T3 fibroblasts expressing the Ha-ras oncogene. *Eur. J. Cell Biol.* **67**, 372–378 (1995).

102. Ritter, M., Wöll, E., Häussinger, D. & Lang, F. Effects of bradykinin on cell volume and intracellular pH in NIH 3T3 fibroblasts expressing the ras oncogene. *FEBS Lett.* **307**, 367–370 (1992).

103. van Rossum, G. D. & Russo, M. A. Ouabain-resistant mechanism of volume control and the ultrastructural organization of liver slices recovering from swelling in vitro. *J. Membr. Biol.* **59**, 191–209 (1981).

104. Ritter, M. *et al.* Activation of $Na^+/H(+)$-exchanger by transforming Ha-ras requires stimulated cellular calcium influx and is associated with rearrangement of the actin cytoskeleton. *Eur. J. Cell Biol.* **72**, 222–228 (1997).

105. Yin, H. L., Hartwig, J. H., Maruyama, K. & Stossel, T. P. Ca^{2+} control of actin filament length. Effects of macrophage gelsolin on actin polymerization. *J. Biol. Chem.* **256**, 9693–9697 (1981).

106. Ritter, M. & Wöll, E. Modification of cellular ion transport by the Ha-ras oncogene: Steps towards malignant transformation. *Cell. Physiol. Biochem.* **6**, 245–270 (1996).

107. Lang, F. *et al.* Effects of inhibitors and ion substitutions on oscillations of cell membrane potential in cells expressing the RAS oncogene. *Pflugers Arch.* **421**, 416–424 (1992).

108. Rosskopf, D., Scholz, W., Lang, H. J., Schölkens, B. A. & Siffert, W. HOE 694 blocks Na^+/H^+ exchange in human B lymphoblasts without influencing proliferation. *Cell. Physiol. Biochem.* **5**, 269–275 (1995).

109. Mills, G. B., Cragoe, E. J., Gelfand, E. W. & Grinstein, S. Interleukin 2 induces a rapid

increase in intracellular pH through activation of a Na^+/H^+ antiport. Cytoplasmic alkalinization is not required for lymphocyte proliferation. *J. Biol. Chem.* **260**, 12500–12507 (1985).

110. Kakinuma, Y., Sakamaki, Y., Ito, K., Cragoe, E. J. & Igarashi, K. Relationship among activation of the Na+/H+ antiporter, ornithine decarboxylase induction, and DNA synthesis. *Arch. Biochem. Biophys.* **259**, 171–178 (1987).

111. Schliess, F., Schreiber, R. & Häussinger, D. Activation of extracellular signal-regulated kinases Erk-1 and Erk-2 by cell swelling in H4IIE hepatoma cells. *Biochem. J.* **309**, 13–17 (1995).

112. Lloyd, A. C. Distinct functions for ERKs? *J. Biol.* **5**, 13 (2006).

113. Higgins, G.M., Anderson, R. M. Experimental pathology of liver: restoration of liver of white rat following partial surgical removal. *AMA Arch Pathol* (1931).

114. Taub, R. Liver regeneration: From myth to mechanism. *Nat. Rev. Mol. Cell Biol.* **5**, 836–847 (2004).

115. Grisham, J. W. A morphologic study of deoxyribonucleic acid synthesis and cell proliferation in regenerating rat liver; autoradiography with thymidine-H3. *Cancer Res.* **22**, 842–849 (1962).

116. Sun, Z., Guo, S. S. & Fässler, R. Integrin-mediated mechanotransduction. *J. Cell Biol.* **215**, 445–456 (2016).

117. Häussinger, D. *et al.* Effect of hepatocyte swelling on microtubule stability and tubulin mRNA levels. *Biochem. Cell Biol.* **72**, 12–19 (1994).

118. Theodoropoulos, P. A. *et al.* Hepatocyte swelling leads to rapid decrease of the G-/total actin ratio and increases actin mRNA levels. *FEBS Lett.* **311**, 241–245 (1992).

119. Zhang, F., Warskulat, U. & Häussinger, D. Modulation of tumor necrosis factor-alpha release by anisoosmolarity and betaine in rat liver macrophages (Kupffer cells). *FEBS Lett.* **391**, 293–296 (1996).

120. Ben-Ze'ev, A. Animal cell shape changes and gene expression. *Bioessays* **13**, 207–12 (1991).

121. Alfieri, R., Petronini, P. G., Urbani, S. & Borghetti, A. F. Activation of heat-shock transcription factor 1 by hypertonic shock in 3T3 cells. *Biochem. J.* **319**, 601–606 (1996).

122. Cohen, D. M., Wasserman, J. C. & Gullans, S. R. Immediate early gene and HSP70 expression in hyperosmotic stress in MDCK cells. *Am. J. Physiol.* **261**, 594–601 (1991).

123. Sheikh-Hamad, D., García-Pérez, A., Ferraris, J. D., Peters, E. M. & Burg, M. B. Induction of gene expression by heat shock versus osmotic stress. *Am. J. Physiol.* **267**, 28–34 (1994).

124. Häussinger, D. & Schliess, F. Cell volume and hepatocellular function. *J. Hepatol.* **22**, 94–100 (1995).

125. Aromataris, E. C., Roberts, M. L., Barritt, G. J. & Rychkov, G. Y. Glucagon activates Ca^{2+} and Cl^- channels in rat hepatocytes. *J. Physiol.* **573**, 611–625 (2006).

126. Espie, P., Guerin, B. & Rigoulet, M. On isolated hepatocytes mitochondrial swelling induced in hypoosmotic medium does not affect the respiration rate. *Biochim. Biophys. Acta - Bioenerg.* **1230**, 139–146 (1995).

127. Skrzydlewska, E., Sulkowska, M., Koda, M. & Sulkowski, S. Proteolytic-antiproteolytic balance and its regulation in carcinogenesis. *World J. Gastroenterol.* **11**, 1251–1266 (2005).

128. Lee, D. H. & Goldberg, A. L. Proteasome inhibitors: valuable new tools for cell biologists. *Trends Cell Biol.* **8**, 397–403 (1998).

129. Mortimore, G. E. & Kadowaki, M. Regulation of protein metabolism in liver. In *Comprehensive Physiology* 553–577, (Wiley, Weinheim, Deutschland, 2001). Prakash, Y.S. (eds).

130. Kristensen, L. O. Associations between transports of alanine and cations across cell membrane in rat hepatocytes. *Am. J. Physiol.* **251**, 575–584 (1986).

131. Hudson, R. L. & Schultz, S. G. Sodium-coupled glycine uptake by Ehrlich ascites tumor cells results in an increase in cell volume and plasma membrane channel activities. *Proc. Natl. Acad. Sci. U. S. A.* **85**, 279–283 (1988).

132. Zhande, R. & Brownsey, R. W. Cell volume and the metabolic actions of insulin. *Biochem. Cell Biol.* **74**, 513–522 (1996).

133. Nagarajan, S. R. *et al.* Lipid and glucose metabolism in hepatocyte cell lines and primary mouse hepatocytes: a comprehensive resource for in vitro studies of hepatic metabolism. *Am. J. Physiol. Metab.* **316**, 578–589 (2019).

134. Häussinger, D., Reinehr, R. & Schliess, F. The hepatocyte integrin system and cell volume sensing. *Acta Physiol. (Oxf).* **187**, 249–255.

135. Meijer, A. J. Hepatocyte swelling: techniques and effects on metabolism. In *The Hepatocyte Review* 147–167 (Springer Dordrecht, Netherlands, 2000). Berry M.N., Edwards A.M. (eds).

136. Boyer, J. L., Graf, J. & Meier, P. J. Hepatic transport systems regulating pHi, cell volume, and bile secretion. *Annu. Rev. Physiol.* **54**, 415–438 (1992).

137. Nathanson, M. H. & Boyer, J. L. Mechanisms and regulation of bile secretion. *Hepatology* **14**, 551–566 (1991).

138. Häussinger, D., Hallbrucker, C., Saha, N., Lang, F. & Gerok, W. Cell volume and bile acid excretion. *Biochem. J.* **288 (Pt 2**, 681–689 (1992).

139. Waldegger, S. *et al.* Mechanisms and clinical significance of cell volume regulation. *Nephrol. Dial. Transplant* **13**, 867–874 (1998).

140. Häussinger, D., Graf, D. & Weiergräber, O. H. Glutamine and cell signaling in liver. *J. Nutr.* **131**, 2509–2514 (2001).

141. Häussinger, D., Saha, N., Hallbrucker, C., Lang, F. & Gerok, W. Involvement of microtubules in the swelling-induced stimulation of transcellular taurocholate transport in perfused rat liver. *Biochem. J.* **291**, 355–360 (1993).

142. Lee, R. C., Feinbaum, R. L. & Ambros, V. The C. elegans heterochronic gene lin-4 encodes small RNAs with antisense complementarity to lin-14. *Cell* **75**, 843–854 (1993).

143. Wightman, B., Ha, I. & Ruvkun, G. Posttranscriptional regulation of the heterochronic gene lin-14 by lin-4 mediates temporal pattern formation in C. elegans. *Cell* **75**, 855–862 (1993).

144. Chalfie, M. Mutations that lead to reiterations in the cell lineages of C. elegans. *Cell* **24**, 59–69 (1981).

145. Ambros, V. & Horvitz, H. R. The lin-14 locus of Caenorhabditis elegans controls the time of expression of specific postembryonic developmental events. *Genes Dev.* **1**, 398–414 (1987).

146. Ferguson, E. L., Sternberg, P. W. & Horvitz, H. R. A genetic pathway for the specification of the vulval cell lineages of Caenorhabditis elegans. *Nature* **326**, 259–267 (1987).

147. Lee, R., Feinbaum, R. & Ambros, V. A short history of a short RNA. *Cell* **116**, 89–92 (2004).

148. Almeida, M. I., Reis, R. M. & Calin, G. A. MicroRNA history: Discovery, recent applications, and next frontiers. *Mutat. Res. Mol. Mech. Mutagen.* **717**, 1–8 (2011).

149. Lee, R. C., Feinbaum, R. L. & Ambros, V. The C. elegans heterochronic gene lin-4 encodes small RNAs with antisense complementarity to lin-14. *Cell* **75**, 843–854 (1993).

150. Wightman, B., Ha, I. & Ruvkun, G. Posttranscriptional regulation of the heterochronic gene lin-14 by lin-4 mediates temporal pattern formation in C. elegans. *Cell* **75**, 855–862 (1993).

151. de Rie, D. *et al.* An integrated expression atlas of miRNAs and their promoters in human and mouse. *Nat. Biotechnol.* **35**, 872–878 (2017).

152. Pasquinelli, A. E. *et al.* Conservation of the sequence and temporal expression of let-7 heterochronic regulatory RNA. *Nature* **408**, 86–89 (2000).

153. Davis, B. N. & Hata, A. Mechanisms of control of microRNA biogenesis. *J. Biochem.* (2010).

154. Li, S.-C. *et al.* Identification of homologous microRNAs in 56 animal genomes. *Genomics* **96**, 1–9 (2010).

155. Ha, M. & Kim, V. N. Regulation of microRNA biogenesis. *Nat. Rev. Mol. Cell Biol.* **15**, 509–524 (2014).

156. Broughton, J. P., Lovci, M. T., Huang, J. L., Yeo, G. W. & Pasquinelli, A. E. Pairing beyond the seed supports microRNA targeting specificity. *Mol. Cell* **64**, 320–333 (2016).

157. Vasudevan, S. Posttranscriptional upregulation by microRNAs. *Wiley Interdiscip. Rev.*

RNA **3**, 311–330 (2012).

158. Makarova, J. A. *et al.* Intracellular and extracellular microRNA: An update on localization and biological role. *Prog. Histochem. Cytochem.* **51**, 33–49 (2016).

159. Chen, X. *et al.* Characterization of microRNAs in serum: a novel class of biomarkers for diagnosis of cancer and other diseases. *Cell Res.* **18**, 997–1006 (2008).

160. Arroyo, J. D. *et al.* Argonaute2 complexes carry a population of circulating microRNAs independent of vesicles in human plasma. *Proc. Natl. Acad. Sci.* **108**, 5003–5008 (2011).

161. Cogswell, J. P. *et al.* Identification of miRNA Changes in alzheimer's disease brain and CSF yields putative biomarkers and insights into disease pathways. *J. Alzheimer's Dis.* **14**, 27–41 (2008).

162. Gallo, A., Tandon, M., Alevizos, I. & Illei, G. G. The majority of microRNAs detectable inserum and saliva is concentrated in exosomes. *PLoS One* **7**, 30679 (2012).

163. Zhou, Q. *et al.* Immune-related microRNAs are abundant in breast milk exosomes. *Int. J. Biol. Sci.* **8**, 118–123 (2012).

164. Ha, M. & Kim, V. N. Regulation of microRNA biogenesis. *Nat. Rev. Mol. Cell Biol.* **15**, 509–524 (2014).

165. Rodriguez, A., Griffiths-Jones, S., Ashurst, J. L. & Bradley, A. Identification of mammalian microRNA host genes and transcription units. *Genome Res.* **14**, 1902–1910 (2004).

166. Hinske, L. C. G., Galante, P. A. F., Kuo, W. P. & Ohno-Machado, L. A potential role for intragenic miRNAs on their hosts' interactome. *BMC Genomics* **11**, 533 (2010).

167. He, C. *et al.* Young intragenic miRNAs are less coexpressed with host genes than old ones: implications of miRNA-host gene coevolution. *Nucleic Acids Res.* **40**, 4002–4012 (2012).

168. Gao, X., Qiao, Y., Han, D., Zhang, Y. & Ma, N. Enemy or partner: relationship between intronic micrornas and their host genes. *IUBMB Life* **64**, 835–840 (2012).

169. Tanzer, A. & Stadler, P. F. Molecular evolution of a microRNA cluster. *J. Mol. Biol.* **339**, 327–335 (2004).

170. Denli, A. M., Tops, B. B. J., Plasterk, R. H. A., Ketting, R. F. & Hannon, G. J. Processing of primary microRNAs by the Microprocessor complex. *Nature* **432**, 231–235 (2004).

171. Alarcón, C. R., Lee, H., Goodarzi, H., Halberg, N. & Tavazoie, S. F. N6-methyladenosine marks primary microRNAs for processing. *Nature* **519**, 482–485 (2015).

172. Marzluff, W. F., Wagner, E. J. & Duronio, R. J. Metabolism and regulation of canonical histone mRNAs: life without a poly(A) tail. *Nat. Rev. Genet.* **9**, 843–854 (2008).

173. Han, J. The Drosha-DGCR8 complex in primary microRNA processing. *Genes Dev.* **18**, 3016–3027 (2004).

174. Okada, C. *et al.* A high-resolution structure of the pre-microRNA nuclear export machinery. *Science.* **326**, 1275–1279 (2009).

175. Zhang, H., Kolb, F. A., Jaskiewicz, L., Westhof, E. & Filipowicz, W. Single processing center models for human Dicer and bacterial RNase III. *Cell* **118**, 57–68 (2004).

176. Yoda, M. *et al.* ATP-dependent human RISC assembly pathways. *Nat. Struct. Mol. Biol.* **17**, 17–23 (2010).

177. Hammond, S. M. Argonaute2, a link between genetic and biochemical analyses of RNAi. *Science.* **293**, 1146–1150 (2001).

178. Kawamata, T. & Tomari, Y. Making RISC. *Trends Biochem. Sci.* **35**, 368–376 (2010).

179. Xu, W., San Lucas, A., Wang, Z. & Liu, Y. Identifying microRNA targets in different gene regions. *BMC Bioinformatics* **15**, 4 (2014).

180. Ellwanger, D. C., Büttner, F. A., Mewes, H.-W. & Stümpflen, V. The sufficient minimal set of miRNA seed types. *Bioinformatics* **27**, 1346–1350 (2011).

181. Jo, M. H. *et al.* Human Argonaute 2 has diverse reaction pathways on target RNAs. *Mol. Cell* **59**, 117–124 (2015).

182. Souret, F. F., Kastenmayer, J. P. & Green, P. J. AtXRN4 degrades mRNA in Arabidopsis and its substrates include selected miRNA targets. *Mol. Cell* **15**, 173–183 (2004).

183. Parker, R. & Song, H. The enzymes and control of eukaryotic mRNA turnover. *Nat. Struct. Mol. Biol.* **11**, 121–127 (2004).

184. Jonas, S. & Izaurralde, E. Towards a molecular understanding of microRNA-mediated gene silencing. *Nat. Rev. Genet.* **16**, 421–433 (2015).

185. Müller, M., Fazi, F. & Ciaudo, C. Argonaute proteins: From structure to function in development and pathological cell fate determination. *Front. Cell Dev. Biol.* **7**, (2020).

186. Braun, J. E., Huntzinger, E. & Izaurralde, E. The role of GW182 proteins in miRNA-mediated gene silencing. *Adv. Exp. Med. Biol.* **768**, 147–163 (2013).

187. Takimoto, K., Wakiyama, M. & Yokoyama, S. Mammalian GW182 contains multiple Argonaute-binding sites and functions in microRNA-mediated translational repression. *RNA* **15**, 1078–1089 (2009).

188. Lian, S. L. *et al.* The C-terminal half of human Ago2 binds to multiple GW-rich regions of GW182 and requires GW182 to mediate silencing. *RNA* **15**, 804–813 (2009).

189. Behm-Ansmant, I. mRNA degradation by miRNAs and GW182 requires both CCR4:NOT deadenylase and DCP1:DCP2 decapping complexes. *Genes Dev.* **20**, 1885–1898 (2006).

190. Christie, M., Boland, A., Huntzinger, E., Weichenrieder, O. & Izaurralde, E. Structure of the PAN3 pseudokinase reveals the basis for interactions with the PAN2 deadenylase and the GW182 proteins. *Mol. Cell* **51**, 360–373 (2013).

191. Braun, J. E. *et al.* A direct interaction between DCP1 and XRN1 couples mRNA decapping to 5′ exonucleolytic degradation. *Nat. Struct. Mol. Biol.* **19**, 1324–1331 (2012).

192. Vasudevan, S. & Steitz, J. A. AU-rich-element-mediated upregulation of translation by FXR1 and Argonaute 2. *Cell* **128**, 1105–1118 (2007).

193. Truesdell, S. S. *et al.* MicroRNA-mediated mRNA translation activation in quiescent cells and oocytes involves recruitment of a nuclear microRNP. *Sci. Rep.* **2**, 842 (2012).

194. Bukhari, S. I. A. *et al.* A specialized mechanism of translation mediated by FXR1a-associated microRNP in cellular quiescence. *Mol. Cell* **61**, 760–773 (2016).

195. Ørom, U. A., Nielsen, F. C. & Lund, A. H. MicroRNA-10a binds the 5′UTR of ribosomal protein mRNAs and enhances their translation. *Mol. Cell* **30**, 460–471 (2008).

196. Barman, B. & Bhattacharyya, S. N. mRNA targeting to endoplasmic reticulum precedes Ago protein interaction and microRNA (miRNA)-mediated translation repression in mammalian cells. *J. Biol. Chem.* **290**, 24650–24656 (2015).

197. Bose, M., Barman, B., Goswami, A. & Bhattacharyya, S. N. Spatiotemporal uncoupling of microRNA-mediated translational repression and target RNA degradation controls microRNP recycling in mammalian cells. *Mol. Cell. Biol.* **37**, (2017).

198. Detzer, A., Engel, C., Wünsche, W. & Sczakiel, G. Cell stress is related to re-localization of Argonaute 2 and to decreased RNA interference in human cells. *Nucleic Acids Res.* **39**, 2727–2741 (2011).

199. Nishi, K. *et al.* Control of the localization and function of a miRNA silencing component TNRC6A by Argonaute protein. *Nucleic Acids Res.* (2015).

200. Gibbings, D. J., Ciaudo, C., Erhardt, M. & Voinnet, O. Multivesicular bodies associate with components of miRNA effector complexes and modulate miRNA activity. *Nat. Cell Biol.* **11**, 1143–1149 (2009).

201. Barrey, E. *et al.* Pre-microRNA and mature microRNA in human mitochondria. *PLoS One* **6**, 202–220 (2011).

202. Zhang, X. *et al.* MicroRNA directly enhances mitochondrial translation during muscle differentiation. *Cell* **158**, 607–619 (2014).

203. Gagnon, K. T., Li, L., Chu, Y., Janowski, B. A. & Corey, D. R. RNAi factors are present and active in human cell nuclei. *Cell Rep.* **6**, 211–221 (2014).

204. Miao, L. *et al.* A dual inhibition: microRNA-552 suppresses both transcription and translation of cytochrome P450 2E1. *Biochim. Biophys. Acta - Gene Regul. Mech.* **1859**, 650–662 (2016).

205. Parker, R. & Sheth, U. P bodies and the control of mRNA translation and degradation. *Mol. Cell* **25**, 635–646 (2007).

206. Liu, J., Valencia-Sanchez, M. A., Hannon, G. J. & Parker, R. MicroRNA-dependent localization of targeted mRNAs to mammalian P-bodies. *Nat. Cell Biol.* **7**, 719–723

(2005).

207. Rajgor, D. *et al.* Mammalian microtubule P-body dynamics are mediated by nesprin-1. *J. Cell Biol.* **205**, 457–475 (2014).

208. Carbonaro, M., O'Brate, A. & Giannakakou, P. Microtubule disruption targets HIF-1α mRNA to cytoplasmic P-bodies for translational repression. *J. Cell Biol.* **192**, 83–99 (2011).

209. Pillai, R. S. Inhibition of translational initiation by let-7 microRNA in human cells. *Science.* **309**, 1573–1576 (2005).

210. Aqeilan, R. I., Calin, G. A. & Croce, C. M. miR-15a and miR-16-1 in cancer: discovery, function and future perspectives. *Cell Death Differ.* **17**, 215–220 (2010).

211. Cimmino, A. *et al.* miR-15 and miR-16 induce apoptosis by targeting BCL2. *Proc. Natl. Acad. Sci. U. S. A.* **102**, 13944–13949 (2005).

212. Shen, J. *et al.* miR-15b and miR-16 induce the apoptosis of rat activated pancreatic stellate cells by targeting Bcl-2 in vitro. *Pancreatology* **12**, 91–99 (2012).

213. Deshpande, A. *et al.* 3'UTR mediated regulation of the cyclin D1 proto-oncogene. *Cell Cycle* **8**, 3592–3600 (2009).

214. Eberle, A., Reinehr, R., Becker, S. & Häussinger, D. Fluorescence resonance energy transfer analysis of proapoptotic CD95-EGF receptor interactions in Huh7 cells. *Hepatology* **41**, 315–326 (2005).

215. Reinehr, R., Becker, S., Höngen, A. & Häussinger, D. The Src family kinase Yes triggers hyperosmotic activation of the epidermal growth factor receptor and CD95. *J. Biol. Chem.* **279**, 23977–23987 (2004).

216. Flynt, A. S. *et al.* miR-8 microRNAs regulate the response to osmotic stress in zebrafish embryos. *J. Cell Biol.* **185**, 115–127 (2009).

217. Weinman, E. J., Cunningham, R., Wade, J. B. & Shenolikar, S. The role of NHERF-1 in the regulation of renal proximal tubule sodium-hydrogen exchanger 3 and sodium-dependent phosphate cotransporter 2a. *J. Physiol.* **567**, 27–32 (2005).

218. Huebert, R. C. *et al.* Aquaporin-1 promotes angiogenesis, fibrosis, and portal hypertension through mechanisms dependent on osmotically sensitive microRNAs. *Am. J. Pathol.* **179**, 1851–1860 (2011).

219. Meijer, A. J., Gimpel, J. A., Deleeuw, G. A., Tager, J. M. & Williamson, J. R. Role of anion translocation across the mitochondrial membrane in the regulation of urea synthesis from ammonia by isolated rat hepatocytes. *J. Biol. Chem.* **250**, 7728–7738 (1975).

220. Kordes, C., Sawitza, I., Götze, S., Herebian, D. & Häussinger, D. Hepatic stellate cells contribute to progenitor cells and liver regeneration. *J. Clin. Invest.* **124**, 5503–5515 (2014).

221. Hellemans, J., Mortier, G., De Paepe, A., Speleman, F. & Vandesompele, J. qBase

relative quantification framework and software for management and automated analysis of real-time quantitative PCR data. *Genome Biol.* **8**, (2008).

222. Livak, K. J. & Schmittgen, T. D. Analysis of relative gene expression data using real-time quantitative PCR and the 2-ΔΔCT method. *Methods* **25**, 402–408 (2001).

223. Benes, V. *et al.* Identification of cytokine-induced modulation of microRNA expression and secretion as measured by a novel microRNA specific qPCR assay. *Sci. Rep.* **5**, 1–14 (2015).

224. Castoldi, M. *et al.* The liver-specific microRNA miR-122 controls systemic iron homeostasis in mice. *J. Clin. Invest.* **121**, (2011).

225. Shen, J. *et al.* miR-15b and miR-16 induce the apoptosis of rat activated pancreatic stellate cells by targeting Bcl-2 in vitro. *Pancreatology* **12**, 91–99.

226. Chawade, A., Alexandersson, E. & Levander, F. Normalyzer: a tool for rapid evaluation of normalization methods for omics data sets. *J. Proteome Res.* **13**, 3114–3120 (2014).

227. Marchini, S. *et al.* Association between miR-200c and the survival of patients with stage I epithelial ovarian cancer: a retrospective study of two independent tumour tissue collections. *Lancet. Oncol.* **12**, 273–285 (2011).

228. Chen, X. *et al.* miR-141 is a key regulator of renal cell carcinoma proliferation and metastasis by controlling EphA2 expression. *Clin. Cancer Res.* **20**, 2617–2630 (2014).

229. van Jaarsveld, M. T. M. *et al.* miR-141 regulates KEAP1 and modulates cisplatin sensitivity in ovarian cancer cells. *Oncogene* **32**, 4284–4293 (2013).

230. Uhlmann, S. *et al.* miR-200bc/429 cluster targets PLCgamma1 and differentially regulates proliferation and EGF-driven invasion than miR-200a/141 in breast cancer. *Oncogene* **29**, 4297–4306 (2010).

231. Vekemans, K. & Braet, F. Structural and functional aspects of the liver and liver sinusoidal cells in relation to colon carcinoma metastasis. *World J. Gastroenterol.* **11**, 5095 (2005).

232. Miranda, K. C. *et al.* A pattern-based method for the identification of MicroRNA binding sites and their corresponding heteroduplexes. *Cell* **126**, 1203–1217 (2006).

233. Gao, Y. *et al.* The roles of microRNA-141 in human cancers: From diagnosis to treatment. *Cell. Physiol. Biochem.* **38**, 427–448 (2016).

234. Lorenz, L. *et al.* Mechanosensing by β1 integrin induces angiocrine signals for liver growth and survival. *Nature* **562**, 128–132 (2018).

235. Schliess, F., Kurz, A. K., vom Dahl, S. & Häussinger, D. Mitogen-activated protein kinases mediate the stimulation of bile acid secretion by tauroursodeoxycholate in rat liver. *Gastroenterology* **113**, 1306–1314 (1997).

236. vom Dahl, S. *et al.* Cell hydration controls autophagosome formation in rat liver in a microtubule-dependent way downstream from p38MAPK activation. *Biochem. J.* **354**, 31 (2001).

237. Häussinger, D. *et al.* Effect of hepatocyte swelling on microtubule stability and tubulin mRNA levels. *Biochem. Cell Biol.* **72**, 12–19 (1994).

238. Malik, S. & Roeder, R. G. Dynamic regulation of pol II transcription by the mammalian Mediator complex. *Trends Biochem. Sci.* **30**, 256–263 (2005).

239. Guo, T. *et al.* miR-338-5p regulates the viability, proliferation, apoptosis and migration of rheumatoid arthritis fibroblast-like synoviocytes by targeting NFAT5. *Cell. Physiol. Biochem.* **49**, 899–910 (2018).

240. Gao, S. *et al.* miR-18a-5p targets FBP1 to promote proliferation, migration, and invasion of liver cancer cells and inhibit cell apoptosis. *Comput. Math. Methods Med.* **2021**, 3334065 (2021).

241. Tang, B. *et al.* MicroRNA-155-3p promotes hepatocellular carcinoma formation by suppressing FBXW7 expression. *J. Exp. Clin. Cancer Res.* **35**, 93 (2016).

242. Cohen, D. M., Wasserman, J. C. & Gullans, S. R. Immediate early gene and HSP70 expression in hyperosmotic stress in MDCK cells. *Am. J. Physiol. Physiol.* **261**, 594-C601 (1991).

243. Sheikh-Hamad, D., Garcia-Perez, A., Ferraris, J. D., Peters, E. M. & Burg, M. B. Induction of gene expression by heat shock versus osmotic stress. *Am. J. Physiol. Physiol.* **267**, 28–34 (1994).

244. Jolesch, A., Elmer, K., Bendz, H., Issels, R. D. & Noessner, E. Hsp70, a messenger from hyperthermia for the immune system. *Eur. J. Cell Biol.* **91**, 48–52 (2012).

245. Kurz, A. K., Schliess, F. & Häussinger, D. Osmotic regulation of the heat shock response in primary rat hepatocytes. *Hepatology* **28**, 774–781 (1998).

246. Westerheide, S. D., Anckar, J., Stevens, S. M., Sistonen, L. & Morimoto, R. I. Stress-inducible regulation of heat shock factor 1 by the deacetylase SIRT1. *Science* **323**, 1063–1066 (2009).

247. Bardeck, N. *et al.* Swelling-induced upregulation of miR-141-3p inhibits hepatocyte proliferation. *JHEP Reports* 100440 (2022).

248. Sardiello, M. *et al.* A gene network regulating lysosomal biogenesis and function. *Science.* **325**, 473–477 (2009).

249. Settembre, C. *et al.* TFEB links autophagy to lysosomal biogenesis. *Science* **332**, 1429–1433 (2011).

250. Warskulat, U., Newsome, W., Noe, B., Stoll, B. & Haussinger, D. Anisoosmotic regulation of hepatic gene expression. *Biol. Chem. Hoppe. Seyler.* **377**, 57–65 (1996).

251. Quinn, P. G. & Yeagley, D. Insulin regulation of PEPCK gene expression: a model for rapid and reversible modulation. *Curr. Drug Targets. Immune. Endocr. Metabol. Disord.* **5**, 423–437 (2005).

252. Christ, B., Nath, A., Bastian, H. & Jungermann, K. Regulation of the expression of the phosphoenolpyruvate carboxykinase gene in cultured rat hepatocytes by glucagon and

insulin. *Eur. J. Biochem.* **178**, 373–379 (1988).

253. Tohyama, Y., Kameji, T. & Hayashi, S. Mechanisms of dramatic fluctuations of ornithine decarboxylase activity upon tonicity changes in primary cultured rat hepatocytes. *Eur. J. Biochem.* **202**, 1327–1331 (1991).

254. Finkenzeller, G., Newsome, W., Lang, F. & Häussinger, D. Increase of c-jun mRNA upon hypo-osmotic cell swelling of rat hepatoma cells. *FEBS Lett.* **340**, 163–166 (1994).

255. Huang, G.-L. *et al.* MiR-200 family and cancer: From a meta-analysis view. *Mol. Aspects Med.* **70**, 57–71 (2019).

256. Tong, S. J. *et al.* Study on effects of miR-141-3p in proliferation, migration, invasion and apoptosis of colon cancer cells by inhibiting Bcl2. *Clin. Transl. Oncol.* (2021).

257. Dong, S. *et al.* LncRNA MEG3 regulates breast cancer proliferation and apoptosis through miR-141-3p/RBMS3 axis. *Genomics* **113**, 1689–1704 (2021).

258. Fontana, A. *et al.* Combined analysis of miR-200 family and its significance for breast cancer. *Sci. Rep.* **11**, 2980 (2021).

259. Liu, C. *et al.* Roles of miR-200 family members in lung cancer: more than tumor suppressors. *Futur. Oncol.* **14**, 2875–2886 (2018).

260. Kong, D., Li, Y., Wang, Z. & Sarkar, F. H. Cancer stem cells and epithelial-to-mesenchymal transition (EMT)-phenotypic cells: Are they cousins or twins? *Cancers (Basel).* **3**, 716–729 (2011).

261. Lamouille, S., Xu, J. & Derynck, R. Molecular mechanisms of epithelial-mesenchymal transition. *Nat. Rev. Mol. Cell Biol.* **15**, 178–196 (2014).

262. Park, S.-M., Gaur, A. B., Lengyel, E. & Peter, M. E. The miR-200 family determines the epithelial phenotype of cancer cells by targeting the E-cadherin repressors ZEB1 and ZEB2. *Genes Dev.* **22**, 894–907 (2008).

263. Zhao, G. *et al.* miRNA-141, downregulated in pancreatic cancer, inhibits cell proliferation and invasion by directly targeting MAP4K4. *Mol. Cancer Ther.* **12**, 2569–2580 (2013).

264. Cheng, H. *et al.* Circulating plasma MiR-141 is a novel biomarker for metastatic colon cancer and predicts poor prognosis. *PLoS One* **6**, 17745 (2011).

265. Nakada, C. *et al.* Genome-wide microRNA expression profiling in renal cell carcinoma: significant down-regulation of miR-141 and miR-200c. *J. Pathol.* **216**, 418–427 (2008).

266. Cheung, C. Y. & Ko, B. C. NFAT5 in cellular adaptation to hypertonic stress - regulations and functional significance. *J. Mol. Signal.* **8**, 5 (2013).

267. Aramburu, J. & López-Rodríguez, C. Brx shines a light on the route from hyperosmolarity to NFAT5. *Sci. Signal.* **2**, 20 (2009).

268. Lee, N., Kim, D. & Kim, W.-U. Role of NFAT5 in the immune system and pathogenesis of autoimmune diseases. *Front. Immunol.* **10**, (2019).

269. Miyakawa, H., Woo, S. K., Dahl, S. C., Handler, J. S. & Kwon, H. M. Tonicity-responsive enhancer binding protein, a rel-like protein that stimulates transcription in response to hypertonicity. *Proc. Natl. Acad. Sci. U. S. A.* **96**, 2538–2542 (1999).

270. Woo, S. K., Lee, S. Do & Kwon, H. M. TonEBP transcriptional activator in the cellular response to increased osmolality. *Pflugers Arch.* **444**, 579–585 (2002).

271. Zhu, H. *et al.* Hyperosmotic stress stimulates autophagy via the NFAT5/mTOR pathway in cardiomyocytes. *Int. J. Mol. Med.* (2018).

272. Bounedjah, O. *et al.* Macromolecular crowding regulates assembly of mRNA stress granules after osmotic stress: new role for compatible osmolytes. *J. Biol. Chem.* **287**, 2446–2458 (2012).

273. Olson, J. M. & Hallahan, A. R. p38 MAP kinase: a convergence point in cancer therapy. *Trends Mol. Med.* **10**, 125–129 (2004).

274. Ko, B. C. B. *et al.* Fyn and p38 signaling are both required for maximal hypertonic activation of the osmotic response element-binding protein/tonicity-responsive enhancer-binding protein (OREBP/TonEBP). *J. Biol. Chem.* **277**, 46085–46092 (2002).

275. Ferraris, J. D. *et al.* Activity of the TonEBP/OREBP transactivation domain varies directly with extracellular NaCl concentration. *Proc. Natl. Acad. Sci. U. S. A.* **99**, 739–744 (2002).

276. Navarro, C. L. *et al.* Lamin A and ZMPSTE24 (FACE-1) defects cause nuclear disorganization and identify restrictive dermopathy as a lethal neonatal laminopathy. *Hum. Mol. Genet.* **13**, 2493–2503 (2004).

277. Yu, K.-R. *et al.* MicroRNA-141-3p plays a role in human mesenchymal stem cell aging by directly targeting ZMPSTE24. *J. Cell Sci.* (2013).

278. Yang, L., Guan, T. & Gerace, L. Lamin-binding fragment of LAP2 inhibits increase in nuclear volume during the cell cycle and progression into S phase. *J. Cell Biol.* **139**, 1077–1087 (1997).

279. Qiu, W. & Kassem, M. miR-141-3p inhibits human stromal (mesenchymal) stem cell proliferation and differentiation. *Biochim. Biophys. Acta* **1843**, 2114–2121 (2014).

280. Vigo, E. *et al.* CDC25A phosphatase is a target of E2F and is required for efficient E2F-induced S phase. *Mol. Cell. Biol.* **19**, 6379–95 (1999).

281. Galaktionov, K., Chen, X. & Beach, D. Cdc25 cell-cycle phosphatase as a target of c-myc. *Nature* **382**, 511–517 (1996).

282. Lin, Y. M., Chung, C. L. & Cheng, Y. S. Posttranscriptional regulation of CDC25A by BOLL is a conserved fertility mechanism essential for human spermatogenesis. *J. Clin. Endocrinol. Metab.* **94**, 2650–2657 (2009).

283. Tomko, R. J. & Lazo, J. S. Multimodal control of Cdc25A by nitrosative stress. *Cancer Res.* **68**, 7457–7465 (2008).

284. Busino, L., Chiesa, M., Draetta, G. F. & Donzelli, M. Cdc25A phosphatase:

combinatorial phosphorylation, ubiquitylation and proteolysis. *Oncogene* **23**, 2050–2056 (2004).

285. Qiu, W. & Kassem, M. miR-141-3p inhibits human stromal (mesenchymal) stem cell proliferation and differentiation. *Biochim. Biophys. Acta - Mol. Cell Res.* **1843**, 2114–2121 (2014).

286. Philip, S., Kumarasiri, M., Teo, T., Yu, M. & Wang, S. Cyclin-dependent kinase 8: A new hope in targeted cancer therapy? *J. Med. Chem.* **61**, 5073–5092 (2018).

287. Haneke, K. *et al.* CDK1 couples proliferation with protein synthesis. *J. Cell Biol.* **219**, (2020).

288. Tadesse, S. *et al.* Targeting CDK2 in cancer: challenges and opportunities for therapy. *Drug Discov. Today* **25**, 406–413 (2020).

289. Porter, D. C. *et al.* Cyclin-dependent kinase 8 mediates chemotherapy-induced tumor-promoting paracrine activities. *Proc. Natl. Acad. Sci. U. S. A.* **109**, 13799–13804 (2012).

290. Firestein, R. *et al.* CDK8 is a colorectal cancer oncogene that regulates beta-catenin activity. *Nature* **455**, 547–551 (2008).

291. Donner, A. J., Ebmeier, C. C., Taatjes, D. J. & Espinosa, J. M. CDK8 is a positive regulator of transcriptional elongation within the serum response network. *Nat. Struct. Mol. Biol.* **17**, 194–201 (2010).

292. Bancerek, J. *et al.* CDK8 kinase phosphorylates transcription factor STAT1 to selectively regulate the interferon response. *Immunity* **38**, 250–262 (2013).

293. Chen, M. *et al.* CDK8/19 Mediator kinases potentiate induction of transcription by NFκB. *Proc. Natl. Acad. Sci. U. S. A.* **114**, 10208–10213 (2017).

294. McDermott, M. S. J. *et al.* Inhibition of CDK8 mediator kinase suppresses estrogen dependent transcription and the growth of estrogen receptor positive breast cancer. *Oncotarget* **8**, 12558–12575 (2017).

295. Broude, E. V *et al.* Expression of CDK8 and CDK8-interacting genes as potential biomarkers in breast cancer. *Curr. Cancer Drug Targets* **15**, 739–749 (2015).

296. Xu, W. *et al.* Mutated K-ras activates CDK8 to stimulate the epithelial-to-mesenchymal transition in pancreatic cancer in part via the Wnt/β-catenin signaling pathway. *Cancer Lett.* **356**, 613–627 (2015).

297. Brägelmann, J. *et al.* Pan-cancer analysis of the mediator complex transcriptome identifies CDK19 and CDK8 as therapeutic targets in advanced prostate cancer. *Clin. Cancer Res.* **23**, 1829–1840 (2017).

298. Galbraith, M. D. *et al.* HIF1A employs CDK8-mediator to stimulate RNAPII elongation in response to hypoxia. *Cell* **153**, 1327–1339 (2013).

299. McDermott, M. S. J. *et al.* Inhibition of CDK8 mediator kinase suppresses estrogen dependent transcription and the growth of estrogen receptor positive breast cancer. *Oncotarget* **8**, 12558–12575 (2017).

300. Bancerek, J. *et al.* CDK8 kinase phosphorylates transcription factor STAT1 to selectively regulate the interferon response. *Immunity* **38**, 250–262 (2013).

301. Zhao, X. *et al.* Regulation of lipogenesis by cyclin-dependent kinase 8-mediated control of SREBP-1. *J. Clin. Invest.* **122**, 2417–2427 (2012).

302. Lindsay, A. K. *et al.* Analysis of Candida albicans mutants defective in the Cdk8 module of mediator reveal links between metabolism and biofilm formation. *PLoS Genet.* **10**, 1004567 (2014).

303. Xie, X.-J. *et al.* CDK8-cyclin C mediates nutritional regulation of developmental transitions through the ecdysone receptor in Drosophila. *PLoS Biol.* **13**, 1002207 (2015).

304. Galbraith, M. D. *et al.* CDK8 kinase activity promotes glycolysis. *Cell Rep.* **21**, 1495–1506 (2017).

305. Kapoor, A. *et al.* The histone variant macroH2A suppresses melanoma progression through regulation of CDK8. *Nature* **468**, 1105–1109 (2010).

306. Firestein, R. *et al.* CDK8 is a colorectal cancer oncogene that regulates β-catenin activity. *Nature* **455**, 547–551 (2008).

307. Adler, A. S. *et al.* CDK8 maintains tumor dedifferentiation and embryonic stem cell pluripotency. *Cancer Res.* **72**, 2129–2139 (2012).

308. DeBerardinis, R. J. & Thompson, C. B. Cellular metabolism and disease: what do metabolic outliers teach us? *Cell* **148**, 1132–1144 (2012).

309. Cantor, J. R. & Sabatini, D. M. Cancer cell metabolism: one hallmark, many faces. *Cancer Discov.* **2**, 881–898 (2012).

310. Vander Heiden, M. G., Cantley, L. C. & Thompson, C. B. Understanding the Warburg effect: the metabolic requirements of cell proliferation. *Science* **324**, 1029–1033 (2009).

311. Godoy, P. *et al.* Recent advances in 2D and 3D in vitro systems using primary hepatocytes, alternative hepatocyte sources and non-parenchymal liver cells and their use in investigating mechanisms of hepatotoxicity, cell signaling and ADME. *Arch. Toxicol.* **87**, 1315–1530 (2013).

312. Bale, S. S. *et al.* In vitro platforms for evaluating liver toxicity. *Exp. Biol. Med. (Maywood).* **239**, 1180–1191 (2014).

313. Dunn, J. C., Tompkins, R. G. & Yarmush, M. L. Long-term in vitro function of adult hepatocytes in a collagen sandwich configuration. *Biotechnol. Prog.* **7**, 237–245 (1991).

314. Busch, G. L. *et al.* Involvement of microtubules in the link between cell volume and pH of acidic cellular compartments in rat and human hepatocytes. *Proc. Natl. Acad. Sci. U. S. A.* **91**, 9165–9169 (1994).

315. Meijer, A. J. *et al.* Cell swelling and the sensitivity of autophagic proteolysis to inhibition by amino acids in isolated rat hepatocytes. *Eur. J. Biochem.* **215**, 449–454 (1993).

316. Michalopoulos, G. K. & DeFrances, M. C. Liver Regeneration. *Science.* **276**, 60–66

(1997).

317. Fausto, N. Liver regeneration. *J. Hepatol.* **32**, 19–31 (2000).

318. Ko, S. *et al.* Hdac1 regulates differentiation of bipotent liver progenitor cells during regeneration via Sox9b and Cdk8. *Gastroenterology* **156**, 187–202 (2019).

319. Lim, C. P. & Cao, X. Structure, function, and regulation of STAT proteins. *Mol. Biosyst.* **2**, 536–550 (2006).

320. Krebs, D. L. & Hilton, D. J. SOCS proteins: negative regulators of cytokine signaling. *Stem Cells* **19**, 378–87 (2001).

321. Durham, G. A., Williams, J. J. L., Nasim, M. T. & Palmer, T. M. Targeting SOCS proteins to control JAK-STAT signalling in disease. *Trends Pharmacol. Sci.* **40**, 298–308 (2019).

322. Campbell, J. S. *et al.* Expression of suppressors of cytokine signaling during liver regeneration. *J. Clin. Invest.* **107**, 1285–1292 (2001).

323. Wüstefeld, T., Rakemann, T., Kubicka, S., Manns, M. P. & Trautwein, C. Hyperstimulation with interleukin 6 inhibits cell cycle progression after hepatectomy in mice. *Hepatology* **32**, 514–522 (2000).

324. Karkampouna, S., Ten Dijke, P., Dooley, S. & Julio, M. K. TGFβ signaling in liver regeneration. *Curr. Pharm. Des.* **18**, 4103–4113 (2012).

325. Alarcón, C. *et al.* Nuclear CDKs drive Smad transcriptional activation and turnover in BMP and TGF-β pathways. *Cell* **139**, 757–769 (2009).

326. Serrao, A. *et al.* Mediator kinase CDK8/CDK19 drives YAP1-dependent BMP4-induced EMT in cancer. *Oncogene* **37**, 4792–4808 (2018).

327. Kretzschmar, M., Doody, J. & Massagué, J. Opposing BMP and EGF signalling pathways converge on the TGF-beta family mediator Smad1. *Nature* **389**, 618–622 (1997).

328. Macias-Silva, M., Li, W., Leu, J. I., Crissey, M. A. S. & Taub, R. Up-regulated transcriptional repressors SnoN and Ski bind Smad proteins to antagonize transforming growth factor-beta signals during liver regeneration. *J. Biol. Chem.* **277**, 28483–28490 (2002).

329. Shi, J.-H. & Line, P.-D. Effect of liver regeneration on malignant hepatic tumors. *World J. Gastroenterol.* **20**, 16167 (2014).

330. Kent, O. A. *et al.* A resource for analysis of microRNA expression and function in pancreatic ductal adenocarcinoma cells. *Cancer Biol. Ther.* **8**, 2013–2024 (2009).

331. Yang, Q., Zheng, M., Yan, J., Wu, J. & Liu, X. Rhynchophylline improves trophocyte mobility potential by upregulating ZEB1 level via the inhibition of miR-141-3p level. *Biosci. Biotechnol. Biochem.* **85**, 280–286 (2021).

332. Sun, Z. *et al.* LINC01296/miR-141-3p/ZEB1-ZEB2 axis promotes tumor metastasis via enhancing epithelial-mesenchymal transition process. *J. Cancer* **12**, 2723–2734 (2021).

333. Häussinger, D. & Reinehr, R. Osmotic regulation of bile acid transport, apoptosis and proliferation in rat liver. *Cell. Physiol. Biochem.* **28**, 1089–1098 (2011).

334. Sommerfeld, A., Reinehr, R. & Häussinger, D. Free fatty acids shift insulin-induced hepatocyte proliferation towards CD95-dependent apoptosis. *J. Biol. Chem.* **290**, 4398–4409 (2015).

335. Gohlke, H., Schmitz, B., Sommerfeld, A., Reinehr, R. & Häussinger, D. $\alpha_5\beta_1$-integrins are sensors for tauroursodeoxycholic acid in hepatocytes. *Hepatology* **57**, 1117–1129 (2013).

336. Schliess, F., Reinehr, R. & Häussinger, D. Osmosensing and signaling in the regulation of mammalian cell function. *FEBS J.* **274**, 5799–5803 (2007).

337. Sackin, H. Stretch-activated potassium channels in renal proximal tubule. *Am. J. Physiol.* **253**, 1253–1262 (1987).

338. Cheng, G., Tse, J., Jain, R. K. & Munn, L. L. Micro-environmental mechanical stress controls tumor spheroid size and morphology by suppressing proliferation and inducing apoptosis in cancer cells. *PLoS One* **4**, 4632 (2009).

339. Dolega, M. E. *et al.* Extracellular matrix in multicellular aggregates acts as a pressure sensor controlling cell proliferation and motility. *Elife* **10**, (2021).

340. Nam, S. & Chaudhuri, O. Mitotic cells generate protrusive extracellular forces to divide in three-dimensional microenvironments. *Nat. Phys.* **14**, 621–628 (2018).

341. Reinehr, R., Sommerfeld, A. & Häussinger, D. The Src family kinases: Distinct functions of c-Src, Yes, and Fyn in the liver. *Biomol. Concepts* **4**, 129–142 (2013).

342. Schliess, F. & Häussinger, D. Cell volume and insulin signaling. *Int. Rev. Cytol.* **225**, 187–228 (2003).

343. Taylor, E. W. The mechanism of colchicine inhibition of mitosis. *J. Cell Biol.* **25**, 145–160 (1965).

344. Dubin, M., Maurice, M., Feldmann, G. & Erlinger, S. Influence of colchicine and phalloidin on bile secretion and hepatic ultrastructure in the rat. Possible interaction between microtubules and microfilaments. *Gastroenterology* **79**, 646–654 (1980).

345. Crawford, J. M., Berken, C. A. & Gollan, J. L. Role of the hepatocyte microtubular system in the excretion of bile salts and biliary lipid: implications for intracellular vesicular transport. *J. Lipid Res.* **29**, 144–156 (1988).

346. Häussinger, D., Saha, N., Hallbrucker, C., Lang, F. & Gerok, W. Involvement of microtubules in the swelling-induced stimulation of transcellular taurocholate transport in perfused rat liver. *Biochem. J.* **291 (Pt 2**, 355–60 (1993).

347. Hu, J.-Y. *et al.* The p38/MAPK pathway regulates microtubule polymerization through phosphorylation of MAP4 and Op18 in hypoxic cells. *Cell. Mol. Life Sci.* **67**, 321–333 (2010).

348. Ou, X.-H. *et al.* p38α MAPK is a MTOC-associated protein regulating spindle assembly,

spindle length and accurate chromosome segregation during mouse oocyte meiotic maturation. *Cell Cycle* **9**, 4130–4143 (2010).

349. JANMEY, P. A. The cytoskeleton and cell signaling: Component localization and mechanical coupling. *Physiol. Rev.* **78**, 763–781 (1998).

350. Gómez, A. M., Kerfant, B. G. & Vassort, G. Microtubule disruption modulates Ca^{2+} signaling in rat cardiac myocytes. *Circ. Res.* **86**, 30–36 (2000).

351. Cohen, P. The twentieth century struggle to decipher insulin signalling. *Nat. Rev. Mol. Cell Biol.* **7**, 867–873 (2006).

352. vom Dahl, S. & Häussinger, D. Nutritional state and the swelling-induced inhibition of proteolysis in perfused rat liver. *J. Nutr.* **126**, 395–402 (1996).

353. Salai, M. *et al.* The inhibitory effects of colchicine on cell proliferation and mineralisation in culture. *J. Bone Joint Surg. Br.* **83**, 912–915 (2001).

354. Lemor, M., de Bustros, S. & Glaser, B. M. Low-dose colchicine inhibits astrocyte, fibroblast, and retinal pigment epithelial cell migration and proliferation. *Arch. Ophthalmol. (Chicago, Ill. 1960)* **104**, 1223–1225 (1986).

6. Acknowledgements

I would like to express my gratitude and my sincere thanks to Professor Dr. Dieter Häussinger and Dr. David Schöler for the opportunity to conduct my PhD thesis in the Clinic for Gastroenterology, Hepatology and Infectious Diseases in Düsseldorf. Furthermore, I would also like to thank Professor Dr. Stephan vom Dahl for taking over the role as PhD advisor.

I would also like to thank Professor Dr. Holger Gohlke for providing his time and his interest in my research topic and for reviewing my PhD thesis.

A special thanks to Dr. Martha Paluschinski for her support, her expertise, and her charming manners since my first workday.

Another special thanks to Dr. Claus Kordes for proof-reading my work and his helpful suggestions, explanations, and constructive criticism over the years.

I would also like to thank my colleagues at the Experimental Hepatology for their helpful support in the laboratory and the pleasant working atmosphere. It has been a pleasure to work with you in such a friendly and welcoming environment.

Last but not least, I would like to thank my parents, my family, my girlfriend, and my friends for their support throughout the entire period of my doctoral thesis.

7. List of Figures

8. List of Tables

9. List of Publications and Scientific Presentations

Publication:

Nils Bardeck, Martha Paluschinski, Mirco Castoldi, Claus Kordes, Boris Görg, Jan Stindt, Tom Luedde, Stephan vom Dahl, Dieter Häussinger, David Schöler

"Swelling-induced upregulation of miR-141-3p inhibits hepatocyte proliferation."

JHEP Reports - 2022, in press

Nils Bardeck, Martha Paluschinski, Mirco Castoldi, Tom Luedde, Dieter Häussinger, Stephan vom Dahl, David Schöler

„*Liver cell swelling leads to upregulation of miR-141-3p in perfused rat liver and primary rat hepatocytes."*

Zeitschrift für Gastroenterologie – January 2021, 59. Edition, Page 9

(Thieme, Stuttgart, Deutschland)

Poster presentation:

"*Liver cell swelling leads to upregulation of miR-141-3p in perfused rat liver and primary rat hepatocytes.*"

37. Annual meeting GASL (29th – 30th January 2021)

10. Curriculum vitae

07/2018 until 06/2021	Research Ph.D. student Heinrich-Heine-Universität, Düsseldorf
10/2017 until 12/2017	Research Assistant Ruhr-Universität Bochum, Bochum
08/2012 until 07/2017	Study: Biology Ruhr-Universität Bochum, Bochum Degree: Master of Science
08/2011 until 07/2012	Study: Bio- and nanotechnology Fachhochschule Südwestfalen, Iserlohn
08/2009 until 07/2011	Training as biological-technical assistant Hans Böckler Berufskolleg, Marl Degree: Biological-technical assistant
08/1999 until 07/2009	Gymnasium Borbeck, Essen Degree: High school diploma

Eidesstattliche Versicherung

Ich, Herr Nils Bardeck, versichere an Eides statt, dass die vorliegende Dissertation von mir selbstständig und ohne unzulässige fremde Hilfe unter Beachtung der „Grundsätze zur Sicherung guter wissenschaftlicher Praxis an der Heinrich-Heine-Universität Düsseldorf“ erstellt worden ist.

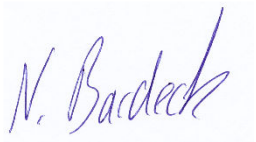

Düsseldorf, der 19. Dezember 2022 Unterschrift